Integration of geological and geophysical data of different quality into the stochastic description of aquifers

Inauguraldissertation

zur

Erlangung der Würde eines Doktors der Philosophie

vorgelegt der

Philosophisch-Naturwissenschaftlichen Fakultät

der Universität Basel

von

Christian Regli

aus Andermatt (UR)

Basel, 2003

Genehmigt von der Philosophisch-Naturwissenschaftlichen Fakultät

auf Antrag von   Prof. Dr. Peter Huggenberger
                   Angewandte und Umweltgeologie
                   Universität Basel

                   Prof. Dr. Warren Barrash
                   Center for Geophysical Investigation of the Shallow Subsurface
                   Boise State University, Boise, USA

            und   Dr. Lukas Rosenthaler
                   Bild- und Medientechnologien
                   Universität Basel

                   Prof. Dr. Stefan Schmid
                   Fakultätsverantwortlicher

                   ....

Basel, den 21. Januar 2003

                                   Prof. Dr. Marcel Tanner
                                   Dekan

to my wife Ursula
and our children Josias, Elena, and Jann

Acknowledgments

The present thesis resulted from my activities during the years 1997 to 2002 at the Geological Institute of the University of Basel. My sincerest thanks are addressed to my supervisor Peter Huggenberger, Professor and Head of the Division of Applied and Environmental Geology at the University of Basel. He was always ready to help and give advice but has also allowed me to develop my own ideas. Working under his leadership has been a real privilege and pleasure. The confidence and friendship that I experienced from him is simply outstanding.

Many thanks are also addressed to Warren Barrash, Professor and Head of the Center for Geophysical Investigation of the Shallow Subsurface at Boise State University. His untiring efforts in thinking along with the writer are invaluable and will always be appreciated. This thesis benefitted substantially from his comments. He accepted to be the co-referent.

Special thanks are addressed to Dr. Lukas Rosenthaler, staff member of the Imaging and Media Lab at the University of Basel. He formed my skills in programming and always had a solution for implementing the geologist's wishes. Also special thanks are addressed to Dr. Martin Rauber, Head of Rauber Consulting at Zürich, who has always been ready to assist me throughout the past five years and to keep conceptual things 'on the right track'.

Over the last five years, different field investigations have been taken place: drilling, georadar, and groundwater sampling surveys as well as tracer tests at high river discharge, which is of course related to wet and cold weather. Mario Kaiser, Majka Rohrmeier, Peter Schwer, and particularly the 'six pack team': Christoph Hecker, Matthias Damo, Rolf Keiser, Judith Kohler, Andreas Märki, and Beat Niederberger participated in the field surveys and did a wonderful job. I shall never forget their long working hours, also nights, under often harsh field conditions. The technique for the continuous input of tracer over a defined time and distributed evenly over the entire cross-section of a river was developed by Hans-Rudolf Rüegg. I express my gratitude to him.

Richard Wülser and his team of the Industrial Services of the City of Basel provided the water supply data and analyzed the chemical and microbiological parameters of groundwater samples, while Markus Zehringer and his team of the Cantonal Laboratory of Basel measured the Radon activities - all their work is most greatly acknowledged.

Thanks are also expressed to Katrin Schneiter and Dr. Karin Bernet for most appreciated suggestions and comments on the manuscripts and improving my English. I trust that they also did a wonderful job in the work you are currently reading.

I shared many special moments of delight, laughter, and support with my colleagues of the division: Adrian Auckenthaler, Daniel Gechter, Lorenz Guldenfels, Ralph Kirchhofer, Dr. Cinzia Miracapillo, Dr. Thomas Noack, Monika Schweizer, Ina Spottke, and Dr. Eric Zechner. Special thanks are also addressed to Antoinette Lüdin for her ever reliable administrative support.

Finally, I must give my sincerest thanks to my wife Ursula for the many hours during which she allowed me to work on my thesis. She obliged me with more affection and understanding than I actually would have earned. Without her love, patience, and support, this thesis would not have been possible. I dedicate this work to her and our children Josias, Elena, and Jann.

TABLE OF CONTENTS

Abstract

Many of the present problems in hydrogeology such as old waste disposal sites and the risk of the infiltration of contaminated riverwater concern the protection of groundwater. Solutions of qualitative and quantitative, site-specific groundwater problems require the knowledge of the site-specific heterogeneity of the subsurface. Therefore, (1) descriptive, (2) structure-imitating, and (3) process-imitating methods are combined:

(1) Sedimentlogical and geophysical data – outcrop, drill-core, and georadar data – are combined in a lithofacies-based interpretation and processed to be used for stochastic simulations of sedimentary structures. This interpretation respects differences in data uncertainty and provides lithofacies probabilities for points along boreholes and grid nodes with arbitrary mesh sizes along georadar sections. The estimation of probabilities that drill-core layer descriptions and radarfacies patterns represent specified lithofacies types is based on the significance of the information included in drill-core layer descriptions and the structural information of radarfacies patterns. The specification of the lithofacies types is based on outcrop data.

(2) GEOSSAV (Geostatistical Environment fOr Subsurface Simulation And Visualization) has been developed for the integration of hard and soft data into the stochastic simulation and visualization of distributions of geological structures and hydrogeological properties in the subsurface. GEOSSAV, an interface to selected geostatistical modules (bicalib, gamv, vargplt, and sisim) from the Geostatistical Software LIBrary, GSLIB (Deutsch and Journel, 1998), can be used for data analysis, variogram computation of regularly or irregularly spaced data, and sequential indicator simulation of subsurface heterogeneities. Sequential indicator simulation, based on various kriging techniques (simple, ordinary, and Bayesian), is suitable for the simulation of either continuous variables such as hydraulic conductivity of an aquifer or chemical concentrations at a contaminated site, or categorical variables which indicate the presence or absence of a particular lithofacies. Export options for finite-difference groundwater models allow either files that characterize single model layers or files that characterize the complete 3D flow model set-up for MODFLOW-based groundwater simulation systems. GEOSSAV has been successfully tested on Microsoft Windows NT 4.0/2000/XP and on SuSE Linux 7.3. The current version is available at http://www.unibas.ch/earth/pract.

(3) The developed lithofacies-based interpretation of geological and geophysical data and the software GEOSSAV was applied on a field example in the groundwater recharge and production area Lange Erlen, a formerly braided river environment near Basel, Northwestern Switzerland. Two different groundwater models are used to simulate a capture zone of a well located near the infiltrating river Wiese, depending on the hydrological variations (river discharge, hydraulic conductivity of the riverbed), the water supply operation, the progress of river restoration, and the heterogeneity of the subsurface. A deterministic, large-scaled groundwater model (1.8 km x 1.2 km) is used to simulate the average behavior of groundwater flow and advective transport. It is also used to assign the hydraulic boundary conditions for a small-scaled groundwater model (550 m x 400 m), which relies on stochastically generated aquifer properties based on site-specific drill-core and georadar data. The stochastic approach in the small-scaled groundwater model does not lead to a clearly defined well capture zone, but to a well capture zone distribution reflecting the uncertainty of the knowledge of the aquifer parameters.

The developed methods and tools allow the integration of geological and geophysical data of different quality into the stochastic description of aquifers. They can be used, e.g., to define and evaluate groundwater protection zones in heterogeneous aquifers associated with infiltration from rivers under changing boundary conditions and under the uncertainty of subsurface heterogeneity.

Kurzfassung

Viele der gegenwärtigen Probleme in der Hydrogeologie wie Altlasten und das Risiko der Infiltration von verschmutztem Flusswasser betreffen den Grundwasserschutz. Lösungen qualitativer und quantitativer, standortspezifischer Grundwasserprobleme erfordern die Kenntnis der standortspezifischen Heterogenität des Untergrundes. Deshalb werden (1) beschreibende, (2) Strukturen-imitierende und (3) Prozess-imitierende Methoden miteinander kombiniert:

(1) Sedimentologische und geophysikalische Daten – Aufschluss-, Bohrkern- und Georadardaten – werden, basierend auf einer Lithofazies-Interpretation, miteinander kombiniert und aufbereitet, so dass sie für die stochastische Simulation von Sedimentstrukturen verwendet werden können. Die vorgestellte Interpretation berücksichtigt Unterschiede in der Datenunsicherheit und liefert als Resultat nicht eine eindeutige lithologische Zuweisung, sondern Wahrscheinlichkeiten von Lithologien für Punkte entlang von Bohrungen und Raster mit beliebigen Maschenweiten entlang von Georadarprofilen. Die Schätzung von Wahrscheinlichkeiten, dass einzelne Schichtbeschreibungen aus Bohrungen und Radarfaziesmuster von Georadarprofilen spezifische Lithologien darstellen, basiert auf der Aussagekraft der in Schichtbeschreibungen enthaltenen Information und der Strukturinformation von Radarfaziesmustern. Die Klassifizierung der Lithologien basiert auf Aufschlussdaten.

(2) GEOSSAV (Geostatistical Environment fOr Subsurface Simulation And Visualization) wurde entwickelt, um harte und weiche geologische und geophysikalische Daten in die stochastische Simulation zu integrieren und die daraus resultierenden Verteilungen von geologischen Strukturen und hydrogeologischen Eigenschaften im Untergrund zu visualisieren. GEOSSAV, eine Schnittstelle zu ausgewählten geostatistischen Module (bicalib, gamv, vargplt, und sisim) der Geostatistischen Software Bibliothek, GSLIB (Deutsch and Journel, 1998), kann für die Datenanalyse, die Variogrammberechnung von regelmässig oder unregelmässig verteilten Daten und für die sequentielle Indikatorsimulation von Heterogenitäten des Untergrundes verwendet werden. Die sequentielle Indikatorsimulation basiert auf verschiedenen Kriging Methoden (simple, ordinary, and Bayesian). Sie ist geeignet für die Simulation von kontinuierlichen Variablen wie der hydraulischen Leitfähigkeit eines Aquifers oder chemischer Konzentrationen bei einem kontaminierten Standort, oder kategorischen Variablen, welche die Gegenwart oder Abwesenheit einer bestimmten Lithofazies anzeigen. Exportmöglichkeiten für Finite-Differenzen Grundwassermodelle erlauben entweder den Export von Dateien, die einzelne Modellschichten oder den vollständigen 3D Modellaufbau von MODFLOW basierten Grundwasser Simulationssystemen charakterisieren. GEOSSAV wurde auf Microsoft Windows NT 4.0/2000/XP und auf SuSE Linux 7.3 erfolgreich getestet. Die aktuelle Version kann unter http://www.unibas.ch/earth/pract herunter geladen werden.

(3) Sowohl die entwickelte lithofazies-basierte Interpretation geologischer und geophysikalischer Daten als auch die Software GEOSSAV wurde in einem Feldbeispiel im Grundwasser Anreicherungs- und Entnahmegebiet Lange Erlen angewandt, einem ehemals verzweigten Flusssystem in der Nähe von Basel, Nordwestschweiz. Zwei verschiedene Grundwassermodelle wurden aufgesetzt, um den Anströmbereich eines in der Nähe des infiltrierenden Flusses Wiese liegenden Brunnens zu simulieren. Die Simulation erfolgte in Abhängigkeit der hydrologischen Veränderungen (Abfluss der Wiese, Durchlässigkeit der Flusssohle), den Pump- und Anreicherungsraten, dem Fortschritt der Flussrevitalisierung und der Heterogenität des Untergrundes. Das deterministische, grossskalige Grundwassermodell (1.8 km x 1.2 km) wurde verwendet um das mittlere Verhalten von Grundwasserfluss und advektivem Transport zu ermitteln. Gleichzeitig wurde dieses Modell für die Zuweisung der hydraulischen Randbedingungen in einem kleinskaligen Grundwassermodell (550 m x 400 m) benutzt, welches stochastisch generierte Aquifereigenschaften enthält, die auf standort-

spezifischen Bohrkern- und Georadardaten basieren. Der stochastische Ansatz im kleinskaligen Grundwassermodell führt nicht zu einem klar definierten Anströmbereich, sondern zu einer Darstellung der Wahrscheinlichkeit, dass ein Punkt auf der Terrainoberfläche zum Anströmbereich des Brunnens gehört.

Die entwickelten Methoden und Werkzeuge ermöglichen die Integration von geologischen und geophysikalischen Daten unterschiedlicher Qualität in die stochastische Beschreibung von Aquiferen. Sie können z.B. verwendet werden, um Grundwasserschutzzonen in heterogenen Aquiferen im Zusammenhang mit infiltrierenden Flüssen bei sich ändernden hydraulischen Randbedingungen und der Unsicherheit bezüglich der Heterogenität des Untergrundes zu eruieren und zu beurteilen.

References

Deutsch, C.V., Journel, A.G., 1998. GSLIB: Geostatistical Software Library and User's Guide, Second Edition, Applied Geostatistics Series. Oxford University Press, Oxford.

Introduction

1. Problems and approaches

Coarse fluvial deposits in river valleys of the alpine foreland commonly are important aquifers for municipal water supplies. In Switzerland, approximately 42% of the total drinking water demand, which is about 1.1 billion m^3/y, is covered by pumped groundwater. In many countries, river valleys have undergone a series of changes since the last century, e.g. in the fields of flood defense, material extraction, industrialization, and agriculture activities. In more recent years, ecological recovery, recreation, transporting systems, and the development of new living or working space have become new issues in public discussions, not at least due to new findings in resource management, sustainability, biodiversity, and flood protection, but also due to the increasing value on mobility. However, the river valleys are relatively narrow and, therefore, the limited space inevitably causes conflicts in utilization. How can all these above-mentioned functions simultaneously be accommodated in the finite space along the rivers? How should the different interests be weighed? What can reasonably be done, and what not?

Many of the present problems such as old waste disposal sites, polluted grounds, and the risk of the infiltration of contaminated river water concern the protection of groundwater, which is legislated in laws and ordinances (e.g., law of water protection, law of pollution control, ordinance of substances, ordinance over the protection of waters against water endangering liquids). To solve such problems, information of the subsurface heterogeneity is required. The importance of the knowledge of the subsurface heterogeneity is often underestimated and this knowledge is difficult to obtain. The main reasons are the relative inaccessibility of the subsurface, the time-scale of subsurface processes, and the high costs of the investigation methods. To get structure information of the subsurface, different approaches are applied and have to be combined: (1) descriptive methods which translate sedimentological facies models into hydro-facies models with characteristic aquifer properties, (2) structure-imitating methods which match sedimentary structures based on geostatistical techniques, and (3) process-imitating methods which solve governing flow and transport equations based on calibration techniques (Koltermann and Gorelick, 1996).

The present knowledge of many aquifer systems only covers the mean behaviour. However, solutions of qualitative and quantitative, site-specific groundwater problems (e.g., definition of well capture zones, river-groundwater interaction, processes downgradient of contaminated sites) require the knowledge of the site-specific heterogeneity of the subsurface. The heterogeneity of hydraulic, chemical, and biological aquifer properties control groundwater flow and transport. For example the risk assessment of drinking water wells and, thus, the definition of well capture zones is one of many application fields, where the subsurface heterogeneity play an important role. Consequently, the following questions are subject of recent research: How does the incorporation of subsurface heterogeneity lead to predictions for large-scaled contamination or solute and particle transport that differ from predictions made by models for homogeneous media? Does the stochastic approach offer insight into observations of field scale transport under heterogeneous conditions?

1.1. Descriptive approach

Large-scale (valley scale) sedimentological features of alluvial groundwater systems, which strongly influence groundwater flow, have been described by Siegenthaler and Huggenberger (1993), Creuzé des Chatelliers et al. (1994), and Bridge et al. (1995). At a medium scale (kilo-

meters to 10s of kilometers), sedimentological models are generally used to delineate trends of hydraulic properties of fluvial sediments (Anderson, 1989; Webb and Davis, 1998; Anderson et al., 1999).

Many of the present groundwater problems in urban areas require knowledge of the subsurface heterogeneity at smaller scales, in the order of 10s to several hundred of meters. At these scales, textural and structural assemblages exist, but they exhibit a puzzling variety of lateral changes in sediment composition and the geometry of erosional boundaries. At the small scale (outcrop scale), coarse-grained fluvial deposits have been successfully described in terms of architectural element analysis (Siegenthaler and Huggenberger, 1993; Asprion and Aigner, 1999) and hydraulic properties (Jussel et al., 1994; Klingbeil et al., 1999). A principal finding of these authors was that coarse-grained fluvial deposits are composed of a limited number of sedimentary structure types, each with characteristic hydraulic properties such as hydraulic conductivity and porosity. The sedimentary structure types may be explained in terms of depositional processes.

Rapid lateral changes significantly complicate the exploration of the sedimentary structures in aquifers. To overcome these difficulties, different investigation methods are applied and partially combined, e.g., ultra-high resolution geophysical methods (Rubin et al., 1992; Huggenberger, 1993; Hyndmann et al., 1994; Hyndman and Gorelick, 1996; Beres et al., 1995; Barrash and Morin, 1997; Barrash and Knoll, 1997; Beres et al., 1999; Dietrich, 1999; Kowalsky et al., 2001), outcrop analysis (Siegenthaler and Huggenberger, 1993; Rauber et al., 1998; Van Dam and Schlager, 2000; Heinz, 2001), modern destruction-poor drilling methods, and the observation of the surface morphology and processes of recent braided river systems. Although these methods provide data of differnt quality, they allow to establish spatial trends of the principal sedimentary structures.

1.2. Structure-imitating approach

The problem of adequately modeling subsurface structures becomes more difficult with increasing heterogeneity and thereby increasing uncertainty with respect to spatial variability of available data. The modeling depends both on the quantity and the quality of available data. In the earth sciences and in many other research disciplines, great efforts have been made within the last 20 years on evaluation and integration of data in the characterization of the subsurface (among others Wingle et al., 1997; Deutsch and Journel, 1998). One of the objectives of all these projects is to model reasonable variations in the subsurface while constraining results as much as possible with available data. Although one particular data set may suggest a wide range of alternatives, if all the available data are combined, the possible solution population should be greatly reduced. Data used in subsurface and groundwater models may be divided into two basic types: 'hard data' and 'soft data' (Poeter and McKenna, 1995). Hard data can be directly obtained and examined. There is uncertainty in hard data, but it is considered small enough to be ignored. Soft data are less precise and/or direct, and so there is greater uncertainty associated with the soft data values. The technique used to model subsurface structures in a site-specific problem should be chosen based on properties under consideration (e.g., lithofacies, hydraulic conductivity, porosity), knowledge of the subsurface, and causes of uncertainty (Ayyub and Gupta, 1997; Weissmann et al., 1999).

For any given data set, there is a multitude of possible interpretations of the subsurface which honor the raw data. To manually simulate and evaluate the alternatives in a deterministic approach would take considerable time, and still only a small portion of the possibilities could be evaluated. This is true even if the subsurface configuration is relatively simple. However, if

the subsurface is strongly heterogeneous or some of the data are hard and some are soft, alternatives can only be simulated and evaluated meaningfully by applying stochastic simulations. In these stochastic simulations, some input parameter values are taken from probability distributions. The solutions are, therefore, also probability distributions of structure types and structure properties which can be examined with statistical methods. The stochastic simulation approach yields not only a probable realization but also a probable fluctuation range of the result (Journel and Huijbregts, 1989; Deutsch and Journel, 1998).

1.3. Process-imitating approach

Investigations regarding hydrogeological processes can only partially be made with field experiments. Water protection measures as well as questions about the sustainable use of groundwater, require the consideration of a broader and broader associated field. Therefore, methods which permit a comparative assessment of different operation options become still more important. Numerical models of physical systems play an important role in decision-making processes, especially in the context of better characterization of parameter distributions and prediction of dynamic behavior of a given system (Reichert and Pahl, 1999). Groundwater models are helpful tools to define well capture zones based on hydrogeological and water supply operation data (e.g., Kinzelbach et al., 1992; Lerner, 1992). They allow to examine the sensitivity of the observed system on changing model parameters and conditions. Groundwater models, however, which do not consider site-specific geological information might not be used for site-specific risk estimation of changing groundwater quality. How accurate a prediction is, depends on how well the models actually represent the system behavior. The more representative realizations of the concerned system behavior are available, the larger is the confidence that the model correctly describes the processes of the system, and that the system is also well understood (Reichert and Pahl, 1999).

This thesis helps to better understand the consequences of geological and geophysical data of different quality on groundwater flow and transport calculations and increases the ability to evaluate and optimize measures on aquifers as well as to quantify and to assess expected consequences of decisions. Consequently, calculation, uncertainty, and assessment of operational alternatives can be separated, the discussion in decision-making processes can be de-emotionalized, and discrepancies can be identified as well (Reichert and Pahl, 1999). A groundwater model based on geological data has accomplished its task if the solution is robust and also is geologically and hydrologically resaonable if the actual parameter values differ, within a certain range, from those of the model (Kinzelbach and Rausch, 1995). The above-mentioned approaches clarify the only restrictedly possible, but after all quantifiable knowledge of subsurface structures and hydrogeological processes. In this sense, the knowledge about subsurface structures and hydrogeological processes is soft, being based on a number of hypotheses and assumptions. Under this conditions, models help to better interpret field data and to understand the sensitivity of data and modeled processes on model results, expressed also in terms of uncertainties.

2. Objectives and scope

The objective of this thesis was to develop and to evaluate a method and a tool which allow the integration of geological and geophysical data of different quality into the stochastic description of aquifers. The essentials of particular aquifer systems have to be recognized and

the differences in data uncertainty have to be respected. The method and the tool have to be applied to a site-specific problem in an environment of coarse fluvial gravel deposits which are typical for braided river systems.

Sedimentlogical and geophysical data - outcrop, drill-core, and georadar data - are combined in a lithofacies-based interpretation and processed to be used for stochastic simulations of sedimentary structures. This interpretation respects differences in data uncertainty and provides lithofacies probabilities for points along boreholes and grid nodes with arbitrary mesh sizes along georadar sections. The estimation of probabilities that drill-core layer descriptions and radarfacies patterns represent specified lithofacies types is based on the significance of the information included in drill-core layer descriptions (e.g., main constituent, quantity, fraction, and sorting of single grain-size categories, color, chemical precipitation, layer thickness, and adjacent layer) and the interpretation of the structural information of radarfacies patterns. The specification of the lithofacies types is based on outcrop data.

GEOSSAV (Geostatistical Environment fOr Subsurface Simulation And Visualization) is introduced, a tool for the integration of hard and soft data into the stochastic simulation and visualization of distributions of geological structures and hydrogeological properties in the subsurface. GEOSSAV, as an interface to selected geostatistical modules (bicalib, gamv, vargplt, and sisim) from the Geostatistical Software LIBrary, GSLIB (Deutsch and Journel, 1998), can be used for data analysis, variogram computation of regularly or irregularly spaced data, and sequential indicator simulation of subsurface heterogeneities. Sequential indicator simulation, based on various kriging techniques (simple, ordinary, and Bayesian), is suitable for the simulation of either continuous variables such as hydraulic conductivity of an aquifer or chemical concentrations at a contaminated site, or categorical variables which indicate the presence or absence of a particular lithofacies. The standard OpenGL API (application programming interface) is used for rendering of 3D data distributions and for slicing perpendicular to the main coordinate axis. Export options for finite-difference groundwater models (e.g. GMS (Environmental Modeling Systems Inc., 2002); PMWIN (Chiang and Kinzelbach, 2001)) allow either files that characterize single model layers (which are saved in ASCII matrix format) or files that characterize the complete 3D flow model set-up for MODFLOW-based groundwater simulation systems (which are saved in bcf package format (Harbaugh and McDonald, 1996)).

The developed lithofacies-based interpretation of geological and geophysical data and the software GEOSSAV is combined with groundwater modeling and applied on a field example in a formerly braided river environment near Basel, Northwestern Switzerland. Two different groundwater models are used to simulate a well capture zone in the heterogeneous aquifer located near the infiltrating river Wiese. A deterministic, large-scaled groundwater model (1.8 km x 1.2 km) is used to simulate the average behavior of groundwater flow and advective transport. It is also used to assign the boundary conditions for a small-scaled groundwater model (550 m x 400 m) which relies on stochastically generated aquifer properties based on site-specific drill-core and georadar data. The small-scaled groundwater model is used to include the large subsurface heterogeneity at the location of interest. The stochastic approach in the small-scaled groundwater model does not lead to a clearly defined well capture zone, but to a plane representation of the probability of a certain surface location belonging to the well capture zone. The models were applied to a study site in Lange Erlen, which is located in an area of artificial groundwater recharge and production. The groundwater at this site contributes to the city's drinking water supply, and the site serves as recreational area to the population of Basel. The river is channelized, but there are initiatives to restore the riverbank to more natural conditions. However, they conflict with the requirements of groundwater protection, especially during flood events. Therefore, a river section of 600 m in the vicinity of an unused and disconnected drinking water well was restored to study changes in the groundwater flow

regime depending on hydrologic variations, water supply operation data, progress of river restoration, and subsurface heterogeneity. The results of the groundwater models are compared with data from two tracer experiments using Uranine and the natural Radon isotope Rn-222, and with physical, chemical, and microbiological data sampled in monitoring wells between the river and the drinking water well.

3. Thesis organization

The thesis is divided into three parts, each representing a standalone article including corresponding references. Part I describes the interpretation of drill-core and georadar data of coarse gravel deposits. It starts by summarizing sedimentological and geophysical field investigations. In the following section, a lithofacies-based interpretation of drill-core layer descriptions and radarfacies types representing specified sedimentary structure types is given. Part I concludes with examples, results, and a discussion of this interpretation method.

Part II presents an user-friendly tool, GEOSSAV, for the integration of hard and soft geological and geophysical data into the stochastic simulation and visualization of subsurface heterogeneities. It starts by describing the integration platform and software resources. In the following sections the central features of GEOSSAV are described, including an account of the geostatistical techniques, the visualization methods, and the data export options. Subsequently, an example is given to illustrate site-specific considerations of heterogeneity in subsurface modeling. This part concludes with a description of hardware and software requirements for running GEOSSAV, planned new developments, and information for acquiring GEOSSAV.

Part III is an application of the developed method and software in combination with groundwater modeling to simulate a well capture zone in a heterogeneous aquifer located near an infiltrating river. It starts with a description of the study site. Then deterministic and stochastic modeling of a well capture zone is presented depending on hydrologic variations, water supply operation data, progress of river restoration, and subsurface heterogeneity, including the generation of distributions of hydrogeological properties. This part concludes with the comparison of results from groundwater models with two tracer experiments and with physical, chemical, and microbiological data.

The appendices are on CD ROMs. Appendix A includes the interpretation of drill-core and georadar data described in part I, Appendix B includes the source code of GEOSSAV described in part II, and Appendix C includes the subsurface and groundwater models as well as the data of field experiments and measurements described in part III. CD ROM 1 is inside, CD ROM 2 is in the archive of the Geological Institute.

References

Anderson, M.P., Aiken, J.S., Webb, E.K., Mickelson, D.M., 1999. Sedimentology and hydrogeology of two braided stream deposits. Sedimentary Geology 129, 501-511.

Anderson, M.P., 1989. Hydrogeologic facies models to delineate large-scale spatial trends in glacial and glaciofluvial sediments. Geological Society of America Bulletin 101, 501-511.

Asprion, U., Aigner, T., 1999. Towards realistic aquifer models: three-dimensional georadar surveys of quaternary gravel deltas (Singen Basin, SW Germany). Sedimentary Geology 129 (3-4), 281-297.

Ayyub, B.M., Gupta, M.M., 1997. Uncertainty Analysis in Engineering and Sciences: Fuzzy Logic, Statistics, and Neural Network Approach. Kluwer Academic, Dordrecht.

Barrash, W., Knoll, W.D., 1997. Research well field for calibrating geophysical measurements against hydrologic parameters. AGU Fall Meeting, San Francisco. CA, EOS, 78 (46), F319.

Barrash, W., Morin, R.H., 1997. Recognition of units in coarse, unconsolidated braided stream deposits from geophysical log data with principal component analysis. Geology 25 (8), 687-690.

Beres, M., Huggenberger, P., Green, A.G., Horstmeyer, H., 1999. Using two- and three-dimensional georadar methods to characterize glaciofluvial architecture. Sedimentary Geology 129, 1-24.

Beres, M., Green, A.G., Huggenberger, P., Horstmeyer, H., 1995. Mapping the architecture of glaciofluvial sediments with three-dimensional georadar. Geology 23 (12), 1087-1090.

Bridge, S.J., Alexander, J., Collier, R.E.L., Gawthropes, R.L., Jarvis, J., 1995. Ground-penetrating radar and coring to study the large-scale structure of point-bar deposits in three dimensions. Sedimentology 42, 839-852.

Chiang, W.-H., Kinzelbach, W., 2001. 3D-Groundwater Modeling with PMWIN. Springer, Heidelberg.

Creuzé des Chatelliers, M., Pointsart D., Bravard, J.-P., 1994. Geomorphology of alluvial groundwater ecosystems. Gibert, J., Danielopol, D.L., Stanford, J.A. (Eds.). Groundwater Ecology. Academic Press, San Diego, California, 157-185.

Deutsch, C.V., Journel, A.G., 1998. GSLIB: Geostatistical Software Library and User's Guide. Oxford University Press, Oxford.

Dietrich, P., 1999. Konzeption und Auswertung gleichstrom-geoelektrischer Tracerversuche unter Verwendung von Sensitivitätskoeffizienten. Tübinger Geowissenschaftliche Arbeiten (TGA), C50, 130.

Environmental Modeling Systems Inc. (EMS-I), 2002. GMS: Groundwater Modeling System, EMS-I, South Jordan, Utah.

Heinz, J., 2001. Sedimentary Geology of Glacial and Periglacial Gravel Bodies (SW-Germany): Dynamic Stratigraphy and Aquifer Sedimentology. Tübinger Geowissenschaftliche Arbeiten C59.

Huggenberger, P., 1993. Radar facies: recognition of facies patterns and heterogeneities within Pleistocene Rhine gravels, NE Switzerland. Best, C.L., Bristow, C.S. (Eds.). Braided Rivers. Geological Society Special Publication 75, 163-176.

Hyndman, D.W., Gorelick, S.M., 1996. Estimating lithologic and transport properties in three dimensions using seismic and tracer data: The Kesterson aquifer. Water Resources Research 32 (9), 2659-2670.

Hyndman, D.W., Harris, J.M., Gorelick, S.M., 1994. Coupled seismic and tracer test inversion for aquifer property characterization. Water Resources Research 30 (7), 1965-1977.

Journel, A.G., Huijbregts, C.J., 1989. Mining Geostatistics. Academic Press, London.

Jussel, P., Stauffer, F., Dracos, T., 1994. Transport modeling in heterogeneous aquifers: 1. Statistical description and numerical generation of gravel deposits. Water Resources Research 30 (6), 1803-1817.

Kinzelbach, W., Rausch, R., 1995. Grundwassermodellierung, Eine Einführung mit Übungen. Gebrüder Bornträger, Berlin.

Kinzelbach, W., Marburger, M., Chiang, W.-H., 1992. Bestimmung von Brunneneinzugsgebieten in zwei und drei räumlichen Dimensionen. Geologisches Jahrbuch, Reihe C, Heft 61, Bundesanstalt für Geowissenschaften und Rohstoffe und Geologische Landesämter in der Bundesrepublick Deutschland, Hannover.

Klingbeil, R., Kleineidam, S., Asprion, U., Aigner, T., Teutsch, G., 1999. Relating lithofacies to hydrofacies: outcrop-based hydrogeological characterisation of Quaternary gravel deposits. Sedimentary Geology 129, 299-310.

Koltermann, C.E., Gorelick, S.M., 1996. Heterogeneity in sediment deposits: A review of structure-imitating, process-imitating, and descriptive approaches. Water Resources Research 32, 2617-2658.

Kowalsky, M.B., Dietrich, P., Teutsch, G., Rubin, Y., 2001. Forward modeling of ground-penetrating radar data using digitized outcrop images and multiple scenarios of water saturation. Water Resources Research, 37 (6), 1615-1625.

Lerner, D.N., 1992. Well catchments and time-of-travel zones in aquifers with recharge. Water Resources Research 28 (10), 2621-2628.

Poeter, E.P., McKenna, S.A., 1995. Reducing uncertainty associated with ground-water flow and transport predictions. Ground Water 33 (6), 899-904.

Rauber, M., Stauffer, F., Huggenberger, P., Dracos, T., 1998. A numerical three-dimensional conditioned/unconditioned stochastic facies type model applied to a remediation well system. Water Resources Research 34 (9), 2225-2233.

Reichert, P., Pahl, C., 1999. Wie können Modelle zu Umweltentscheiden beitragen? EAWAG news 47d, 3-5.

Rubin, Y., Mavko, G., Harris, J., 1992. Mapping permeability in heterogeneous aquifers using hydrologic and seismic data. Water Resources Research 28 (7), 1809-1816.

Siegenthaler, C., Huggenberger, P., 1993. Pleistocene Rhine gravel: deposits of a braided river system with dominant pool preservation. Best, J.L., Bristow, C.S. (Eds.). Braided Rivers. Geological Society Special Publication 75, 147-162.

Van Dam, R., Schlager, W., 2000. Identifying causes of ground-penetrating radar reflections using time-domain reflectometry and sedimentological analyses. Sedimentology 47, 435-449.

Webb, E.K., Davis, J.M., 1998. Simulation of the spatial heterogeneity of geologic properties: An overview. Fraser, G.S., Davis, J.M. (Eds.). Hydrogeologic models of sedimentary aquifers. SEPM, Concepts in Hydrogeology and Environmental Geology 1, 1-24.

Weissmann, G.S., Carle, S.F., Fogg, G.E., 1999. Three-dimensional hydrofacies modeling based on soil surveys and transition probability geostatistics. Water Resources Research, 35 (6), 1761-1770.

Wingle, W.L., Poeter, E.P., McKenna, S.A., 1997. UNCERT: A Geostatistical Uncertainty Analysis Package Applied to Groundwater Flow and Contaminant Transport Modeling. Colorado School of Mines, Golden, Colorado.

Interpretation of drill-core and georadar data of coarse gravel deposits

Christian Regli [a], Peter Huggenberger [a], Martin Rauber [b]

[a] Department of Earth Sciences, Applied and Environmental Geology, University of Basel,
Bernoullistr. 16, 4056 Basel, Switzerland

[b] Rauber Consulting, Technoparkstr. 1, 8005 Zürich, Switzerland

Interpretation of drill-core and georadar data
of coarse gravel deposits

Christian Regli [a], Peter Huggenberger [a], Martin Rauber [b]

[a] *Department of Earth Sciences, Applied and Environmental Geology, University of Basel, Bernoullistr. 16, 4056 Basel, Switzerland*
[b] *Rauber Consulting, Technoparkstr. 1, 8005 Zürich, Switzerland*

Abstract

Pollution in the shallow subsurface has led to an increasing need of understanding how to quantitatively characterize both the heterogeneity of gravel aquifers and the influence of heterogeneity on groundwater flow and solute transport. Models play an important role in decision-making processes, especially in the context of better characterizing and in forecasting the behavior of a given geological system. The objective of the present paper is the derivation of a lithofacies-based interpretation of outcrop, drill-core, and ground-penetrating radar (GPR or georadar) data of different quality. The presented method allows a probability estimation of drill-core layer descriptions and radarfacies patterns representing defined sedimentary structure types. The method includes a determination of initial structure-type probabilities for grain-size categories and combinations thereof described in drill-core layer descriptions as well as a subsequent differentiation of these structure-type probabilities in an iterative process considering additional information like main constituent, quantity, fraction, and sorting of single grain-size categories, color, chemical precipitation, layer thickness, and adjacent layer. The radarfacies types are calibrated with drill cores located in the vicinity of georadar sections. The calibration process consists of the assignment of the calculated structure-type probabilities from the drill-core layer descriptions to the corresponding radarfacies types considering the proportion in thickness between drill-core layers and georadar structures. The structure-type probabilities can be given for points along boreholes and grid nodes with arbitrary mesh sizes along georadar sections. The method is applied to field examples from the Rhine/Wiese aquifer near Basel, Switzerland. The resulting structure-type probabilities can be used for conditioning stochastic simulations of geological models. However, the conditioned stochastic simulation of the Rhine/Wiese aquifer is the topic of another paper. The results show the importance of a detailed sedimentological analysis of outcrops and drill-cores as well as its significance on the distinction of sedimentary structure types.

Keywords: drill-core analysis, ground-penetrating radar, aquifer stratigraphy, site characterization, heterogeneity, geostatistics

1. Introduction

The coarse fluvial deposits of the alpine forelands, e.g., river valleys in Switzerland, France, and Austria, are important groundwater aquifers for municipal water supplies. Natural hetero-

geneities of these sediments, including sedimentary structures and textures, result in heterogeneities of the hydraulic, chemical, and biological aquifer properties which control the behavior of groundwater flow and solute transport. For many hydrogeological problems, e.g., definition of well capture zones, river-groundwater interaction, and contaminant transport behavior, the knowledge of heterogeneity is crucial (Rauber et al., 1998). Information on heterogeneity can be of quite different character and quality: (1) outcrop information (e.g., sedimentological classification) is usually sparse, (2) borehole information (e.g., drill-core description, pumping test) provides only a limited view of subsurface properties, and (3) geophysical information (e.g., seismic, ground-penetrating radar (GPR or georadar)), although often powerful for delineating sedimentary structures, only provides an indication to possible lithofacies.

The problem of adequately modeling subsurface uncertainties becomes more difficult with increasing heterogeneity. The uncertainty depends both on the quantity and on the quality of available data. The geostatistical technique used to model uncertainty in a specific context should be chosen considering the features of the phenomenon under consideration, the knowledge of the subsurface, and the causes of uncertainty (Ayyub and Gupta, 1997).

Several recent studies have investigated the use of geophysical, borehole, and outcrop data to characterize subsurface sedimentary and hydraulic properties (e.g., Beres and Haeni, 1991; Rubin et al., 1992; Copty et al., 1993; Huggenberger, 1993; Hyndman et al., 1994; Beres et al., 1995; Copty and Rubin, 1995; Hubbard et al., 1997; Langsholt et al., 1998; Hubbard et al., 1999; Beres et al., 1999; Asprion and Aigner, 1999; Miller et al., 2000), and to use these data to support groundwater flow and solute transport modeling (e.g., Poeter and McKenna, 1995; McKenna and Poeter, 1995; Hyndman and Gorelick, 1996; Rauber et al., 1998). These studies suggest that high-resolution geophysical data can be helpful delineating aquifer structures as well as estimating hydraulic aquifer properties. As these data typically provide two-dimensional information about the subsurface, conditioned stochastic simulation techniques are commonly used to generate probability distributions of the aquifer properties at locations where no data exist (Deutsch and Journel, 1998; Journel and Huijbregts, 1989; and others). Kunstmann and Kinzelbach (1998) studied several methods to quantify model output uncertainty under given input parameter uncertainty. They considered the stochastic simulation to be the method of choice for almost any quantification of model uncertainties.

The estimation of parameter values at locations without data is very important. The determination of the conditioning data is very important as well, because the conditioning of stochastic simulations strongly influences the simulation results, e.g., groundwater flow pattern and transport behavior (Schafmeister, 1997). In most cases the conditioning is based on facies analysis. A facies is considered a homogeneous, isotropic or anisotropic unit which is hydrogeologically relevant for groundwater flow and solute transport (Anderson, 1989). Depending on the data acquisition method, both lithofacies (e.g., from outcrop and/or drill-core descriptions) and radarfacies, with corresponding hydraulic properties, can be distinguished.

On the theoretical and computational side, geostatistical techniques and visualisation tools are available for the representation of heterogeneity in models. However, techniques, which allow the integration of data of different quality to condition geological or groundwater flow and transport models are still an area of major research. At the outcrop scale, coarse-grained fluvial deposits have been successfully described in terms of architectural element analysis (Siegenthaler and Huggenberger, 1993) and hydraulic properties (Jussel et al., 1994). A principal finding of these authors was that the coarse-grained fluvial deposits are composed of a limited number of sedimentary structure types, each with characteristic hydraulic properties, e.g., porosity and hydraulic conductivity. Recent research also demonstrates the possibility of fully three-dimensional facies analysis using georadar and outcrop analysis (e.g. Beres et al., 1999). Particular time 'slices' or subhorizontal image surfaces are used as a tool for determi-
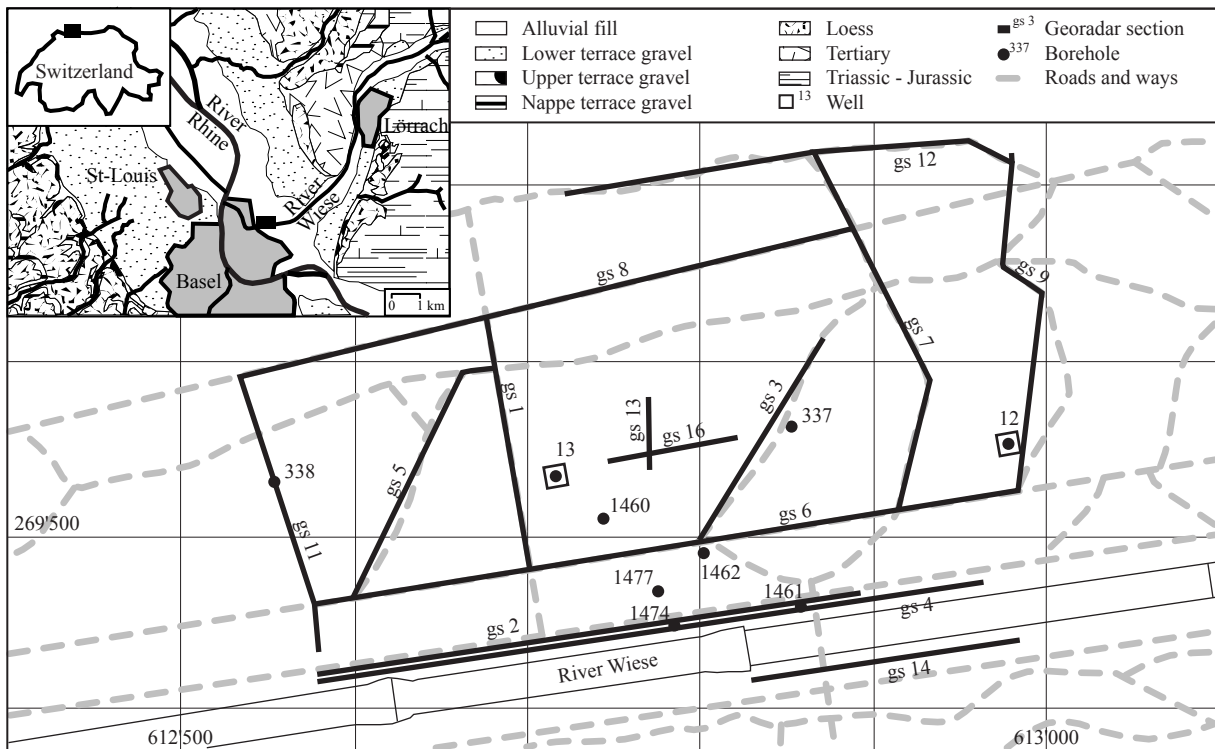
Fig. 1. Geological map of the region of Basel in Northwestern Switzerland and map of the study site showing locations of boreholes and traces of georadar sections.

ning the strikes of inclined layers and for depicting the connectivity and spatial relations of the main sedimentary structure types. In most cases, however, three-dimensional geophysical surveys are not possible because of trees, buildings, and installations. Similarly, outcrop analysis is often restricted to a small number of exposures or excavations. In most practical problems, drilling is one of the most common used methods to determine aquifer thickness, groundwater table, and bedrock surface. However, only limited information on heterogeneity is extracted. Possible causes are: (1) no information on geometry and interconnection of sedimentary structures, (2) main lithofacies responsible for fast water conducts such as open-framework gravel are overlooked, (3) existence of drill-core descriptions of different geologists which cannot easily be integrated into a coherent deterministic concept.

For example, about 3'000 drill-core descriptions from Basel are stored in a data base (Noack, 1993; Noack, 1997). Starting at the beginning of the 20th century, these descriptions often differ from the standard classification systems (e.g., unified soil classification system (USCS)) and important sedimentary structure types, such as the highly permeable open-framework gravel, are generally overlooked due to smearing with overlying and underlying layers during the drilling process. The occurrence and the size of the open-framework gravel, however, determine the variance of the hydraulic conductivity and the correlation length in coarse gravel deposits (e.g., Jussel et al., 1994). For these two reasons, there generally is an important gap between outcrop and drill-core descriptions. The strong association of open-framework gravel to the related structure type open-framework/bimodal gravel couplets (Jussel et al., 1994) has led to the idea that drill-core descriptions might also be used to identify sedimentary structure types from older boreholes.

The objective of the present paper is the derivation of a lithofacies-based interpretation of outcrop, drill-core, and ground-penetrating radar data which represent data of different quality. The presented method allows a probability estimation of drill-core layer descriptions and radar-facies types representing defined sedimentary structure types. The structure-type probabilities
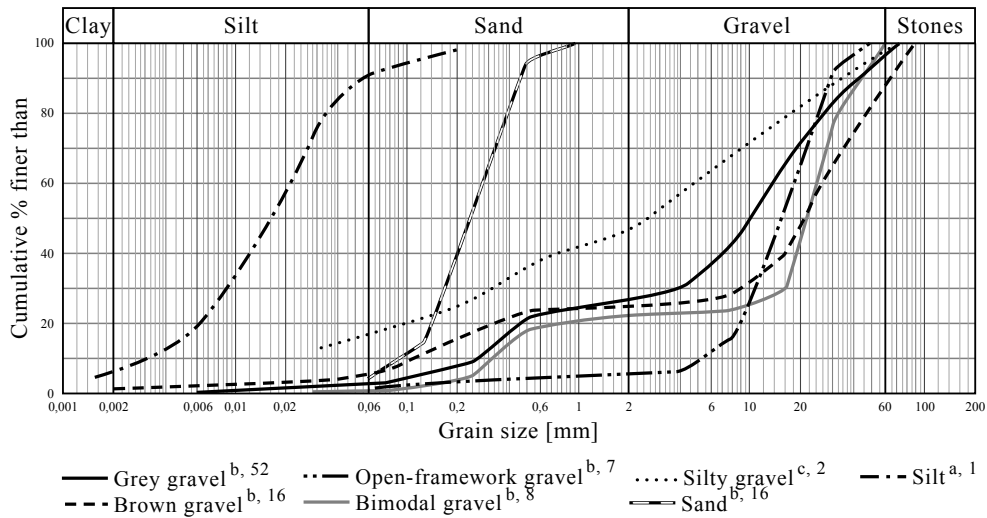
Fig. 2. Typical grain-size distribution [cumulative wt%] of the sedimentary texture types from [a] Huggenberger et al. (1988), [b] Jussel et al. (1994), and [c] Rohrmeier (2000); [52] number of samples.

can be given for points along boreholes and grid nodes with arbitrary mesh sizes along georadar sections. The method is applied on field examples from the Rhine/Wiese aquifer near Basel. The resulting structure-type probabilities can be used for conditioning stochastic simulations of geological models. However, the conditioned stochastic simulation of the Rhine/Wiese aquifer is the topic of another paper.

2. Results of field investigations

2.1. Sedimentological and hydrological investigations

Heterogeneities of natural gravel deposits in Northeastern Switzerland were investigated in unweathered outcrops by Siegenthaler and Huggenberger (1993) and Jussel et al. (1994). Siegenthaler and Huggenberger (1993) proposed a model of the Pleistocene Rhine gravel aquifer using a limited number of sedimentary structure types based on fluvio-dynamic interpretations of processes in a braided river system. Jussel et al. (1994) examined the sedimentary structure types with a focus on hydraulic parameters.

Outcrop and drill-core analyses show that the sedimentary structure types, which are geometric features detectable in the aquifer, are composed of one or two sedimentary texture types. The classification of the sedimentary texture types includes data on grain-size distribution, color, and sorting. In literature, the term 'lithofacies' (e.g. Miall, 1996, p. 79, table 4.1) is probably nearest to 'sedimentary texture types'. The sedimentary structure types are defined based on bounding surfaces and fill. The fill may be characterized by the sedimentary texture types and the layering. In the literature, the term 'architectural element' (e.g. Miall, 1996, p. 93, table 4.3) is probably nearest to 'sedimentary structure types'. However, the significance of lithofacies and architectural element in literature often differs from author to author.

In general, the sedimentary texture and structure types are easily recognizable in outcrops due to color variations caused by the presence or absence of silt and clay in the gravel, which also results in different water contents. Therefore, color attributes are used for texture-type names such as 'gray gravel' or 'brown gravel'. The structure-type names are derived from these texture-type names. Consequently, the sedimentary structure types comprise gray gravel (GG), brown gravel (BG), alternating gray and brown gravel layers (GG/BG), open-framework gravel

(OW), open-framework/bimodal gravel couplets (OW/BM), sand lenses (SA), and silt lenses (SI).

Fig. 1 shows the geological map of the region of Basel in Northwestern Switzerland and the study site. In the ancient confluence of the main river Rhine and its tributary Wiese the physical processes were expected to be the same as upstream. Therefore, the same sedimentary texture and structure types as described by Siegenthaler and Huggenberger (1993), Jussel et al. (1994), and Rauber et al. (1998) are expected and were actually found. However, the sediments are from different source areas with distinct geological units, which allow a clear assignment of the sediments to the source areas. Due to changing dynamics, caused by the significant widening of the Rhine Valley at Basel, the character of the fluvial system also include elements, which are typical for the braided-meandering transition (e.g., point-bar deposits). For this reason, the existing lithofacies scheme (Siegenthaler and Huggenberger, 1993) has to be expanded with the new texture type 'silty gravel' (SG) which forms sedimentary structures as well. The distinction of this texture and structure type is based on outcrop and georadar investigations, drill-core descriptions, and grain-size analyses. The occurrence of silty gravel may either be caused by the braided-meandering transition of the fluvial system character at Basel or by the sedimentation of fine material in the backwater of the tributary Wiese, which results from the high discharge in the main river Rhine.

The silty gravel is a very poorly sorted gravel with a sand fraction of nearly 30% and a silt and clay fraction of nearly 20%. The color of the gravel is brownish (Rohrmeier, 2000). The grain-size distribution of the various recurring texture types, which are arranged from the different works to see the heterogeneity of these deposits, are represented in Fig. 2. The variability of the hydraulic aquifer properties of the sedimentary structure types is outlined in Jussel et al. (1994). The compiled data revealed large differences in hydraulic conductivity between the sedimentary structure types (Rauber et al., 1998, p. 2227, table 1).

2.2. Geophysical investigations

Sedimentological information from outcrops is usually sparse, and borehole information only provides a limited view of subsurface properties. The georadar technique is a non-destructive geophysical method capable of resolving heterogeneities at the scale of observable sedimentary structures. It allows one to identify the spatial arrangement (e.g., location, geometry, and interconnectness) of erosion surfaces separating sedimentological units. The georadar technique turned out to be a powerful tool for mapping sedimentary structures in coarse gravel deposits of the shallow subsurface (up to 20 m).

For the georadar survey in Northwestern Switzerland near Basel (Fig. 1), a pulseEKKO IV georadar system with a 1'000 V transmitter was used (Sensors & Software Inc., 1993). The transmitting and receiving antennae were separated by 2 m and the recording step size was 0.25 m. Tests showed that 50 MHz antennae allow a resolution of the aquiclude surface, the main erosion boundaries and the large sedimentary structures to a depth of the aquiclude at approximately 13-18 m. The excellent penetration depth of electromagnetic waves in these Rhine/Wiese gravel deposits may be explained by the low electrical conductivities of the pore- and groundwater (100-150 µS/cm).
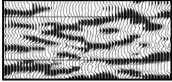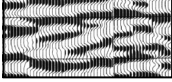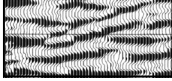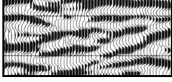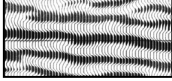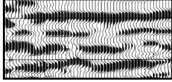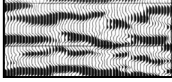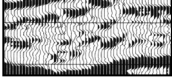
The vertical resolution depends on the radar-wave frequency of the applied georadar system and is equal to a quarter of the wavelength (Jol and Smith, 1991) and is of the order of 0.5 m. According to the theory, reflections of low conductive geological materials occur when electromagnetic waves meet boundaries between lithological units of contrasting dielectric constants. Such reflections can occur either at the change of water content within the same texture

type, or at the boundary between two distinct structure types. Due to the low and constant electrical conductivities of the gravel deposits, the influence of electrical conductivity may be neglected for this particular aquifer. Reflection coefficients for the main lithofacies transitions of gravel deposits have been derived for saturated and non-saturated conditions (Huggenberger, 1993). Compared with the results from the 100 and 200 MHz antennae (Huggenberger, 1993; Beres et al., 1999), the erosion surfaces, which separate the main sedimentary structures, and some of the larger internal structures are expected to be resolved. Due to the larger wavelengths of the 50 MHz antennae, only few transitions of alternating sequences of open-framework and bimodal gravels may be portrayed on the georadar sections. The presented example (see section 3.2., Fig. 6), however, illustrates that even the main sedimentary structures may be delineated. Furthermore, it seems that in this particular case the georadar response of small features (e.g., fine scale bedding), the clutter effects (Annan and Chua, 1988), are minimized. As a consequence, the 50 MHz antennae allow to delineate the significant sedimentological features of coarse, electrically low conductive sediments at the scale of the required model resolution.

Radarfacies type	Reflection pattern	Interpretation
Trough shaped (ts)		
Oblique parallel (op)		
Oblique tangential (ot)		
Oblique sigmoidal (os)		
Parallel continous (pc)		
Parallel discontinous (pd)		
Subparallel oblique (so)		
Reflection poor (rp)		

Fig. 3. *Two-dimensional radarfacies types of coarse gravel deposits as seen in vertical sections, primarily valid for 50 MHz antennae, slightly modified from Beres et al. (1999); reflection patterns (middle column), interpreted horizons (left column).*

In this paper, some examples of two-dimensional georadar surveys conducted in the floodplain of the ancient confluence of the main river Rhine and its tributary Wiese near Basel are reported. The georadar grid was oriented approximately parallel and perpendicular to the ancient main and tributary flow directions. After acquisition, the georadar data were time-zero adjusted. The pairs of linear arrivals in expanding spread soundings (or common midpoint (CMP); Beres et al., 1999), that intersect at zero traveltime and at zero offset, represent the intersection of the air- and the groundwave. This point is used to define the reference zeropoint for the different georadar profiles. Further processing steps included trace editing, data merging, bandpass filtering, and automatic gain control with a window of 0 ns to 500 ns.

Huggenberger (1993), and Beres et al. (1995, 1999) investigated heterogeneities of Rhine gravel deposits in Northeastern Switzerland. Different radarfacies types have been distinguished based on established concepts of seismic stratigraphy and radarfacies analysis (e.g., Hardage, 1987; Beres and Haeni, 1991). The radarfacies types observed in vertical sections are trough shaped (ts), oblique parallel (op), oblique tangential (ot), parallel continuous (pc), parallel discontinuous (pd), and reflection poor (rp). The same radarfacies types could be recognized in the Rhine/Wiese gravel deposits near Basel in Northwestern Switzerland. At this location, two additional radarfacies types, 'oblique sigmoidal' (os) and 'subparallel oblique' (so), could be distinguished. The distinction of these radarfacies types is based on reflection pattern analysis and the applied georadar system configuration (Rohrmeier, 2000).

The radarfacies types are already described in earlier works (Huggenberger, 1993; Beres et al., 1999). The oblique sigmoidal (os) radarfacies type, which was found in the Rhine/Wiese gravel deposits near Basel, represents sequences that are inclined towards their lower and upper boundary with tangential bottom and top reflections. In the subparallel oblique (so) radarfacies type, which was also found in the Rhine/Wiese gravel deposits, one observes sequences that are subhorizontal, mostly discontinuous and sometimes distinctly inclined layered. The different radarfacies types representing the heterogeneity of these deposits are represented in Fig. 3. They are primarily valid for 50 MHz antennae.

3. Interpretation of data

Outcrop, borehole, and geophysical information represent data of different quality and scale. Due to the easy access to undisturbed sedimentary structures and textures, outcrop and laboratory investigations of representative samples provide the most reliable, hard data. However, only few outcrops are available for study.

Drilling destroys the microfabric and smears the boundaries of adjacent layers. A drill-core layer description is typically not very detailed and does not clearly indicate an explicit texture or structure type, even if a grain-size analysis is available (e.g., overlapping ranges of grain-size distribution of different sedimentary texture types; Jussel, 1992, p. 40, figs. 2.5a-d). Furthermore, the individual drill-core descriptions vary considerably between geotechnical and sedimentological aspects. Pumping tests provide conductivity data which represent mean values averaged over relatively large volumes. They do not provide definite information on geometry and dimensions of subsurface structures. Therefore, drill-core and pumping-test data are considered soft data.

With the non-destructive georadar technique, sedimentary structures can be delineated. The relationship between reflection patterns and sedimentary structure types is often ambiguous. The reflection patterns only provide an indication to possible sedimentary structure types. Since georadar data are more uncertain than drill-core data, they are subsequently considered soft data.

The following interpretation of data of different quality and scale is qualitatively illustrated in Fig. 4. For this interpretation, three steps are necessary. In a first step, the sedimentary structure types were classified from outcrop data (Siegenthaler and Huggenberger, 1993; Jussel et al., 1994; Rohrmeier, 2000; Fig. 4a). In a second step, for drill-core data, the probability of correct classification is estimated based on layer descriptions (see section 3.1.; Fig. 4b), and in a last step, drill-core layers and corresponding radarfacies types are related (see section 3.2.; Fig. 4c).

3.1. Interpretation of drill-core data

Sedimentological drill-core descriptions primarily include information on grain size, but also 'additional information' such as main constituent, quantity, fraction, and sorting of single grain-size categories, color, chemical precipitation, layer thickness, and adjacent layer. Based on this additional information, the probabilities of representing specific sedimentary structure types, which are defined by outcrop data (Siegenthaler and Huggenberger, 1993; Jussel et al., 1994; Rohrmeier, 2000) can be differentiated. If further additional information is available, the probability that a layer description represents a specific sedimentary structure type (structure-

a   Outcrop data

Classification of sedimentary structure types

b   Drill-core data

Probability estimation for drill-core layer descriptions

Borehole 1460

c   Georadar data

Relation between borehole layers and radarfacies types
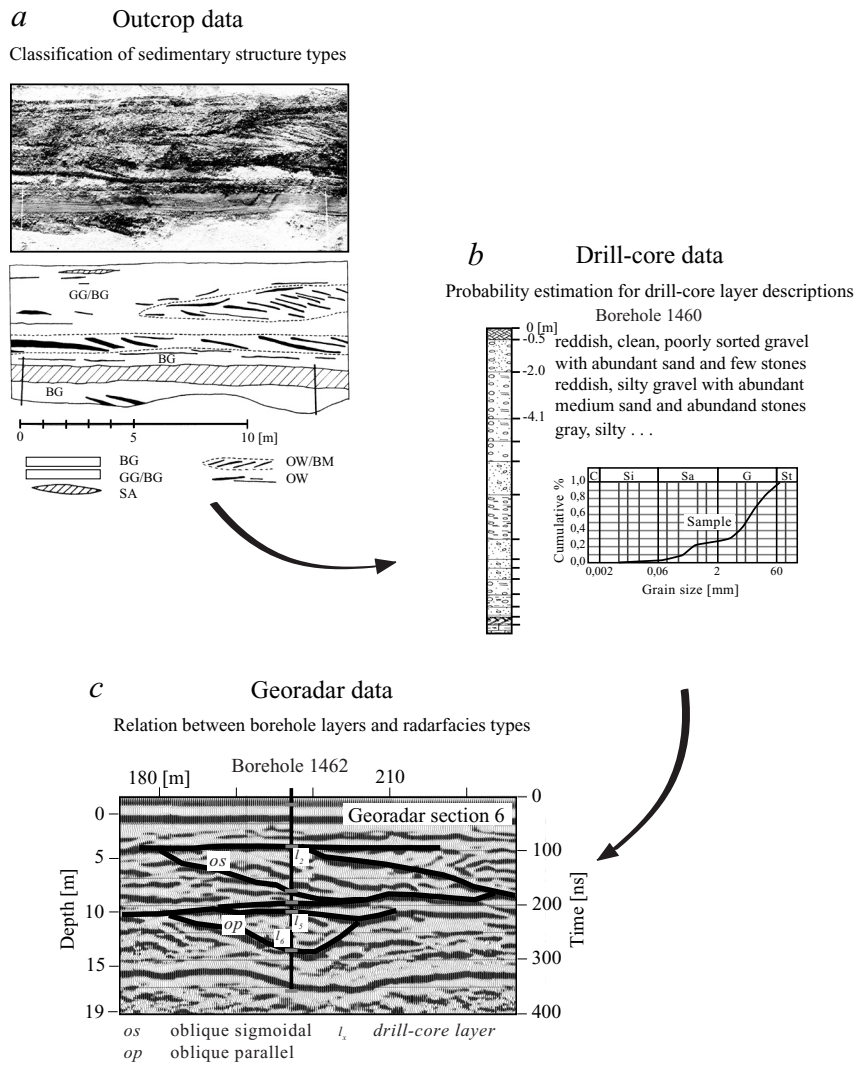
Fig. 4. *Interpretation of data of different quality and scale: (a) classification of the sedimentary structure types from outcrop data (Siegenthaler and Huggenberger, 1993; Jussel et al., 1994; Rohrmeier, 2000), (b) probability estimation of correct classification based on drill-core layer description, and (c) relation between borehole layers and corresponding radarfacies types.*

type probability) increases. The estimation of the structure-type probabilities for a drill-core layer description is obtained in two steps:

In a first step, grain-size categories, mentioned in drill-core layer descriptions, are used for an initial probability estimation. This is done by a (1) determination of average grain-size distribution for the structure types which are then used for an (2) estimation of 'initial structure-type probabilities': (1) Most sedimentary structure types are composed of one single texture type with the exception of open-framework/bimodal gravel couplets and alternating gray and brown gravel layers, which can be inclined or layered horizontally. Bimodal gravel itself does not represent a structure type. Based on the grain-size distribution of the different texture types (Fig. 2), grain-size distribution for the structure types are derived (Table 1). This is done as follows: for the structure types composed of one single texture type, the grain-size distribution is identical. For the structure types composed of two texture types, the grain-size distribution was determined by the arithmetic mean of the contents of the grain-size categories. (2) Based on the values in Table 1, the initial structure-type probabilities for grain-size categories and combinations thereof are derived (Table 2). This is done as follows: the structure-type probabilities for the single grain-size categories are determined by the normalization of the grain-size distribu-

Table 1. *Typical grain-size distribution [cumulative wt%] of the sedimentary structure types: OW: open-framework gravel, OW/BM: open-framework/bimodal gravel couplets, GG: gray gravel, BG: brown gravel, GG/BG-horizontal: alternating gray and brown gravel, horizontally layered, GG/BG-inclined: alternating gray and brown gravel, inclined, SG: silty gravel, SA: sand, SI: silt.*

Sedimentary structure type Grain-size category	OW	OW/BM	GG	BG	GG/BG horizontal	GG/BG inclined	SG	SA	SI
Silt (and clay)	1	1	3	6	5	5	17	4	91
Sand	6	15	27	25	27	27	48	100	100
Gravel	100	100	97	88	93	93	98		
Stones			100	100	100	100	100		

tion values over all structure types. The structure-type probabilities for combinations of grain-size categories are determined by the arithmetic mean of the structure-type probabilities of the single grain-size categories.

In a second step, additional information from the drill-core layer descriptions, listed in Table 3, is used for the further differentiation of the sedimentary structure-type probabilities. Each kind of additional information is typical for a subset of sedimentary structure types and is given a relative weighting factor $w_{relative}$ =]1;0.1[. The relative weighting factor is estimated based on the significance of the additional information for determining a specific structure type, and on the relative importance of the structure type for groundwater flow and transport. A relative weighting factor of 1 is given for a strong association with a given kind of additional information, a relative weighting factor of 0.1 is given for a weak one. The differentiation of the sedimentary structure-type probabilities follows an iterative process, where each kind of additional information is considered using the following equation:

$$P_{st,l,i} = P_{st,l,i-1} W_{st,l,i,ai\pm} \tag{1}$$

Table 2. *Initial sedimentary structure-type probabilities [%] for grain-size categories and combinations thereof grouped according to the number of constituents in a drill-core layer description.*

Sedimentary structure type Grain-size category	OW	OW/BM	GG	BG	GG/BG horizontal	GG/BG inclined	SG	SA	SI
Silt	1	1	2	5	3	3	13	3	69
Sand	2	6	10	8	9	9	13	39	4
Gravel	19	17	15	13	13	13	10	0	0
Stones	0	0	9	37	23	23	8	0	0
Silt, sand	1	3	6	6	6	6	13	23	36
Silt, gravel	10	9	8	9	8	8	11	2	35
Silt, stones	0	0	6	21	13	13	10	2	35
Sand, gravel	11	12	12	10	11	11	11	20	2
Sand, stones	1	3	10	22	16	16	10	20	2
Gravel, stones	9	9	12	25	18	18	9	0	0
Silt, sand, gravel	7	8	9	8	9	9	12	14	24
Silt, gravel, stones	7	6	9	18	13	13	10	1	23
Sand, gravel, stones	7	8	12	19	15	15	10	13	1
Silt, sand, stones	1	2	7	16	12	12	11	15	24
Silt, sand, gravel, stones	5	6	9	16	12	12	11	11	18

Table 3. *Additional information in drill-core layer descriptions and relative weighting factor $w_{relative}$ [ ] with indication of the sedimentary structure type, for which the additional information is typical. The color separation above and below -5.0 m arises from the different geology of the source areas: above -5.0 m the deposits consists exclusively of Wiese gravels, below -5.0 m the deposits consists of Rhine and Wiese gravels.*

Additional information (Iteration number)	Typical sedimentary structure types	Relative weighting factor $(w_{relative})$
(1) Main constituent		1
Silt	SI	
Sand	SA	
Gravel	OW, OW/BM, GG, BG, GG/BG-h / -i, SG	
(3) Quantity of (clay)-silt-(sand)		0.7
Clean	OW, OW/BM, GG, GG/BG-h / -i, SA	
Few silt / silty	BG, GG/BG-h, GG/BG-i, SA	
Few silt and sand	OW, OW/BM	
Much silt / clayish	SG	
(4) Quantity of sand		0.7
Few sand, 3-15%	OW/BM, BG, SG, SI	
Abundant sand, 16-30%	GG, BG, GG/BG-h / -i, SG	
Much sand, 31-49%	GG, SG, SA	
(10) Quantity of gravel		0.25
Few gravel, 3-15%	SA, SI	
Abundant gravel, 16-30%	SA, SI	
Much gravel, 31-49%	SA, SI	
(11) Quantity of stones		0.25
Few stones	OW/BM, GG, BG, GG/BG-h / -i, SG, SA	
Abundant stones	GG, BG, GG/BG-h / -i	
Much stones	BG	
(5) Fraction of sand		0.55
Fine sand	BG, GG/BG-h / -i, SA, SI	
Medium sand	OW/BM, GG, BG, GG/BG-h / -i, SG, SA	
Coarse sand	OW/BM, GG, SA	
(8) Fraction of gravel		0.4
Fine gravel	GG, SG, SA, SI	
Medium gravel	OW, OW/BM, GG, GG/BG-h / -i, SA	
Coarse gravel	OW/BM, BG, GG/BG-h / -i	
(2) Open-framework gravel		0.85
Open-framework gravel	OW, OW/BM	
Fe- / Mg-precipitation	OW, OW/BM	
(6) Sorting of sand		0.55
Well sorted	OW/BM, GG, SA	
Poorly sorted	OW, BG, GG/BG-h / -i, SG, SA	
(9) Sorting of gravel		0.4
Well sorted	OW, OW/BM, SA	
Poorly sorted	GG, BG, GG/BG-h / -i, SG, SA	
(7) Color (above –5.0 m)		0.55
Gray	OW, OW/BM, GG	
Brown	GG, BG, SG, SA, SI	
Gray-brown	GG, BG, GG/BG-h / -i, SG, SA, SI	
(7) Color (below –5.0 m)		0.55
Gray	OW, OW/BM, GG, SG, SA, SI	
Brown	BG	
Gray-brown	GG/BG-h / -i, SA	
(12) Thickness of layer		0.25
Thin, < 0.25 m	OW	
Normal, 0.25 - 2.5 m	OW/BM, GG, BG, GG/BG-h / -i, SG, SA, SI	
Thick, > 2.5 m	BG	

Table 3. (continued)

Additional information (Iteration number)	Typical sedimentary structure types	Relative weighting factor $(w_{relative})$
(13) Adjacent layer		0.1
SA	SI	
OW, OW/BM, GG	BG, GG/BG-h / -i, SG	
BG, GG/BG-h / -i, SI, SG	OW, OW/BM, GG, SA	

where $P_{st,l,i}$ are the probabilities of the sedimentary structure types ($st = 1,...,m$) for a drill-core layer description ($l = 1,...,o$) after an iteration ($i = 1,...,p$). The probabilities of the structure types of the preceding iteration $P_{st,l,i-1}$, for which the additional information ($ai = 1,...,n$) is typical ($ai+$), are multiplied with the weighting factor $W_{st,l,i,ai+}$. The probabilities of the structure types of the preceding iteration, for which the additional information is not typical ($ai-$), are multiplied with the weighting factor $W_{st,l,i,ai-}$. This notation is summarized in the factor $W_{st,l,i,ai\pm}$. The weighting factors are expressed as follows:

$$W_{st,l,i,ai+} = \left(\frac{100}{\sum\limits_{st=1}^{m} P_{st,l,i-1,ai+}} \right)^{w} \qquad W_{st,l,i,ai+} > 1 \qquad (2)$$

$$W_{st,l,i,ai-} = 1 + \frac{\sum\limits_{st=1}^{m} P_{st,l,i-1,ai+}\left(1 - W_{st,l,i,ai+}\right)}{\sum\limits_{st=1}^{m} P_{st,l,i-1,ai-}} \qquad W_{st,l,i,ai-} < 1 \qquad (3)$$

where $\sum_{st=1}^{m} P_{st,l,i-1,ai+}$ is the sum of the probabilities of those structure types of the preceding iteration for which the additional information presently taken into account is typical; while $\sum_{st=1}^{m} P_{st,l,i-1,ai-}$ is the sum of the probabilities of those structure types of the preceding iteration for which the additional information presently taken into account is not typical. To ensure that the sum of the structure type probabilities equals 100 after each iteration (Eq. (1)), a normalization is included in Eq. (2), while Eq. (3) is related to Eq. (2). The exponent:

$$w = w_{relative}c \qquad 0 < w < 1 \qquad (4)$$

contains both the relative weighting factor of the additional information and the factor representing the general confidence in the drill-core description $c =]0.9;0.1[$. A factor of confidence of 0.9 is given for high confidence in the drill-core description (e.g., due to detailed drill-core analysis based on the USCS and additional sedimentological details). A factor of confidence of 0.1 is given for little confidence in the drill-core description (e.g., due to bad drill-core analysis or wash drilling).

Various types of weighting factors (e.g., general form x, x^y, etc. for $W_{st,l,i,ai+}$; $W_{st,l,i,ai-}$ is related to $W_{st,l,i,ai+}$) were tested with 56 drill-core descriptions from 5 drill cores (Fig. 1, boreholes 1460, 1461, 1462, 1474, 1477) to push a strong and balanced differentiation between the structure-type probabilities during the iteration process. The weighting factors in their present forms correspond very well to this criterion (see examples in section 4.). Because $W_{st,l,i,ai+} > 1$, the
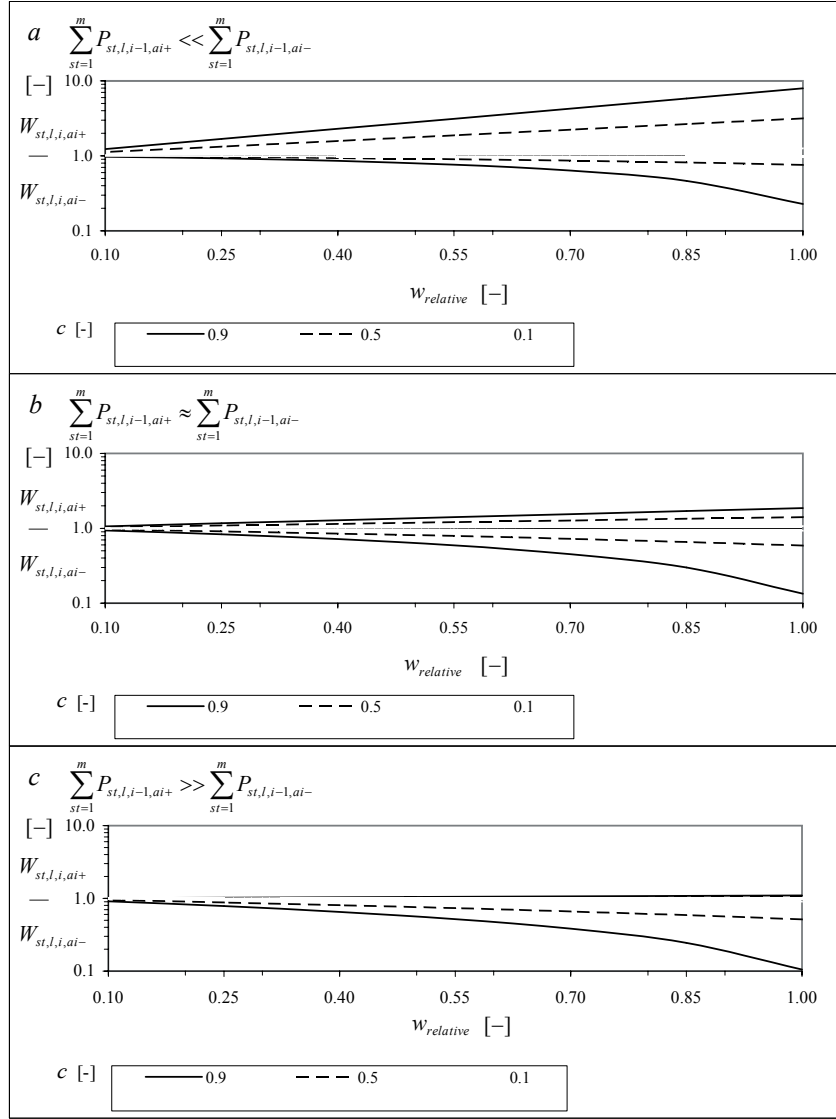
Fig. 5. *Influence of additional information from drill-core layer descriptions on the differentiation of sedimentary structure types. Relationship between the relative weighting factor of additional information $w_{relative}$ [ ], the factor taking into account the general confidence in the drill-core description c [ ], and the weighting factors $W_{st,l,i,ai+}$ [ ] and $W_{st,l,i,ai-}$ [ ], which are used for the calculation of the sedimentary structure-type probabilities in an iterative process: (a) The sum of the probabilities of those structure types of the preceding iteration for which the additional information is typical ($\sum_{st=1}^{m} P_{st,l,i-1,ai+}$) is much smaller than the sum of the probabilities of those structure types for which the additional information is not typical ($\sum_{st=1}^{m} P_{st,l,i-1,ai-}$), (b) the corresponding sums of the structure-type probabilities of the preceding iteration are approximately equal, (c) the sum of the probabilities of those structure types of the preceding iteration for which the additional information is typical is much larger than the sum of the probabilities of those structure types for which the additional information is not typical. Note the logarithmic scale of the y-axis.*

probability values of the indicated structure types are increased. Because $W_{st,l,i,ai-} > 1$, the probability values of the non-indicated structure types are decreased.

The relationship of the parameters $w_{relative}$, c, and $W_{st,l,i,ai\pm}$ is illustrated in Fig. 5. If $\sum_{st=1}^{m} P_{st,l,i-1,ai+} \ll \sum_{st=1}^{m} P_{st,l,i-1,ai-}$ (Fig. 5a), the weighting factor $W_{st,l,i,ai+}$ can become very large depending on the choice of $w_{relative}$ and c. Consequently, the probability of the indicated structure types increases significantly with additional information. At the same time, the weighting factor $W_{st,l,i,ai-}$ becomes only a little smaller than 1 and, therefore, the probability values of the not indicated structure types decrease only slightly. The opposite happens if $\sum_{st=1}^{m} P_{st,l,i-1,ai+} \gg \sum_{st=1}^{m} P_{st,l,i-1,ai-}$ (Fig. 5c). In this case, the weighting factor $W_{st,l,i,ai-}$ be-

comes very small and the probability of the structure types which are not indicated, decreases significantly with additional information. At the same time, the weighting factor $W_{st,l,i,ai+}$ becomes only a little larger than 1 and, therefore, the probability values of the indicated structure types increases only slightly. A balance occurs when $\sum_{st=1}^{m} P_{st,l,i-1,ai+} \approx \sum_{st=1}^{m} P_{st,l,i-1,ai-}$ (Fig. 5b).

## 3.2. Interpretation of georadar data

Georadar data (e.g., reflection profiles) provide two-dimensional images allowing subdivision of the subsurface into zones between prominent reflections with different reflection patterns. According to the interpretation concepts of Hardage (1987), and Beres and Haeni (1991), a radarfacies type may be defined as a mappable, three-dimensional sedimentary structure with a reflection pattern differing from those in adjacent structures. The geometry of these structures can be delineated by (1) the more continuous reflections, and (2) the types of reflection patterns within a certain visible structure. In addition, an angular unconformity between prominent reflections can be an indicator of an erosional surface which separates different sedimentary structures. Because automated selection of reflections produces poor results, manual selection is preferred.

Transformation of the reflections from traveltime to depth requires information on the velocity distribution. The velocity field of the georadar waves is derived from CMPs. Semblance velocity analysis (e.g., Beres et al., 1999) shows interval velocities between 7 and 11 cm/ns (mean at 9.5 cm/ns) for the different CMPs. Depending on the velocity field, linear or more complex velocity functions have to be considered for the transformation of the reflections from traveltime to depth. Due to the accuracy of the vertical resolution (0.5 m) and the variance of the wave velocity in comparison with the resolution of the lithological units in drill cores (0.5 m), a constant velocity is acceptable in a first step. For more complex velocity functions, calibration curves transforming individual boundaries from two-way traveltime to depths including interpolation schemes for differing neighboring velocity logs have to be considered (Copty and Rubin, 1995).

The radarfacies types (Fig. 3) are calibrated with the interpreted drill cores located in the vicinity of the georadar sections. The calibration process consists of the assignment of the calculated sedimentary structure-type probabilities from the drill-core layer descriptions (see section 3.1.) to the corresponding radarfacies types using the following equation:

$$P_{st,rf} = \sum_{l=1}^{s} P_{st,l} \frac{h_l}{h_{rf}} \tag{5}$$

where $P_{st,rf}$ is the probability of the sedimentary structure types ($st = 1,...,m$) for a reflection pattern of a defined radarfacies type ($rf = 1,...,q$). The structure-type probabilities of those drill-core layers ($l = 1,...,s$), which are part of the georadar structure, are added according to the proportion in thickness between the drill-core layer and the georadar structure (h_l/h_{rf}). If the thickness of the drill-core layer is equal to or larger than the one of the georadar structure, an adjustment of the structure-type probabilities is superfluous. Fig. 6 shows this relation for the oblique sigmoidal and the oblique parallel radarfacies types with a portion of the georadar section 6 and the borehole 1462 (Fig. 1). The differences in thickness of drill-core layers and georadar structures depend on the discrepancy of the resolution accuracy between the visual drill-core analysis (few centimeters) and the frequency-dependent georadar mapping (e.g., for 50 MHz antennae few decimeters).
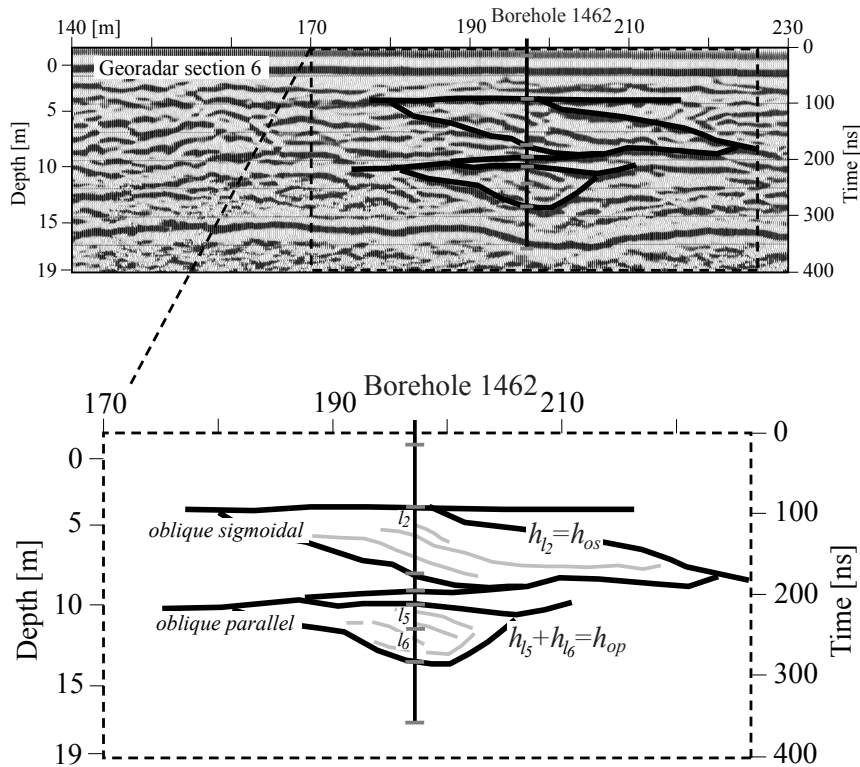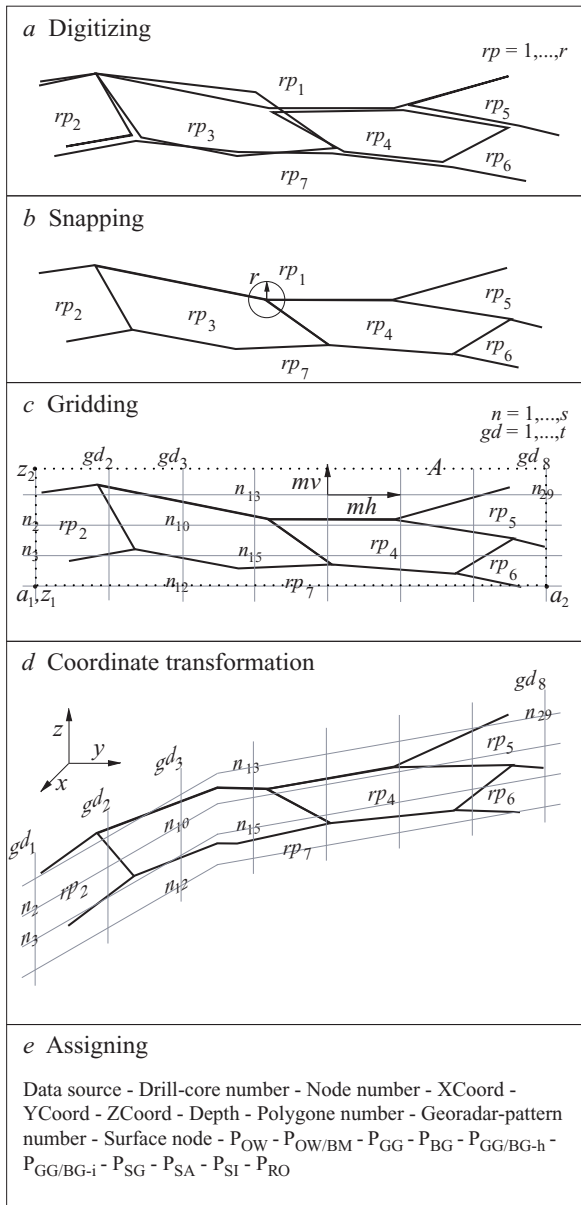
Fig. 6. *Assignment of the sedimentary structure-type probabilities from the drill-core layer descriptions to the corresponding radarfacies types according to the proportion in thickness between the drill-core layer and the georadar structure; here shown for the oblique sigmoidal and the oblique parallel radarfacies types within a portion of georadar section 6 (gs 6) and borehole 1462 located in this section.*

3.3. Transformation of reflection patterns into point data

For the application of georadar data in subsurface modeling, the two-dimensional images of georadar sections have to be transferred into point data. Data processing is necessary, once facies analysis is performed. The processing of the available data is schematically illustrated in Fig. 7 and consists of (a) digitizing reflection pattern boundaries, (b) snapping common points of neighboring polygons (georadar structures), (c) gridding polygons and generating nodes (gridpoints), (d) transforming relative into absolute coordinates, and (e) assigning data to nodes.

The digitization of the reflection patterns ($rp = 1,...,r$) is carried out with digicps-3, a plug-in code to the digitizing software CPS-3 (Radian Corporation, 1992). Usually the points of neighboring polygons are not coincident. For the successive data processing steps, supplemental program routines were written in C. The snapping tool allows for the input of the radius (r) in which polygon points shall be snapped. The gridding tool allows for the input of the area of the georadar section ($A = a_1,a_2,z_1,z_2$) to be gridded and the input of the horizontal (mh) and vertical (mv) mesh sizes between nodes. Nodes ($n = 1,...,s$) with the same a coordinates but various z coordinates are grouped into a 'georadar borehole' ($gd = 1,...,t$). The data density has to be chosen in a way that georadar structures are clearly shown. The coordinate transformation tool changes relative two-dimensional coordinates (a,z) into absolute three-dimensional coordinates (x,y,z). Finally, the assigning tool allows for the arrangement of all information such as data source (georadar or borehole), borehole number, node number, x, y and z coordinates, depth, polygon number, reflection-pattern number, detail whether surface node or not, probabilities of the sedimentary structure types OW, OW/BM, GG, BG, GG/BG-h, GG/BG-i, SG, SA, SI, and RO (rock) to the corresponding nodes. The data are in a comma-separated-value (csv) format,

a Digitizing

b Snapping

c Gridding

d Coordinate transformation

e Assigning

Data source - Drill-core number - Node number - XCoord - YCoord - ZCoord - Depth - Polygone number - Georadar-pattern number - Surface node - P_{OW} - $P_{OW/BM}$ - P_{GG} - P_{BG} - $P_{GG/BG-h}$ - $P_{GG/BG-i}$ - P_{SG} - P_{SA} - P_{SI} - P_{RO}

Fig. 7. *Transformation of reflection patterns into point data: (a) digitizing of georadar pattern boundaries; (b) snapping of common polygon points; (c) gridding of polygons and generating nodes (gridpoints); (d) transformation of relative into absolute coordinates; (e) assigning of data to nodes.*

with each node in a separate line and each information separated by a comma. Sub-surface modeling software requires spatial coordinates (x,y,z) as well as data such as sedimentary structure types, probability details, hydraulic and geotechnical parameters, etc., obtained at the nodal location.

4. Examples, results, and discussion

4.1. Differentiation of sedimentary structure types from drill-core layer descriptions

The differentiation of the sedimentary structure types by the method presented in section 3.1. is shown with two examples. Example 1: For instance, the description of layer 5 from borehole 1477 (Fig. 1) - clean, poorly sorted gravel with abundant medium and coarse sand and abundant stones, gray appearance, normal thickness, and a lower layer of rather silty gravel types - contains several kinds of additional information (Table 3), which allow the differentiation of individual structure-type probabilities. Starting with the probability values for 'sand, gravel, stones' (Table 2, line 13), the subsequent iterations (Fig. 8) lead to a variably strong differentiation of the structure-type probabilities depending on the additional information and the factor of confidence in the drill-core description. The choice of the order of the iterations strongly affects the intermediate probabilities, but has almost no effect on the final probability values, as shown with fine vertical lines.

Example 2: Various orders of additional information were studied using 56 drill-core layer descriptions from boreholes 1460, 1461, 1462, 1474, and 1477 (Fig. 1). Fig. 9 shows the final mean probabilities of the sedimentary structure types and their absolute deviations after considering all available additional information. An increase in confidence not only leads to a stronger differentiation of the final mean structure-type probabilities (y axis), but also to an increase in the maximum deviation of the final mean structure-type probabilities (x axis). In general, the maximum deviations from the final mean structure-type probabilities are smaller than 3% for structure types that are clearly distinguished from each other (Fig. 9a).

a Factor of confidence *c* = 0.9

b Factor of confidence *c* = 0.5
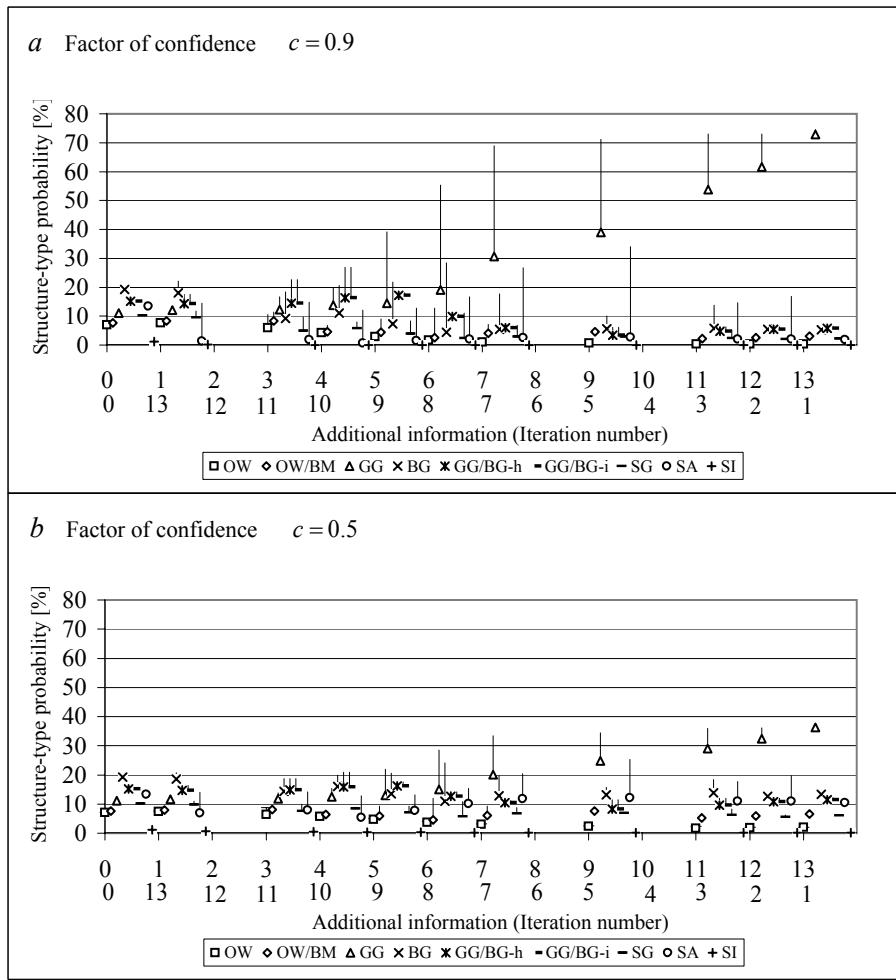
Fig. 8. *Differentiation of the sedimentary structure-type probabilities [%] based on the order of the additional information and the factor of confidence in the drill-core description; shown for layer 5 from borehole 1477. The fine vertical lines indicate the range of the structure-type probabilities depending on the order of the additional information taken into account.*

4.2. Redundancy of the interpretation method

The probability estimation of a drill-core layer description representing a specific sedi-mentary structure type, presented in section 3.1, includes two steps: (1) the initial probability estimation for grain-size categories and combinations thereof (Table 2), using grain-size distri-butions of the sedimentary structure types (Table 1), and (2) the further differentiation of the structure-type probabilities taking into account the available additional information (Table 3). Consequently, at both steps information on grain-size distribution is interpreted. The multiple interpretation of this information is reasonable in this case. First, in the case where no additional information is available (e.g., older, scarce drill-core descriptions), the initial probability values already represent a discrete differentiation of the structure types. Second, applying the USCS classification, not all additional information concerning the quantity of the different grain-size categories (Table 3), can occur together. In most practical cases, however, the descriptions are not available in such detail.
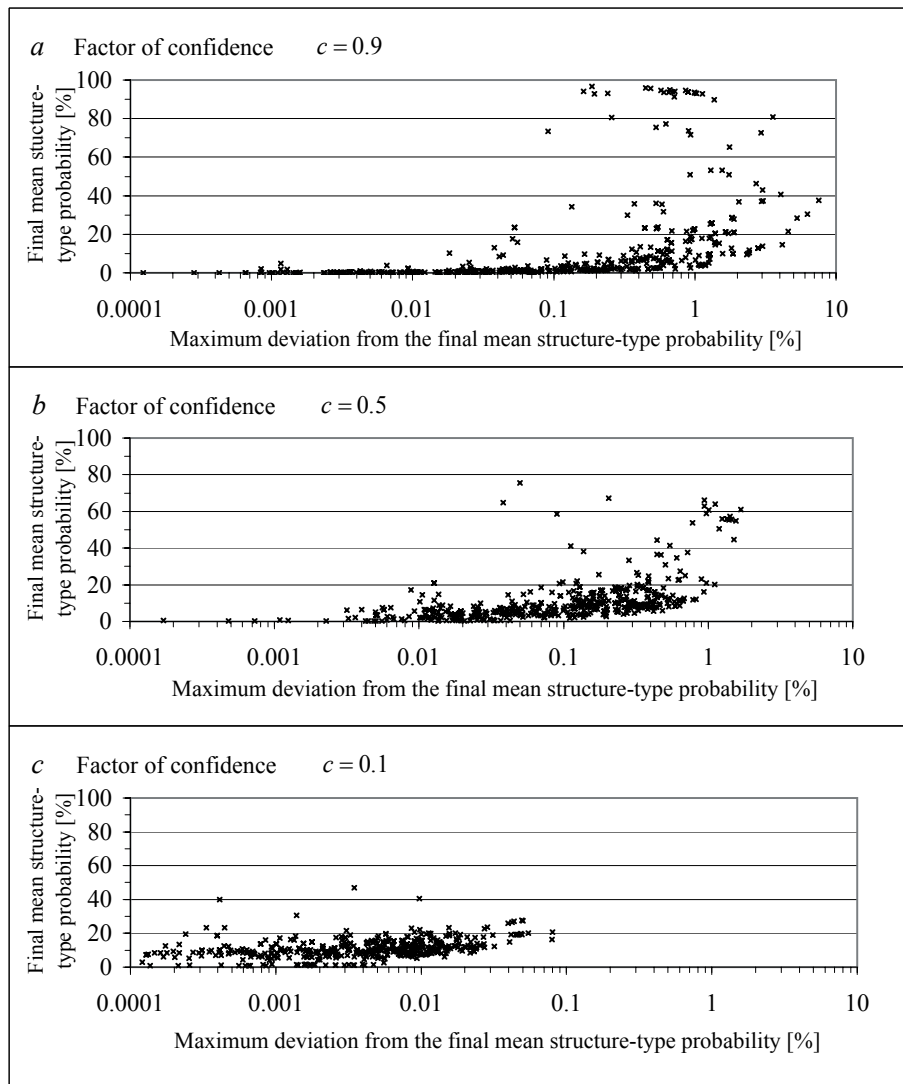
Fig. 9. *Final mean probabilities of the sedimentary structure types and their maximum deviations as a function of the order of additional information and the factor of confidence in the drill-core description. The data refer to 56 drill-core layer descriptions from boreholes 1460, 1461, 1462, 1474, and 1477.*

4.3. Probability matrix for radarfacies types

The assignment of the calculated structure-type probabilities to the radarfacies types by the method presented in section 3.2. leads to a probability matrix (Table 4). This assignment is shown in Fig. 6 for the oblique sigmoidal and the oblique parallel radarfacies types. The matrix also contains an estimate as well as calculated probability values. The estimate is based on sedimentological considerations and the comparison of georadar patterns with outcrop observations after excavation (Beres et al., 1999).

5. Conclusions

Fluvial and glaciofluvial deposits in Northwestern Switzerland are strongly heterogeneous. They consist of different, well-defined sedimentary structure types. Depending on the data acquisition method, lithofacies or radarfacies with different features were characterized. Outcrop and laboratory investigations of representative samples concerning hydraulic properties

Table 4. *Sedimentary structure-type probabilities [%] for different radarfacies types. The probability values are given for different factors of confidence in the drill-core description, and estimates based on sedimentological considerations and the comparison of georadar patterns with outcrop observations after excavation.*

Radarfacies type / Sedimentary structure type		OW	OW/BM	GG	BG	GG/BG horizontal	GG/BG inclined	SG	SA	SI
Trough shaped	Estimated	0	50	25	0	0	5	2	15	3
	$c = 0.9$	13	81	1	2	0	0	3	0	0
	$c = 0.5$	16	41	7	9	4	4	9	4	6
	$c = 0.1$	8	10	9	15	11	11	11	10	15
Oblique parallel	Estimated	0	50	20	0	0	8	7	15	0
	$c = 0.9$	8	31	20	7	9	9	15	0	1
	$c = 0.5$	9	16	14	11	11	11	15	6	7
	$c = 0.1$	6	9	11	14	12	12	12	12	12
Oblique tangential	Estimated	0	30	10	0	0	8	30	20	2
	$c = 0.9$	4	21	13	7	5	5	44	0	1
	$c = 0.5$	6	13	10	12	9	9	26	5	10
	$c = 0.1$	6	8	10	13	11	11	13	12	16
Oblique sigmoidal	Estimated	0	7	5	0	0	8	50	25	5
	$c = 0.9$	1	9	4	7	2	2	73	0	2
	$c = 0.5$	4	10	7	12	6	6	37	4	14
	$c = 0.1$	6	7	9	12	10	10	15	11	20
Parallel continous	Estimated	0	5	25	5	15	0	0	35	15
	$c = 0.9$	0	1	1	0	1	2	0	94	1
	$c = 0.5$	2	6	8	5	6	6	3	64	0
	$c = 0.1$	5	6	12	13	12	12	9	29	2
Parallel discontinous	Estimated	0	7	35	15	30	0	0	10	3
	$c = 0.9$	1	1	6	37	22	22	9	1	1
	$c = 0.5$	3	4	10	23	17	17	13	7	6
	$c = 0.1$	6	7	9	11	10	10	13	14	20
Subparallel oblique	Estimated	0	2	20	20	35	5	3	15	0
	$c = 0.9$	2	6	24	20	19	19	7	3	0
	$c = 0.5$	4	7	16	18	16	16	9	10	4
	$c = 0.1$	7	8	11	14	13	13	11	12	11
Reflection poor	Estimated	0	0	25	25	15	0	0	25	10
	$c = 0.9$	3	4	6	15	11	11	17	32	1
	$c = 0.5$	5	6	9	15	12	12	12	22	7
	$c = 0.1$	7	8	10	14	13	13	11	10	14

provide the most reliable data, and are considered hard data. Drill-core and georadar data are fuzzy to some extent and are, therefore, considered soft data. The georadar data are more uncertain than the drill-core data with respect to the indication of sedimentary structure types.

The method presented respects these differences of data uncertainty and allows a lithofacies-based interpretation of outcrop, drill-core, and georadar data. The lithofacies scheme is based on fluvio-dynamic considerations and is suitable for the interpretation of the radarfacies. The result is a probability estimation of drill-core layer descriptions and radarfacies types representing defined sedimentary structure types. The method includes a determination of initial structure-type probabilities for grain-size categories and combinations thereof described in drill-core layer descriptions as well as a following differentiation of these structure-type probabilities in an iterative process considering additional information like main constituent, quantity, fraction, and sorting of single grain-size categories, color, chemical precipitation, layer thickness, and adjacent layer. The radarfacies types are calibrated with drill cores located in the vicinity of georadar sections. The calibration process consists of the assignment of the calculated struc-

ture-type probabilities from the drill-core layer descriptions to the corresponding radarfacies types considering the proportion in thickness between drill-core layers and georadar structures. The structure-type probabilities can be given for points along boreholes and grid nodes with arbitrary mesh sizes along georadar sections.

The resulting structure-type probabilities can be used for conditioning stochastic simulations of geological models. However, the conditioned stochastic simulation of the Rhine/Wiese aquifer is the topic of another paper.

The results show the importance of a detailed sedimentological analysis of outcrops and drill cores, and its significance on the distinction of sedimentary structure types. The method presented allows a differentiation between the highly permeable open-framework gravel and open-framework/bimodal gravel couplets, which are only rarely described in the classic literature on coarse braided river stratigraphy. As these sedimentary structure types show a high hydraulic conductivity, they act as preferential pathways and therefore strongly influence transport behavior. In addition, older outcrop and drill-core data can also be interpreted and integrated in the lithofacies scheme.

Acknowledgments

References

Anderson, M.P., 1989. Hydrogeologic facies models to delineate large-scale spatial trends in glacial and glaciofluvial sediments. Geological Society of America Bulletin 101, 501-511.

Annan, A.P., Chua, L.T., 1988. Ground penetrating radar performance predictions. Pilon, J.A. (Ed.). Ground Penetrating Radar. Geological Survey of Canada, Paper 90-4.

Asprion, U., Aigner, T., 1999. Towards realistic aquifer models: three-dimensional georadar surveys of quaternary gravel deltas (Singen Basin, SW Germany). Sedimentary Geology 129 (3-4), 281-297.

Ayyub, B.M., Gupta, M.M., 1997. Uncertainty Analysis in Engineering and Sciences: Fuzzy Logic, Statistics, and Neural Network Approach. Kluwer Academic, Dordrecht.

Beres, M., Huggenberger, P., Green, A.G., Horstmeyer, H., 1999. Using two- and three-dimensional georadar methods to characterize glaciofluvial architecture. Sedimentary Geology 129, 1-24.

Beres, M., Green, A.G., Huggenberger, P., Horstmeyer, H., 1995. Mapping the architecture of glaciofluvial sediments with three-dimensional georadar. Geology 23 (12), 1087-1090.

Beres, M., Haeni, F.P., 1991. Application of ground-penetrating radar methods in hydrogeologic studies. Ground Water 29 (3), 375-386.

Copty, N., Rubin, Y., 1995. A stochastic approach to the characterisation of lithofacies from surface seismic and well data. Water Resources Research 31 (7), 1673-1686.

Copty, N., Rubin, Y., Mavko, G., 1993. Geophysical-hydrological identification of field permeabilities through bayesian updating. Water Resources Research 29 (8), 2813-2825.

Deutsch, C.V., Journel, A.G., 1998. GSLIB: Geostatistical Software Library and User's Guide, Second Edition, Applied Geostatistics Series. Oxford University Press, Oxford.

Hardage, B.A., 1987. Seismic Stratigraphy. Geophysical Press, London.

Hubbard, S.S., Rubin, Y., Majer, E., 1999. Spatial correlation structure estimation using geophysical and hydrogeological data. Water Resources Research 35 (6), 1809-1825.

Hubbard, S.S., Rubin, Y., Majer, E., 1997. Ground-penetrating-radar assisted saturation and permeability estmation in bimodal systems. Water Resources Research 33 (5), 971-990.

Huggenberger, P., 1993. Radar facies: recognition of facies patterns and heterogeneities within Pleistocene Rhine gravels, NE Switzerland. Best, C.L., Bristow, C.S. (Eds.). Braided Rivers. Geological Society Special Publication 75, 163-176.

Huggenberger, P., Siegentaler, C., Stauffer, F., 1988. Grundwasserströmung in Schottern: Einfluss von Ablagerungsformen auf die Verteilung von Grundwasserfliessgeschwindigkeit. Wasserwirtschaft 78 (5), 202-212.

Hyndman, D.W., Gorelick, S.M., 1996. Estimating lithologic and transport properties in three dimensions using seismic and tracer data: The Kesterson aquifer. Water Resources Research 32 (9), 2659-2670.

Hyndman, D.W., Harris, J.M., Gorelick, S.M., 1994. Coupled seismic and tracer test inversion for aquifer property characterization. Water Resources Research 30 (7), 1965-1977.

Jol, H.M., Smith, D.G., 1991. Ground-penetrating radar of northern lacustrine deltas. Canadian Journal of Earth Sciences 28 (12), 1939-1947.

Journel, A.G., Huijbregts, C.J., 1989. Mining Geostatistics. Academic Press, New York.

Jussel, P., Stauffer, F., Dracos, T., 1994. Transport modeling in heterogeneous aquifers: 1. Statistical description and numerical generation of gravel deposits. Water Resources Research 30 (6), 1803-1817.

Jussel, P., 1992. Modellierung des Transports gelöster Stoffe in inhomogenen Grundwasserleitern. Dissertation ETH Zürich, Nr. 9663.

Kunstmann, H., Kinzelbach, W., 1998. Quantifizierung von Unsicherheiten in Grundwassermodellen. Mathematische Geologie 2, 3-15.

Langsholt, E., Kitterod, N.-O., Gottschalk, L., 1998. Development of three-dimensional hydrostratigraphical architecture of the unsaturated zone based on soft and hard data. Ground Water 36 (1), 104-111.

McKenna, S.A., Poeter, E.P., 1995. Field example of data fusion in site characterization. Water Reseources Research 31 (12), 3229-3240.

Miall, A.D., 1996. The Geology of Fluvial Deposits: Sedimentary Facies, Basin Analysis and Petroleum Geology. Springer, Berlin.

Miller, R.B., Castle, J.W., Temples, T.J., 2000. Deterministic and stochastic modeling of aquifer stratigraphy, South Carolina. Ground Water 38 (2), 284-295.

Noack, T., 1997. Geologische Datenbank der Region Basel - Konzept und Anwendungen. Mitteilungen der Schweizerischen Gesellschaft für Boden- und Felsmechanik 133, 13-18.

Noack, T., 1993. Geologische Datenbank der Region Basel. Eclogae Geologicae Helveticae 86 (1), 283-301.

Poeter, E.P., McKenna, S.A., 1995. Reducing uncertainty associated with ground-water flow and transport predictions. Ground Water 33 (6), 899-904.

Radian Corporation, 1992. CPS-3, User's Manual. Radian Corporation, Austin, London.

Rauber, M., Stauffer, F., Huggenberger, P., Dracos, T., 1998. A numerical three-dimensional conditioned/unconditioned stochastic facies type model applied to a remediation well system. Water Resources Research 34 (9), 2225-2233.

Rohrmeier, M., 2000. Geologische Modelle im Anströmbereich von Wasserfassungen. Diplomarbeit, Universität Basel.

Rubin, Y., Mavko, G., Harris, J., 1992. Mapping permeability in heterogeneous aquifers using hydrologic and seismic data. Water Resources Research 28 (7), 1809-1816.

Schafmeister, M.-T., 1997. Parameter estimation for ground-water models by indicator kriging. GeoENV I - Geostatistics for Environmental Applications, Proceedings of the Geostatistics for Environmental Applications Workshop, Lisbon, Portugal, 18-19 November 1996. Soares, A., Gomez-Hernandez, J., Froidevaux, R. (Eds.). Quantitative Geology and Geostatistics 9, 165-176.

Sensors & Software Inc., 1993. PulseEKKO Software user's guide. Sensors & Software Inc., Mississauga, Ontario.

Siegenthaler, C., Huggenberger, P., 1993. Pleistocene Rhine gravel: deposits of a braided river system with dominant pool preservation. Best, C.L., Bristow, C.S. (Eds.). Braided Rivers. Geological Society Special Publication 75, 147-162.

Part II

GEOSSAV: a simulation tool for subsurface applications

Christian Regli [a], Lukas Rosenthaler [b], Peter Huggenberger [a]

[a] Department of Earth Sciences, Applied and Environmental Geology, University of Basel, Bernoullistr. 16, 4056 Basel, Switzerland

[b] Imaging and Media Lab, University of Basel, Bernoullistr. 32, 4056 Basel, Switzerland

GEOSSAV: a simulation tool for subsurface applications

Christian Regli [a], Lukas Rosenthaler [b], Peter Huggenberger [a]

[a] Department of Earth Sciences, Applied and Environmental Geology, University of Basel, Bernoullistr. 16, 4056 Basel, Switzerland
[b] Imaging and Media Lab, University of Basel, Bernoullistr. 32, 4056 Basel, Switzerland

Abstract

GEOSSAV (Geostatistical Environment fOr Subsurface Simulation And Visualization) is a tool for the integration of hard and soft data into the stochastic simulation and visualization of distributions of geological structures and hydrogeological properties in the subsurface. GEOSSAV, as an interface to selected geostatistical modules (bicalib, gamv, vargplt, and sisim) from the Geostatistical Software LIBrary, GSLIB (Deutsch and Journel, 1998), can be used for data analysis, variogram computation of regularly or irregularly spaced data, and sequential indicator simulation of subsurface heterogeneities. Sequential indicator simulation, based on various kriging techniques (simple, ordinary, and Bayesian), is suitable for the simulation of continuous variables such as hydraulic conductivity of an aquifer or chemical concentrations at a contaminated site, and categorical variables which indicate the presence or absence of a particular lithofacies. The software integration platform and development environment of GEOSSAV is Tcl with its graphical user interface, Tk, and a number of Tcl/Tk extensions. The standard OpenGL API is used for rendering 3D data distributions and for slicing perpendicular to the main coordinate axis. Export options for finite-difference groundwater models allow either files that characterize single model layers (which are saved in ASCII matrix format) or files that characterize the complete 3D flow model set-up for MODFLOW-based groundwater simulation systems (which are saved in block-centered flow package files (Harbaugh and McDonald, 1996)). GEOSSAV can be used whenever stochastic solutions are preferred to solve site-specific heterogeneity problems, e.g., in the field of hydrology, groundwater, groundwater and/or soil contamination, site remediation, air pollution, and ecology. An example from the Rhine/Wiese aquifer near Basel demonstrates the application of GEOSSAV on geostatistical data analysis and subsurface visualization. GEOSSAV has been successfully tested on Microsoft Windows NT 4.0/2000/XP and on SuSE Linux 7.3. The current version is available at http://www.unibas.ch/earth/pract.

Keywords: software, geostatistics, soft kriging, variogram modeling, sequential indicator simulation, heterogeneity, aquifer stratigraphy

1. Introduction

Numerical models of physical systems play an important role in decision-making processes, especially in the context of better characterization of parameter distributions and prediction of dynamic behavior of a given system. In the earth sciences and in many other research disciplines, great efforts have been made within the last 20 years on evaluation and integration of data in the characterization of the subsurface (among others Wingle et al., 1997; Deutsch

and Journel, 1998). One of the objectives of all these projects is to model reasonable variations in the subsurface while constraining results as much as possible with available data. Although one particular data set may suggest a wide range of alternatives, if all the available data are combined, the possible solution population should be greatly reduced.

Data used in subsurface models may be divided into two basic types: 'hard data' and 'soft data' (Poeter and McKenna, 1995). Hard data can be directly obtained and relate directly to the phenomenon being modeled. Examples of hard data include outcrop data and, in some cases, drill-core data because these explicitly define sedimentary structure types (in the following called structure types or lithofacies types) and properties. There is measurement or interpretation uncertainty in hard data, but it is considered small enough to be ignored. Soft data are less precise and generally indirect, thus greater uncertainties are associated with the soft data values. Soft data may not be honored exactly in conditional simulations (e.g., Wingle et al., 1997).

Ground-penetrating radar (GPR or georadar) data is an example of soft data. Georadar systems measure the dielectric constant of the subsurface (Sensors & Software Inc., 1993), which is dependent on the water content of the sedimentary structure types. The formation of reflection patterns is dependent on the reflection coefficient at contrast surfaces between different structure types (Huggenberger, 1993). Generally, the interpretation of georadar data is based on reflection pattern analysis and the applied georadar system configuration (Huggenberger, 1993; Beres et al., 1999). Therefore, only imprecise estimates can be made about structure type, structure properties, and location (Regli et al., 2002). As shown in another example, often hydraulic conductivity is not measured directly but is deduced from structure characteristics such as grain-size distribution data (e.g., Sudicky, 1986; Hess et al., 1992) or from pumping tests (Furger, 1990).

Subsurface heterogeneity is one of several important factors (e.g., boundary conditions, groundwater recharge) for modeling groundwater flow. In practice, the subsurface heterogeneity is often underestimated. In the following discussion, only the subsurface heterogeneity is considered. All other factors influencing groundwater flow are not taken into account.

Accurate modeling of subsurface parameter distributions becomes more difficult with increasing heterogeneity and uncertainty with respect to spatial variability of available data. The uncertainty depends both on the quantity and the quality of available data. The technique used to model subsurface structures for a site-specific problem should be chosen specifically for the properties under consideration (e.g., lithofacies type, hydraulic conductivity, porosity), the knowledge of the subsurface, and the causes of uncertainty (Ayyub and Gupta, 1997; Weissmann et al., 1999). For example, in a study area where only two structure types are present, relatively few alternative interpretations may be likely based on the raw data. However, although each model realization of parameter distributions may honor the data exactly, subsequent process modeling with each alternative realization (e.g., groundwater flow and transport modeling) can generate significantly different outcomes (Poeter and McKenna, 1995). In more heterogeneous media, alternative interpretations are possible and this increases the number of spatial parameter distributions that may be generated to honor the data.

In order to evaluate this inherent uncertainty, computers can be used to create multiple alternative realizations of the subsurface. Once multiple realizations are created, output from subsequent modeling (e.g., groundwater flow and transport modeling) can be used to compare modeled and field conditions. If a groundwater model response clearly does not match field observations, the possible subsurface configuration can be rejected even though it may satisfy statistical requirements of data distributions (Poeter and McKenna, 1995). Of the remaining realizations that appear reasonable, the modeled distributions may be further evaluated for the conditions already modeled or for future conditions that may be added. With computerized
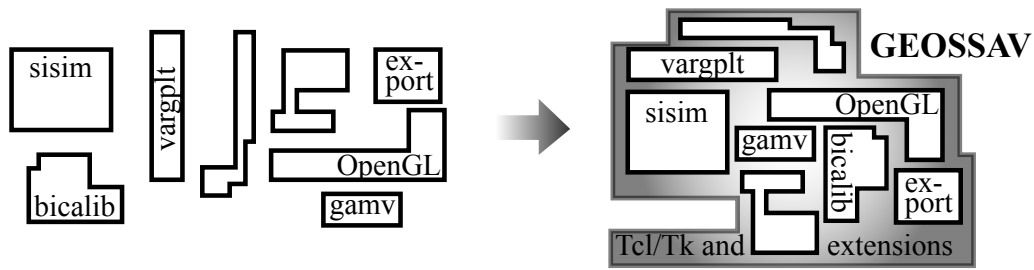
Fig. 1. *The various modules integrated within GEOSSAV. Gamv computes the spatial variability of regularly or irregularly spaced data. Sisim is used for the sequential indicator simulation of categorical and continuous variables, and bicalib is used for considering soft data in the indicator formalism. OpenGL supports visualization of the data and the results in two and three dimensions. Export options allow files to be generated in data formats for use in other applications.*

routines, a sufficient number of realizations may be evaluated so that a statistically robust assessment of the reasonable alternatives may be achieved (Wingle et al., 1997).

Stochastic simulation implies sampling from conditional distributions and consequently the spatial models are samples from a multivariate distribution characterizing the spatial phenomenon. Until now it was relatively inconvenient to perform different steps of generating and visualizing realizations of subsurface heterogeneities that can be easily exported into existing groundwater simulation systems. Among others this is caused: (1) by user-unfriendly aspects of codes (e.g., GSLIB codes), (2) due to the fact that the different steps of subsurface modeling have to be completed with several independent tools (e.g., SAGE2001 for variogram calculation and modeling (Isaaks & Co., 1999), GSLIB codes for subsurface simulation, VTK for visualization (Schroeder et al., 2001)), and (3) by the different export routines which are needed to transform modeled parameter distributions in data formats usable in subsequent modeling systems. In addition, many of these tools are platform dependent (e.g., UNCERT (Wingle et al., 1997)).

Therefore, a tool was developed that combines geostatistical analysis, simulation, visualization, and data export. In this paper a user-friendly tool for subsurface simulation and visualization, GEOSSAV (Geostatistical Environment fOr Subsurface Simulation And Visualization), is described. GEOSSAV is a software package developed to aid hydrogeologists using geostatistics to simulate and visualize the distribution of structure types and properties in the subsurface. This package is developed in a way that spatial data from other research disciplines may be analyzed (e.g., groundwater, groundwater and/or soil contamination, site remediation, air pollution, and ecology). It allows the modeler to: (1) import hard and soft field data or data from a pre-existing database, (2) update soft data using a bivariate calibration method (Deutsch and Journel, 1998), (3) compute and visualize spatial variability of data by variogram analysis, (4) generate distributions of structure types and structure properties of the subsurface using sequential indicator simulation based on a choice of kriging techniques (simple, ordinary, and Bayesian), and (5) visualize the data and the modeled spatial distributions in two and three dimensions by 3D rendering and slicing perpendicular to the main coordinate axis. Furthermore, once spatial distributions of structure types and structure properties have been generated, data files for 2D and 3D finite-difference groundwater flow and transport models can be created.

This paper starts by describing the integration platform and software resources. In the following sections the central features of GEOSSAV are described, including an account of the geostatistical techniques, the visualization methods, and the data export options. Subsequently, an example is given to illustrate site-specific considerations of heterogeneity in subsurface modeling. This paper concludes with a description of hardware and software requirements for running GEOSSAV, planned new developments, and information for acquiring GEOSSAV.
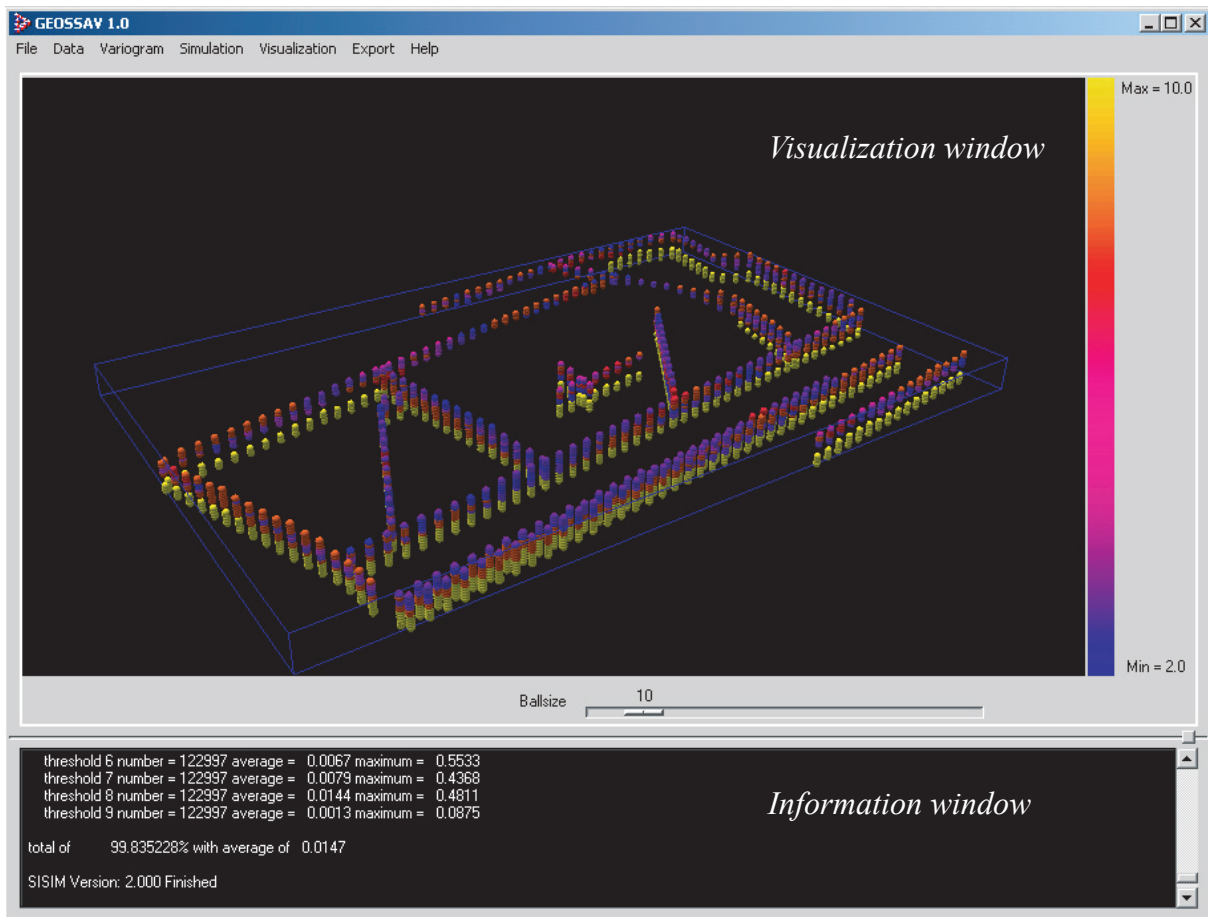
Fig. 2. Main GEOSSAV window with the menu bar for the pull-down menus, the window for the visualization of input and output data, and the window for error checking.

2. Integration platform and software resources

GEOSSAV consists of an integration platform and individual simulation, visualization, and export modules, as shown in Fig. 1. The software integration platform and development environment for GEOSSAV is Tcl (Tool command language) and its graphical user interface Tk (Toolkit; (Ousterhout, 1994)). In addition, some of the Tcl/Tk extensions (Harrison, 1997) such as [incr Tcl], [incr Tk], [incr Widgets], and TkTable are integrated into GEOSSAV. Tcl/Tk was chosen because of its speed of use, breadth of functionality, flexibility for cross-platform deployment, and ease of integrating new extensions such as rendering 3D graphics through the OpenGL API (application programming interface). In addition, Tcl/Tk and its extensions allow the integration of diverse software resources irrespective of the programming language (e.g., Fortran, C/C++) in which they are written.

Compiled GSLIB modules without any enhancements are integrated into GEOSSAV: The sequential indicator simulation module 'sisim' (Deutsch and Journel, 1998) requires information about the spatial variability of the regularly or irregularly spaced data, which can be computed with the variogram module 'gamv' and then visualized with the module 'vargplt' and a PostScript display device (Deutsch and Journel, 1998). The indicator kriging approach allows the modeling of single property classes, represented by indicators, using single indicator variograms. In addition, the sisim algorithm is able to account for soft data. The integration of soft data in the indicator formalism is made possible by the Markov-Bayes option for cokriging using the module 'bicalib' (Deutsch and Journel, 1998).

The open, standardized API OpenGL (Open Graphics Library; (Fosner, 1997; Wright and Sweet, 2000)) has been integrated in the Tcl/Tk environment and is used for rendering of the 3D data distributions and for slicing perpendicular to the main coordinate axis. Export formats are compatible with widely used finite-difference groundwater modeling environments (e.g., ASMWIN (Chiang et al., 1998); GMS (Environmental Modeling Systems Inc., 2002); PMWIN (Chiang and Kinzelbach, 2001)). Also data may be exported as individual files for single model layers (saved in ASCII matrix files) or as data files characterizing the complete 3D model set-up for MODFLOW-based groundwater simulation systems and saved in block-centered flow (bcf) package files (Harbaugh and McDonald, 1996). Groundwater flow and transport simulation is external to GEOSSAV.

Fig. 2 shows the main GEOSSAV window. The upper area is the visualization window where the input and output data are shown. Here all the hard and soft input data are displayed for error checking and the output data are shown for plausibility checking. The lower area is an information window where the standard output of all modules is shown. That is, all of the output that would be seen at the prompt is shown here for error checking. The single modules (e.g., for data processing, simulation, visualization, final control, and data export) are placed in the corresponding pull-down menus. The 'File' menu controls the project settings. The 'Data' menu is for processing the input data (e.g., bivariate calibration of soft data). The 'Variogram', 'Simulation', 'Visualization', 'Export', and 'Help' menus are self-explanatory. When selecting a module from the pull-down menus, a corresponding dialog box for parameter input is opened (e.g., Figs. 4, 5, 6, 7, 9). The dialog box is designed to require the input of all options, which are necessary for running the module. The parameters can be written to a parameter file and the module can be executed.

3. Geostatistical techniques

3.1. Stochastic simulation

Stochastic simulation is the process of drawing multiple, equally probable realizations of random variables (RVs) from a random function (RF) model. The realizations represent possible images of spatial distributions of the data values $z(\boldsymbol{u})$ over the field A. Each realization reflects the spatial properties that have been imposed on the RF model $Z(\boldsymbol{u})$. The more properties are inferred from the sample data and integrated in the RF model through the simulation algorithm, the higher the accuracy will be of the RF model and the resultant simulated realizations in representing the heterogeneity of the spatial phenomenon (Deutsch and Journel, 1998). The conceptual framework of the stochastic simulation approach is shown in Fig. 3. Based on the variogram computation of the hard input data and the following stochastic simulation, e.g., sequential indicator simulation, various equally probable realizations are generated, which represent images of the reality. The simulation is conditional if the resulting realizations honor data values at their locations.

The various realizations have to reproduce the input proportions within a defined accuracy: If the cumulative distribution functions (cdf) or the probability density functions (pdf) of the input data are significantly different from those of the resulting probabilistic model, then this possible subsurface configuration has to be rejected. Moreover, the accepted realizations should be applied to reality to compare measured and calculated data. If a model response clearly does not match field observations, the possible subsurface configuration has to be rejected. On the other hand, if a model response matches field observations, the possible subsurface configuration represents a probable realization of the reality. The different steps of stochastic simulation are described in the sections 3.2. – 3.3.
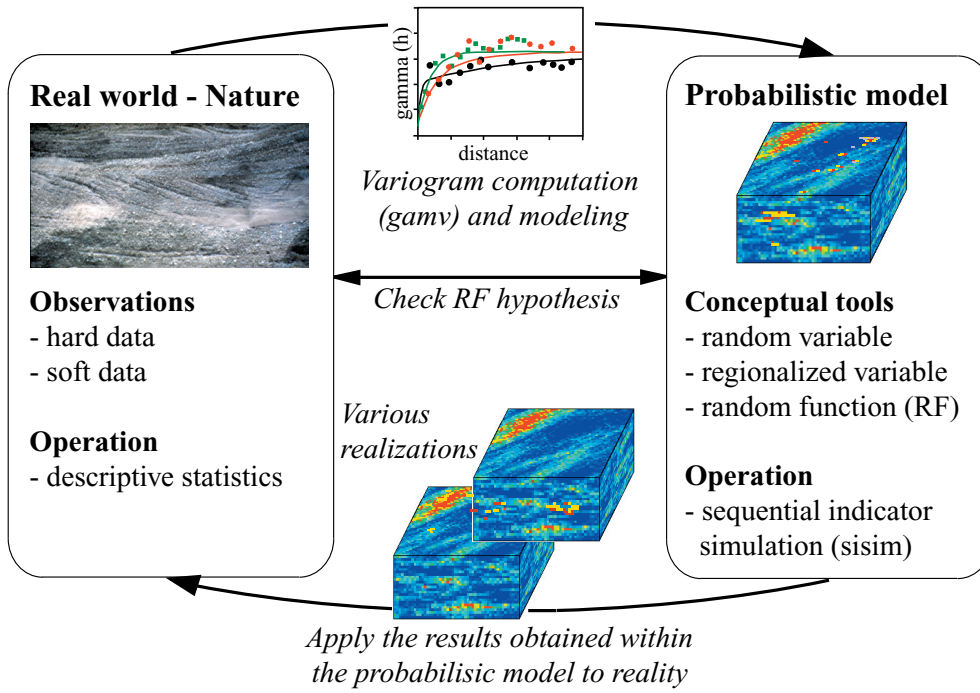
Fig. 3. *Conceptual framework of the stochastic simulation approach, modified from Pannatier (1996). Based on the variogram modeling of the hard input data and the following stochastic simulation (e.g., sequential indicator simulation), various equiprobable realizations are generated and checked for consistency with the random function hypothesis. The results obtained within the probabilistic model should be checked by comparison of measured and calculated data.*

3.2. Variogram computation of irregularly spaced data

Modeling spatial variability of data is the key to any subsurface simulation. The variogram describes the spatial correlation of data as a function of the separation vector $\boldsymbol{h}$ (lag) between two data points. The indicator variogram for continuous variables such as hydraulic conductivity of an aquifer or concentrations over a contaminated site, or categorical variables, indicating the presence or absence of a particular lithofacies, is computed on a constructed indicator variable. This requires either the specification of a continuous variable and cutoff or a categorical variable and category to create the indicator transform. For the cutoff z_k (threshold) and data value $z(\boldsymbol{u}_\alpha)$, or the category s_k and data value $s(\boldsymbol{u}_\alpha)$, the indicator transform $i(\boldsymbol{u}_\alpha; z_k \ or \ s_k)$ is defined as (Deutsch and Journel, 1998):

$$i(\boldsymbol{u}_\alpha; z_k \ or \ s_k) = \begin{cases} 1, \text{ if } z(\boldsymbol{u}_\alpha) \le z_k \text{ (continuous variable), or 1,} \\ \text{if } s(\boldsymbol{u}_\alpha) = s_k \text{ (categorical variable)} \\ 0, \text{ otherwise} \end{cases} \tag{1}$$

where $\boldsymbol{u}_\alpha$ refers to a particular data location.

The indicator variogram, written for a specific category, is defined as half of the average squared increment between two indicators separated by $\boldsymbol{h}$ (Deutsch and Journel, 1998):

$$\gamma_I(\boldsymbol{h}; s_k) = \frac{1}{2N(\boldsymbol{h})} \sum_1^{N(h)} [i(\boldsymbol{u}; s_k) - i(\boldsymbol{u} + \boldsymbol{h}; s_k)]^2 \tag{2}$$

where $N(\boldsymbol{h})$ is the number of pairs, $i(\boldsymbol{u}; s_k)$ is the indicator at the start or tail of the pair, and $i(\boldsymbol{u} + \boldsymbol{h}; s_k)$ is the corresponding end or head indicator.

Experimental variograms derived on the basis of data, have to be fitted using licit variogram models in order to satisfy the requirements. The variogram models are demanded in the sequential indicator simulation module for determining kriging weights. Several of the terms are used to describe variogram models: the sill refers to the maximum value of the variogram model, the range corresponds to the maximum distance of spatial correlation, and the nugget refers to the behavior of the variogram model at lags $h \rightarrow 0$. A variogram model consists of an isotropic or anisotropic nugget effect, a positive definite variogram structure (spherical model, exponential model, gaussian model, power model, hole effect model), and parameters defining the geometric anisotropy.

The module gamv from Deutsch and Journel (1998) can be used for spatial data analysis and variogram computation of irregularly spaced data in three dimensions. In fact, ten experimental measures of spatial variability can be computed (variogram, cross variogram, covariance, correlogram, general relative variogram, pairwise relative variogram, variogram of logarithms, madogram, indicator variogram for continuous variables, and indicator variogram for categorical variables).

Fig. 4. *Dialog box for the irregularly spaced data variogram computation, used for data input and output as well as for lag and variogram specification (directions, variables, and variogram types).*

Variogram implementation

Fig. 4 shows the dialog box for the module gamv 2.000 in GEOSSAV. The first register (top panel of Fig. 4) is used for data input *{Input}*, data output *{Output}*, and lag specifications *{Lags}*. In general, the separation vector h is specified with some direction and distance tolerance. Experience shows that many directional sample variograms are required to obtain a reasonably representative model of 3D spatial variability.

The second register (bottom panel of Fig. 4) is used for variogram specifications *{Variograms}*. The module can handle many different directions, cutoffs or categories, and variogram types in a single pass. The azimuth is measured clockwise from North, and the dip is measured in negative degrees down from horizontal. Angular half-window tolerances are required for both the azimuth and the dip (Deutsch and Journel, 1998, p.49, fig. III.2). These tolerances may overlap, causing pairs to report to more than one direction and lag vector. The angle tolerances are restricted once the deviations from the direction vector exceed the horizontal or the vertical bandwidth. The results of the variogram computation are written into an output file.

The module vargplt from Deutsch and Journel (1998) takes the output format used by gamv and creates graphical displays for PostScript display devices. This module provides no facility for interactive model variogram fitting. Based on the experimental variogram, parameters of a
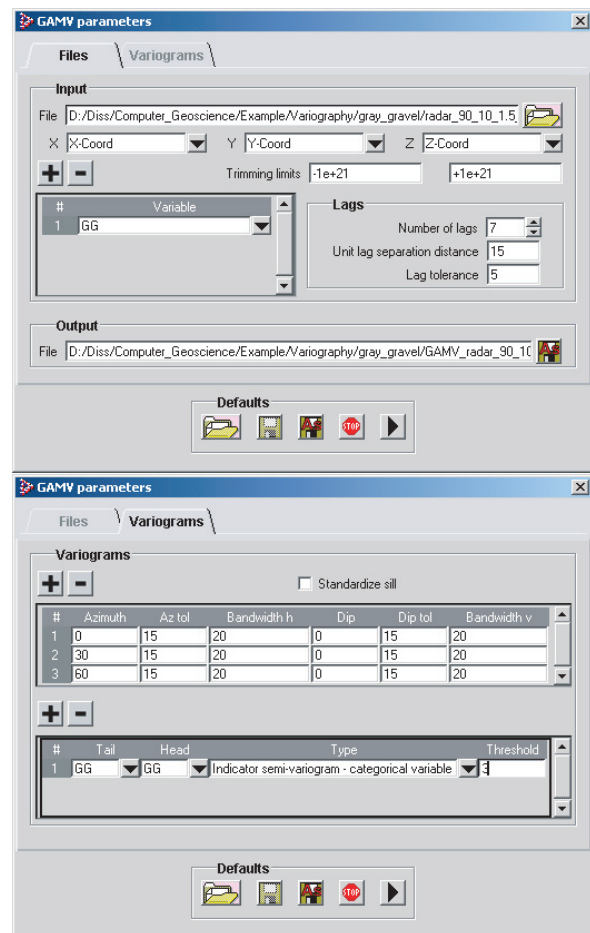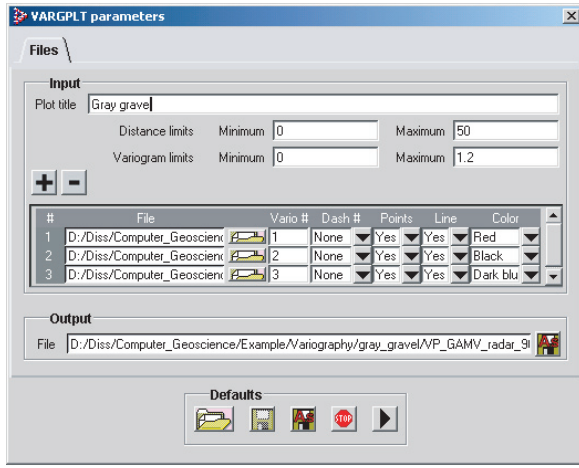
Fig. 5. *Dialog box for variogram plotting, used for specifying and creating graphical displays for PostScript display devices.*

model variogram have to be determined (e.g., with VARIOWIN from Pannatier (1996); SAGE 2001 from Isaaks & Co (2001)).

Fig. 5 shows the dialog box for the module vargplt 2.000 in GEOSSAV, calling for a plot title, distance and variogram limits, as well as files containing the calculated experimental variograms *{Input}*. For every single variogram, display specifications can be indicated. The graphical displays are written into an output file *{Output}* that can be visualized in public PostScript viewing programs (e.g., GSview).

3.3. Sequential indicator simulation

Sequential indicator simulation is suitable for the simulation of continuous and integer-coded categorical variables. Simple indicator kriging (SIK) or ordinary indicator kriging (OIK) can be selected for simulation. The indicator kriging process is repeated for a series of K cutoffs z_k, $k = 1,...,K$, which discretize intervals of variability of the continuous variable, or for a series of K categories s_k, $k = 1,...,K$, which represent different lithofacies types. The cdf (working with continuous variables), built by assembling the K indicator kriging estimates, represents a probabilistic model for the uncertainty about the non-sampled value $z(\boldsymbol{u})$. In the case of categorical variables, the pdf corresponding to each category represents the uncertainty about the non-sampled category $s(\boldsymbol{u})$. For the categorical variable $s(\boldsymbol{u})$, e.g., set to 1 if a specific lithofacies type prevails at location $\boldsymbol{u}$, set to 0 if not, the indicator kriging of $s(\boldsymbol{u})$ provides a model for the probability that $s(\boldsymbol{u})$ be one. For the continuous variable $z(\boldsymbol{u})$ the correct selection of the cutoffs z_k, at which indicator kriging takes place, is essential. By defining too many cutoffs or categories, the computation becomes needlessly tedious, by marking too few, the details of the distribution are lost. The indicator methodology is a non-parametric approach to creating a useful distribution for modeling distributions, which can only be described inadequately by the mean and the variance of the data due to their poly-modal form (Schafmeister, 1999).

For a specific category, the SIK estimate, i.e. the probability that s_k prevails at location $\boldsymbol{u}$, is written as a linear combination of the n nearby indicator-coded data (Deutsch and Journel, 1998):

$$\left[i(\boldsymbol{u};s_k)\right]^*_{SK} = \left[Prob\left\{S(\boldsymbol{u}) = s_k \mid (n)\right\}\right]^*_{SK} = \sum_{\alpha=1}^{n}\lambda_\alpha(\boldsymbol{u};s_k)i(\boldsymbol{u}_\alpha;s_k) + \left[1 - \sum_{\alpha=1}^{n}\lambda_\alpha(\boldsymbol{u};s_k)\right]F(s_k) \qquad (3)$$

where $F(s_k)$ is the stationary prior probability of category s_k, and the $\lambda_\alpha(\boldsymbol{u};s_k)$'s are the SIK weights corresponding to category s_k, which depend on the closeness of the data considered for the estimation. These weights are given by the SIK system (Deutsch and Journel, 1998):

$$\sum_{\beta=1}^{n}\lambda_\beta(\boldsymbol{u};s_k)C_I(\boldsymbol{u}_\beta - \boldsymbol{u}_\alpha;s_k) = C_I(\boldsymbol{u} - \boldsymbol{u}_\alpha;s_k), \quad \alpha = 1,...,n \qquad (4)$$

$C_I(\boldsymbol{h};s_k) = Cov\{I(\boldsymbol{u};s_k),I(\boldsymbol{u}+\boldsymbol{h};s_k)\}$ are the requisite indicator covariances. The variogram models are converted into equivalent covariance models, because the kriging system is more easily solved with covariance matrices. For K categories s_k, SIK requires K indicator covariances $C_I(\boldsymbol{h};s_k)$ in addition to the K pdf values $F(s_k)$.

OIK is the most commonly used variant of the SIK algorithm, whereby the sum of the kriging weights is constrained equal to 1 (OIK constraint). If data is abundant, OIK within moving data neighborhoods may be considered; this amounts to re-estimating locally the prior pdf values $F(s_k)$ (Deutsch and Journel, 1998).

Median indicator kriging calls for a single indicator variogram that is used for all categories. It is used if the sample indicator variograms appear proportional to each other. Only one single indicator kriging system needs to be solved with the resulting weights being used for all categories. It is, therefore, a particularly simple and fast procedure.

The major advantage of the indicator kriging approach to generate posterior conditional distributions is its ability to account for soft data. As long as the soft data can be coded into prior local probability values, indicator kriging can be used to integrate that information into a posterior probability value. The prior information can take one of the following forms (Deutsch and Journel, 1998):

(1) local hard indicator data $i(\boldsymbol{u}_\alpha;z_k)$ or $i(\boldsymbol{u}_\alpha;s_k)$ originating from local hard data $z(\boldsymbol{u}_\alpha)$ or $s(\boldsymbol{u}_\alpha)$, respectively:

$i(\boldsymbol{u}_\alpha;z_k)=1$, if $z(\boldsymbol{u}_\alpha) \le z_k$, $=0$ if not (continuous variables), or

$i(\boldsymbol{u}_\alpha;s_k)=1$, if $s(\boldsymbol{u}_\alpha) = s_k$, $=0$ if not (categorical variables) $\qquad$ (5)

(2) local hard indicator data $j(\boldsymbol{u}_\alpha;z_k)$ originating from ancillary information that provides hard inequality constraints on the local value $z(\boldsymbol{u}_\alpha)$. This type of prior information is valid only for continuous variables. If $z(\boldsymbol{u}_\alpha) \in (a_a,b_b)$, then:

$$j(\boldsymbol{u}_\alpha;z_k) = \begin{cases} 0, \text{ if } z(\boldsymbol{u}_\alpha) \le a_\alpha \\ \text{undefined (missing indicator data), if } z(\boldsymbol{u}_\alpha) \in (a_a,b_b) \\ 1, \text{ if } z(\boldsymbol{u}_\alpha) > b_\alpha \end{cases} \qquad (6)$$

(3) local soft indicator data $y(\boldsymbol{u}_\alpha;z_k)$ or $y(\boldsymbol{u}_\alpha;s_k)$ originating from ancillary information providing prior probabilities of the value $z(\boldsymbol{u}_\alpha)$ or the category $s(\boldsymbol{u}_\alpha)$, respectively:

$y(\boldsymbol{u}_\alpha;z_k) = Prob\{Z(\boldsymbol{u}_\alpha) \le z_k \mid local\ ancillary\ information\}, \in [0,1]$ (continuous variables); or

$y(\boldsymbol{u}_\alpha;s_k) = Prob\{S(\boldsymbol{u}_\alpha) = s_k \mid local\ ancillary\ information\}, \in [0,1]$ (categorical variables) $\qquad$ (7)

(4) global prior information common to all locations $\boldsymbol{u}$ within the area A:

$F(z_k) = Prob\{Z(\boldsymbol{u}) \le z_k\}$, $\forall \boldsymbol{u} \in A$, (continuous variables), or

$F(s_k) = Prob\{S(\boldsymbol{u}) = s_k\}$, $\forall \boldsymbol{u} \in A$, (categorical variables) $\qquad$ (8)

At any location $\boldsymbol{u} \in A$, prior information about the value $z(\boldsymbol{u})$ or the category $s(\boldsymbol{u})$ is characterized by any one of the four previous types of prior information. The indicator kriging

process consists of a Bayesian updating of the local prior cdf or pdf into a posterior cdf or pdf using information supplied by neighboring local prior cdfs or pdfs, written for a specific category (Deutsch and Journel, 1998):

$$\left[Prob\left\{S(\boldsymbol{u})=s_k \mid (n+n')\right\}\right]^*_{SK} = \lambda_0(\boldsymbol{u})F(s_k)+\sum_{\alpha=1}^{n}\lambda_\alpha(\boldsymbol{u};s_k)i(\boldsymbol{u}_\alpha;s_k)+\sum_{\alpha'=1}^{n'}\upsilon_{\alpha'}(\boldsymbol{u};s_k)y(\boldsymbol{u}'_a;s_k) \quad (9)$$

The $\lambda_\alpha(\boldsymbol{u};s_k)$'s are the weights attached to the n neighboring hard indicator data of Eq. (5), the $\upsilon_{\alpha'}(\boldsymbol{u};s_k)$'s are the weights attached to the n' neighboring soft indicator data of Eq. (7), and λ_0 is the weight attributed to the global prior pdf. To ensure unbiasedness, λ_0 is usually set to (Deutsch and Journel, 1998):

$$\lambda_0(\boldsymbol{u})=1-\sum_{\alpha=1}^{n}\lambda_\alpha(\boldsymbol{u};s_k)-\sum_{\alpha'=1}^{n'}\upsilon_{\alpha'}(\boldsymbol{u};s_k) \quad (10)$$

The conditional probability density function model of Eq. (9) can be seen as an indicator cokriging that pools information of different types: the hard i indicator data and the soft y prior probabilities. If the soft information is not present or is ignored ($n'=0$), Eq. (9) reverts to the SIK of Eq. (3).

Bivariate calibration of soft data

Soft information can be considered. If the spatial variability of the soft variable y is represented using the same covariance model $C_I(\boldsymbol{h};s_k)$ as the indicator hard variable i, no posterior updating of prior probability values $y(\boldsymbol{u}'_a;s_k)$ at soft data locations $\boldsymbol{u}'_a$ is possible, i.e. the soft data are also treated as hard data.

Most often, the soft data originates from information related to, but different from the hard data. Thus, the soft y indicator spatial distribution is likely different from that of the hard i indicator data. The Markov-Bayes algorithm (see Eq. (9)) should be considered in order to perform full updating of all prior pdfs that are not already hard. The soft indicator data covariance and cross-covariance for a specific category are calibrated from the hard indicator covariance model, whereby (Deutsch and Journel, 1998):

$$C_{IY}(\boldsymbol{h};s_k)=B(s_k)C_I(\boldsymbol{h};s_k), \quad \forall \boldsymbol{h} \quad (11)$$

$$C_Y(\boldsymbol{h};s_k)=B^2(s_k)C_I(\boldsymbol{h};s_k), \quad \forall \boldsymbol{h}>0$$

$$C_Y(\boldsymbol{h};s_k)=\left|B(s_k)\right|C_I(\boldsymbol{h};s_k), \quad \boldsymbol{h}=0$$

The coefficients $B(s_k)$ corresponding to each secondary data s_k is obtained from calibration of the soft y data to the hard i data (Deutsch and Journel, 1998):

$$B(s_k)=m^{(1)}(s_k)-m^{(0)}(s_k) \in [-1,+1] \quad (12)$$

with:

$$m^{(1)}(s_k)=E\left\{Y(\boldsymbol{u};s_k)\mid I(\boldsymbol{u};s_k)=1\right\}$$

$$m^{(0)}(s_k)=E\left\{Y(\boldsymbol{u};s_k)\mid I(\boldsymbol{u};s_k)=0\right\}$$
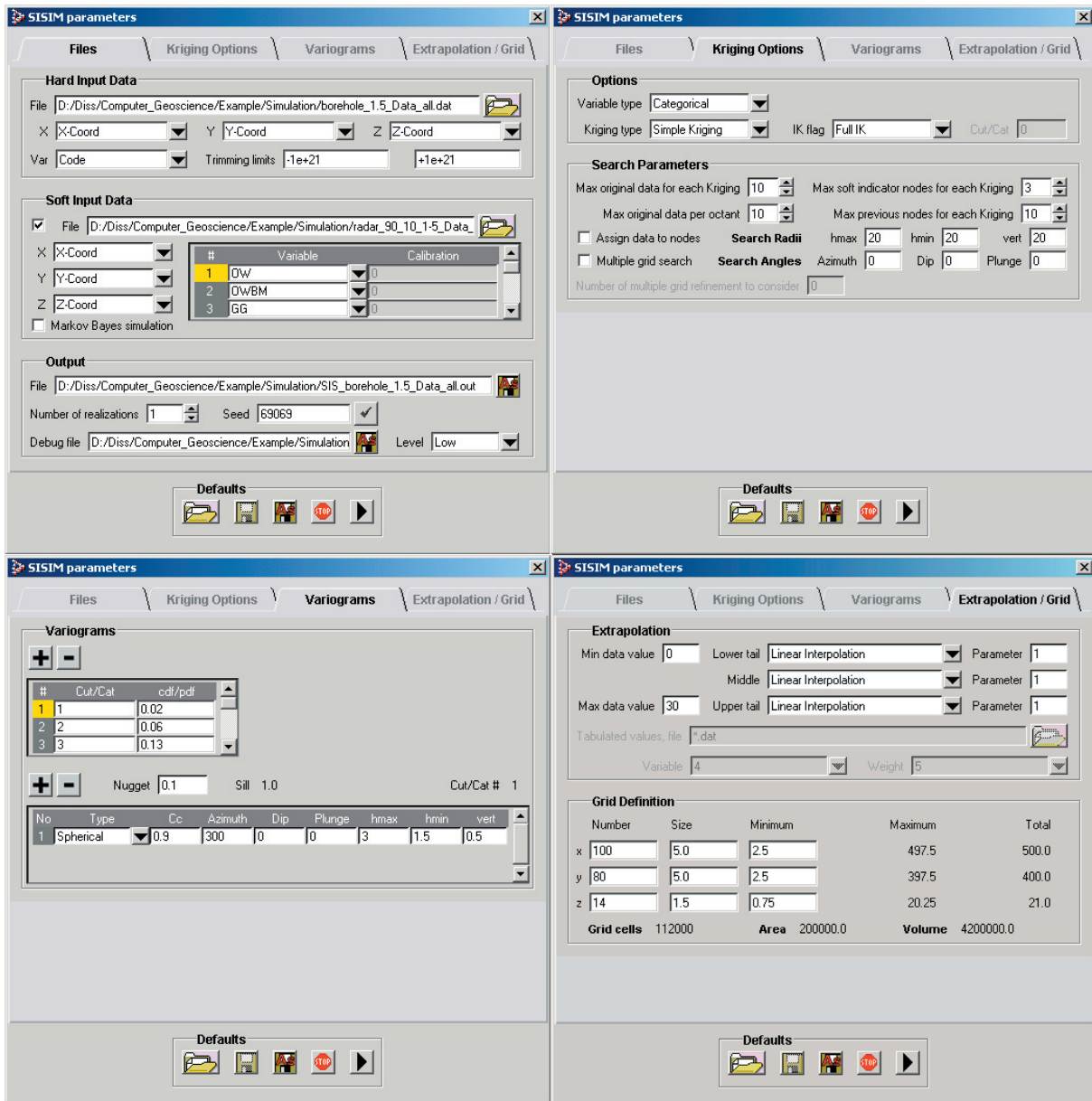
Fig. 6. Dialog box for the sequential indicator simulation, used for hard and soft data input, data output, output control, and for specifying kriging options, search parameters, variogram, extrapolation, and grid information.

Consider a calibration data set $\{y(\boldsymbol{u}_\alpha;s_k),i(\boldsymbol{u}_\alpha;s_k),\ \alpha=1,...,n\}$ where the soft probabilities $y(\boldsymbol{u}_\alpha;s_k)$ valued in $[0,1]$ are compared to the actual hard values $i(\boldsymbol{u}_\alpha;s_k)$ valued 0 or 1. $m^{(1)}(s_k)$ is the mean of the y values corresponding to $i=1$; the best situation is when $m^{(1)}(s_k)=1$, that is, when all y values exactly predict the outcome $i=1$. Similarly, $m^{(0)}(s_k)$ is the mean of the y values corresponding to $i=0$, best being when $m^{(0)}(s_k)=0$.

The parameter $B(s_k)$ measures how well the soft y data separates the two actual cases $i=1$ and $i=0$. The best case is when $B(s_k)=\pm 1$, and the worst case is when $B(s_k)=0$; that is, $m^{(1)}(s_k)=m^{(0)}(s_k)$. The case $B(s_k)=-1$ corresponds to soft data predictably wrong and is best handled by correcting the wrong probabilities $y(\boldsymbol{u}_\alpha;s_k)$ into $1-y(\boldsymbol{u}_\alpha;s_k)$. If $B(s_k)=1$, the soft prior probability data $y(\boldsymbol{u}'_\alpha;s_k)$ in Eq. (9) is treated as hard indicator data and therefore not updated. Conversely, if $B(s_k)=0$, the soft data $y(\boldsymbol{u}'_\alpha;s_k)$ is ignored; i.e. their weights in Eq. (9) become zero.

The sequential indicator simulation principle is an extension of kriging to include all data available within a neighborhood of the location u, including the original data and all previously simulated values. The steps in the sequential indicator simulation are as follows:

- In the first step, a grid network and coordinate system is established.

- In the second step, the data is assigned to the nearest grid node. If there are multiple data, only the closest data is assigned to the nearest grid node.

- In the third step, a random path through all grid nodes is determined. For a node in the random path:

  (1) the nearby data and previously simulated grid nodes are searched, and

  (2) the conditional distribution is estimated by indicator kriging (Eq. (9)).

  (3) From this distribution a simulated value or category, respectively, is randomly drawn and set as hard data for the simulation at the next node. The next node in the random path is selected and the steps (1)-(3) are repeated. This way, the simulation grid is built up sequentially.

- In the last step, the results are checked. The data and the global proportions have to be honored, and the simulation has to look reasonable.

Indicator simulation implementation

Fig. 6 shows the dialog box for the module sisim 2.000 in GEOSSAV. The first register (Fig. 6, top left hand side) is used for hard data input *{Hard Input Data}* and soft data input *{Soft Input Data}*, data output, and output control *{Output}*.
The column numbers for the x, y, and z coordinates and the variable to be simulated have to be specified. One or two of the coordinate column numbers can be set to zero, which indicates that the simulation is 2D or 1D. The range of data values can be reduced, and all values strictly less than the lower trimming limit and strictly greater than the upper trimming limit are ignored *{Trimming limits}*.

Soft information pertaining to continuous variables (cdf data) should steadily increase form 0 to 1, and soft information pertaining to categorical variables (pdf data) must be between 0 and 1 and the sum equal to 1. If the Markov-Bayes option *{Markov-Bayes simulation}* for cokriging with soft indicator data is activated, then the $B(s)$ calibration parameters have to be specified (see Bivariate calibration of soft data). The soft indicator data, i.e. the prior probability pdfs of type Eq. (7), are derived from calibration scattergram using the module bicalib. Fig. 7 shows the dialog box for the module bicalib 2.000 in GEOSSAV, calling for secondary and calibration data values. The secondary data file *{Secondary data}* contains secondary data that have to be integrated in the stochastic simulation. The calibration data file *{Calibration scatterplot}* contains pairs of primary and secondary data as well as declustering weights. The cutoffs or categories of the primary and the secondary variable has to be specified *{Thresholds}*. The module bicalib computes the prior distributions and the $B(s)$ calibration parameters. The prior distributions are written into an output file *{Output}* and the $B(s)$ parameters are written into a reporting file from which they must be transferred to the sisim parameter file.

The number of realizations *{Number of realizations}* to be generated as well as a random number *{Seed}*, which is used to determine the random path through all of the grid nodes of each realization, is entered in the first register (Fig. 6, top left hand side). For output control a debugging file is written, depending on the debugging level.

The second register (Fig. 6, top right hand side) includes the kriging options and the search parameters. The kriging options *{Options}* specify the variable type (continuous or categorical variable), the kriging type (SIK or OIK), and whether a full indicator kriging is performed at each grid node to establish the conditional distribution *{IK flag}*. If a median indicator kriging is performed, then the variogram corresponding to the selected cutoff or category *{Cut/Cat}*, respectively, is used for all cutoffs or categories. Only one kriging system needs to be solved, and, therefore, the computing time is significantly reduced.

The search parameters *{Search Parameters}* specify the maximum number of original data, the maximum number of original data per octant, the maximum number of soft data, and the maximum number of previously simulated nodes that will be used to simulate another grid node. If the data are not assigned to nodes *{Assign data to nodes}*, then the data and previously simulated grid nodes are searched separately. The data is searched with a super block search and the previously

Fig. 7. *Dialog box for the bivariate calibration of soft data, used for specifying the secondary and calibration data required to compute the B(s) calibration parameters that are needed in the sequential indicator simulation program sisim if the Markov-Bayes option is selected.*

simulated nodes are searched with a spiral search. If the data are assigned to nodes, then a spiral search is used. If a multiple grid search will be performed *{Multiple grid search}*, then the grid will be refined depending on the refinement number to be specified, otherwise a standard spiral search will be considered. Details of the search strategies can be found in Deutsch and Journel (1998). In addition, the search parameters also specify the orientation and the radii of the search ellipsoid *{Search Radii / Search angles}* containing the data and the previously simulated nodes used for a node simulation.

In the third register (Fig. 6, bottom left hand side) the variogram information used for the simulation has to be entered *{Variograms}*. The number of cutoffs or categories, the cutoff values or category codes, and the global cdf or pdf values are specified in a tabular format. For each cutoff or category the isotropic nugget constant and for each nested variogram structure: the structure model (spherical model, exponential model, gaussian model, power model, hole effect model), the sill contribution, the anisotropy angles, the maximum and minimum horizontal and the vertical range defining the geometric anisotropy have to be specified (Deutsch and Journel, 1998, fig. II.4). More structure models can be added using the + button above the table. There is no need to standardize the variogram to a unit sill since only the relative shape of the variogram affects the kriging weights.

The last register (Fig. 6, bottom right hand side) includes extrapolation information and grid conventions. The extrapolation information *{Extrapolation}* is only used when considering continuous variables. The minimum and maximum data values have to be entered, the extrapolation of the lower and upper tail of the distribution as well as the interpolation within the middle of the distribution have to be specified. The possible types of interpolation / extrapolation schemes used for going beyond a discrete cdf are: (1) linear interpolation between
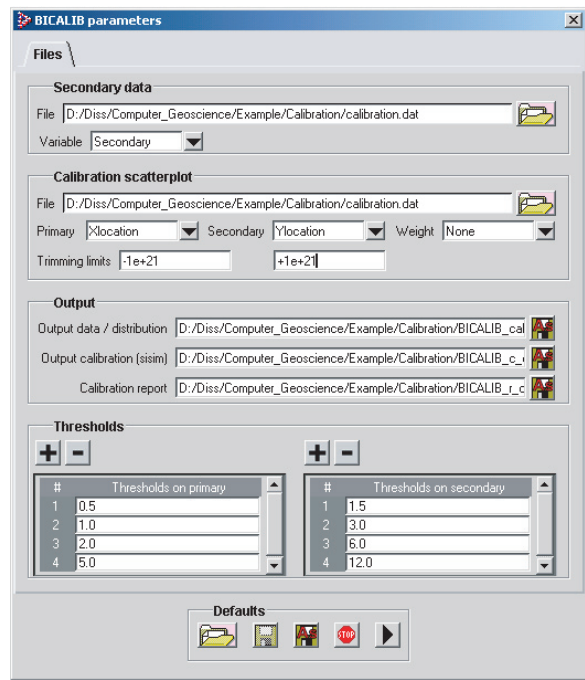
bounds, (2) power interpolation between bounds, (3) linear interpolation between tabulated quantiles, and (4) hyperbolic extrapolation at the upper tail (Deutsch and Journel, 1998). The parameter refers to the power if the power model interpolation is selected. If linear interpolation between tabulated quantiles is selected for any of the three regions, a file with tabulated values has to be read, specifying the column numbers for the values and declustering weights. If declustering weights are not used, the class probability is split equally between the subclasses defined by the tabulated values.

The grid convention *{Grid Definition}* adapted for the simulation is the following: *x* axis is associated with East, grid node indices increase from 1 to *nx* in the positive *x* direction; *y* axis is associated with North, grid node indices increase from 1 to *ny* in the positive *y* direction; and *z* axis is associated with elevation, grid node indices increase from 1 to *nz* in the positive *z* direction. Consequently, the grid represents a relative coordinate system. The coordinate system is established, specifying the number and size of grid cells in *x*, *y*, and *z* direction, and the coordinates at the center of the first cell. For a site-specific problem, the three axes can be associated to any absolute coordinate system that is appropriate. Therefore, a coordinate transformation must be performed.

4. Visualization methods

The OpenGL API, which is an open standard, is integrated into GEOSSAV for 3D rendering and slicing perpendicular to the main coordinate axis. OpenGL is a software interface that allows the rendering of 2D and 3D graphics images, works independently of the platform (Win32, MacOS, and virtually all variants of Unix), and uses available hardware acceleration as provided by modern graphics adapters. OpenGL is a depth buffer based rendering system for hidden surface removal (Wright and Sweet, 2000). It supports different shading models and texture mapping. The geometrical model has to be built of primitives such as points, lines, and polygons. The surface properties of these primitive objects can be adjusted in terms of color, reflectance, shininess, etc. It incorporates both orthonormal and perspective viewing models for adjusting the virtual camera. The rendered scene is lighted by one or more virtual light sources whose type, color, brightness etc. can be adjusted. Due to hardware acceleration, even complicated 3D models can be manipulated interactively (rotation, zoom, and pan). Details of OpenGL programming and matrix mathematics can be found for example in Fosner (1997) and Wright and Sweet (2000).

In addition, selected planes perpendicular to the main coordinate axis are visualized in scaled size. This allows a detailed visual analysis of single slices and, by continuous slicing through the simulated volume, of the completely simulated property field.

5. Data export options

The export modules generate files that specify the spatial distribution of hydraulic parameters (e.g., hydraulic conductivity, porosity) as either: (1) ASCII matrix files which characterize properties of single model layers or (2) block-centered flow (bcf) package files for the complete 3D flow model set-up for MODFLOW-based (Harbaugh and McDonald, 1996) groundwater simulation systems. The ASCII matrix and the bcf files can be loaded into 2D or 3D finite-difference groundwater model systems (e.g., ASMWIN (Chiang et al., 1998); GMS (Environmental Modeling Systems Inc., 2002); PMWIN (Chiang and Kinzelbach, 2001)) and can be used for flow and transport simulations.

Data export implementation

Fig. 8 shows the options for generating export files depending on the variable type used in the stochastic simulation, and Fig. 9 shows the corresponding dialog box for the export of bcf files. The simulation input file *{Simulation Input}* contains the output data from the stochastic simulation: in case of continuous variables, already the distribution of parameter values under study (e.g., hydraulic conductivity, porosity); in case of categorical variables, the distribution of simulated categories such as lithofacies types. If the variable type is continuous, no replacement has to be made. The parameter values of the stochastic simulation are written directly either into ASCII matrix or into bcf files depending on the selected export module. If the variable type is categorical, first the spatial distributed lithofacies types have to be replaced by hydraulic parameter values (e.g., hydraulic conductivity, porosity); subsequently the corresponding values will be written either into ASCII matrix or into bcf files *{Characterization Input}*.

The replacement of the spatial distributed lithofacies types by hydraulic parameter values is done using a random generator from Press et al. (1988). The input mean values and standard deviations of the hydraulic parameters and lithofacies types have to be specified as logarithm values. The simulated lithofacies types can be replaced either by the mean values or by random values generated from the defined distributions. The output values are not given as logarithm values. For data export an existing bcf file is taken to create several bcf files corresponding to the data of the stochastic simulation and the export parameters *{Modflow Input / Output}*. For subsequent external flow simulations, MODFLOW requires either hydraulic conductivity or transmissivity values depending on the layer type of each model layer (Harbaugh and McDonald, 1996). For models with more than one model layer, MODFLOW requires the input of the vertical conductance term between two model layers, known as vertical leakance (vcont). In order to export bcf files, the vcont arrays have to be
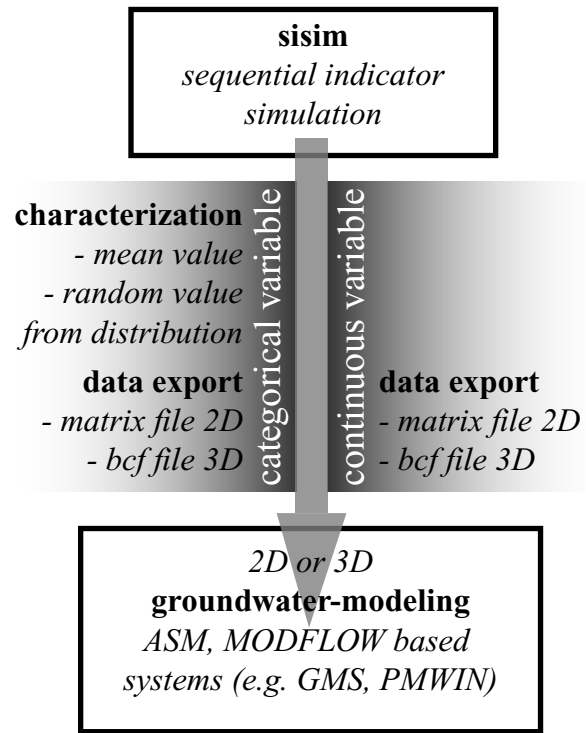
Fig. 8. *Options for generating export files depending on the variable type used in the stochastic simulation. Categorical variables (lithofacies) have to be replaced by a property under study (e.g., hydraulic conductivity), each lithofacies characterized by mean value and standard deviation. The export programs generate either (1) ASCII matrix files for the characterization of single model layers or (2) block-centered flow (bcf) package files for the characterization of the complete 3D flow model set-up for MODFLOW based groundwater simulation systems.*

Fig. 9. *Dialog box for the export of block-centered flow (bcf) package files. An existing bcf file is taken to create several bcf files corresponding to the simulation and characterization input parameters.*

calculated for all layers except the bottom layer, because MODFLOW assumes that the bottom layer is underlain by impermeable material. Vcont is calculated using the following equation (Chiang and Kinzelbach, 2001):

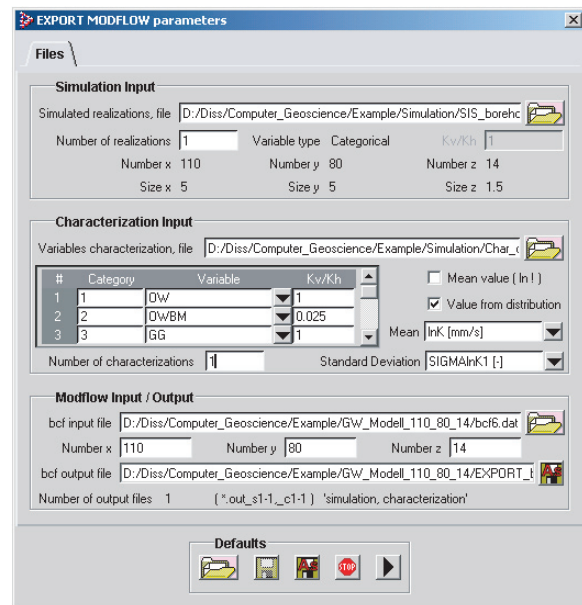$$vcont = \frac{2}{\dfrac{\Delta V_l}{(K_z)_{j,i,l}} + \dfrac{\Delta V_{l+1}}{(K_z)_{j,i,l+1}}}$$ (13)

where ΔV_l and ΔV_{l+1} are the thicknesses of layers l and $l+1$, and $(K_z)_{j,i,l}$ and $(K_z)_{j,i,l+1}$ are the vertical hydraulic conductivities of column j, row i, and layers l and $l+1$, respectively. If the variable type is categorical, the ratio of vertical to horizontal hydraulic conductivity of each single category is considered. If the variable type is continuous, a global ratio of vertical to horizontal hydraulic conductivity is considered. The remaining data of the read bcf file is taken on as it is.

When selecting ASCII matrix files for 3D data export, properties of the subsurface are exported in single model layers. Vertical and horizontal information has to be exported separately and the vertical conductance has to be calculated running MODFLOW.

6. Example

6.1. Data

GEOSSAV was applied to generate the aquifer structures of a well capture zone (in the order of several hundred of meters). The structures were simulated on a 550 m x 400 m x 22 m grid and subsequently exported to a finite-difference groundwater flow and advective transport model to simulate a river restoration pilot project in the region of Basel, Northwestern Switzerland. Particularly, the groundwater simulation of this portion of the Rhine/Wiese aquifer, described in Regli et al. (2003), includes simulation of changing well capture zones depending on subsurface heterogeneity, hydrologic variations, water supply operation data, and progress of river restoration.

The study site is located in the area of the ancient confluence of the main river Rhine (with flow to the Northwest) and its tributary Wiese (with flow to the Southwest). The average discharge of the river Rhine over the last 110 years amounts to 1'052 m³/s and is therefore around 90 times larger than the average discharge of the tributary Wiese with 11.4 m³/s over the last 68 years (Bundesamt für Wasser und Geologie, 2001).

Drill-core data from five boreholes and georadar data from 14 vertical georadar sections (total length of all sections 3'040 m) have been examined. The unconfined aquifer consists of Quaternary unconsolidated coarse alluvial deposits. Tertiary marls underlie these gravels and are considered impermeable for the purposes of the model. The aquifer thickness varies between 13 and 18 meters. The lower 80% of the aquifer consists of Rhine gravel and the upper 20% of Wiese gravel (Zechner et al., 1995). This may be explained as due to the reworking of the Wiese gravel by the river Rhine under landscape-shaping conditions whereby the top sequence of Wiese gravel would be preserved until the next shift of the active channel area of the river Rhine. The Rhine and Wiese sediments are easily distinguished lithologically because the sediments come from different source areas with distinct geological units. Also, within these two stratigraphic units a number of sedimentary structures are recognized that were generated by sedimentary processes in the braided fluvial system. Lithofacies types associated with the sedimentary structures for this area include (Regli et al., 2002): open-framework gravel (OW),
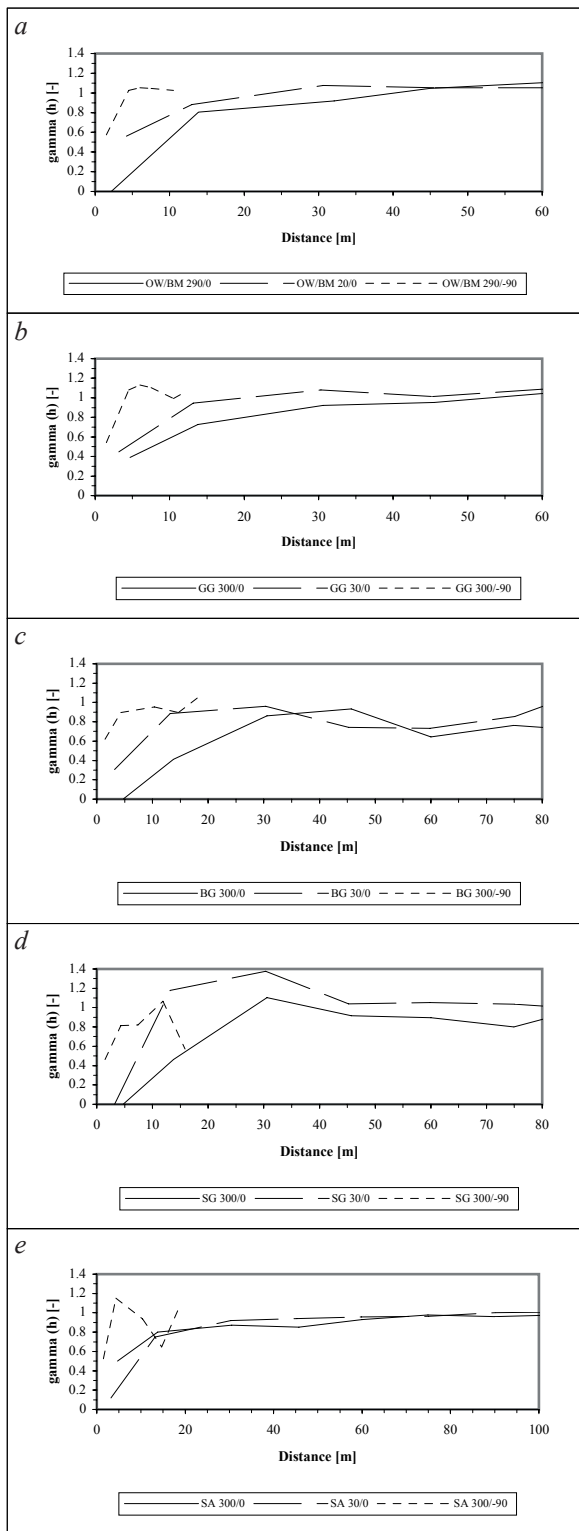
Fig. 10. *Experimental indicator variograms of (a) OW/ BM: open-framework/bimodal gravel couplets, (b) GG: gray gravel, (c) BG: brown gravel, (d) SG: silty gravel, and (e) SA: sand. The directional variograms are given for specified azimuth and dip (e.g., 240/0) which characterize the geometric anisotropy of the sedimentary structure types. The parameters of the model variograms are given in Table1.*

open-framework/bimodal gravel couplets (OW/BM), gray gravel (GG), brown gravel (BG), alternating gray and brown gravel layers (GG/BG), horizontally layered or inclined, silty gravel (SG), sand lenses (SA), and silt lenses (SI).

For the georadar investigations, described in Regli et al. (2002), a pulseEKKO IV georadar system with a 1'000 V transmitter was used (Sensors & Software Inc., 1993). The transmitting and receiving antennae were separated by 2 m and the recording step size was 0.25 m. The 50 MHz antennae used for this study allow recognition of the basal aquiclude surface, the main erosion boundaries within the coarse alluvial deposits, and the larger sedimentary structures down to the aquiclude at approximately 13-18 m depth. According to Jol and Smith (1991) and Huggenberger (1993), the vertical resolution depends on the georadar-wave frequency and is equal to a quarter of the wavelength, or 0.5 m in this case. Due to the relatively long wavelengths of the 50 MHz antennae, few transitions of alternating sequences of open-framework and bimodal gravel may be distinguished on the georadar sections. However, the main sedimentary structures as described above could be delineated.

The drill-core and georadar data are interpreted based on Regli et al. (2002). This lithofacies-based interpretation of hard outcrop, soft drill-core and georadar data respects differences in data uncertainty and provides lithofacies probabilities for points along boreholes and grid nodes with arbitrary mesh sizes in horizontal and vertical direction along georadar sections. The locations of the boreholes and the traces of the georadar sections used for the simulation are shown in the visualization window of Fig. 2. The sampled data from the georadar sections are at nodes of grids separated by 10 m x 1.5 m. In this case, the proportion of sampled aquifer material represented by drill-core compared with georadar data is about 1:90.

Table 1. *Variogram information of Rhine and Wiese gravel used for the sequential indicator simulation to define the geometric anisotropy of the sedimentary structure types: OW: open-framework gravel, OW/BM: open-framework/ bimodal gravel couplets, GG: gray gravel, BG: brown gravel, GG/BG-horizontal: alternating gray and brown gravel, horizontally layered, GG/BG-inclined: alternating gray and brown gravel, inclined, SG: silty gravel, SA: sand, SI: silt. Values in italics are estimates since adequate data for reliably computing proportions was not available for these lithofacies; [a] data from Rauber et al. (1998), valid for Rhine gravel aquifers in Northeastern Switzerland; the isotropic nugget constants are 0.1; the Cc values (variance contribution of nested variogram structures) are 0.9; the variogram models are exponential; the dips and plunges are 0.*

Sedimentary structure type / Variogram parameter	OW	OW/BM	GG	BG	GG/BG horizontal	GG/BG inclined	SG	SA	SI
Probability density function [a]	0.019	0.053	0.094	0.158	0.578	0.044	–	0.050	0.004
Probability density function	*0.02*	0.06	0.13	0.05	*0.50*	*0.05*	0.03	0.15	*0.01*
Azimuth [°]	*300*	290	300	300	*300*	*300*	300	300	*300*
Max. horiz. range [m]	*3*	40	53	60	*80*	*8*	40	115	*3*
Min. horiz. range [m]	*1.5*	26	22	35	*40*	*4*	15	70	*1.5*
Vertical range [m]	*0.5*	4	4	10	*10*	*2*	9	4	*0.5*

6.2. Variogram computation and indicator simulation

The variogram computation is based on the drill-core and georadar data. The data interpretation method of Regli et al. (2002) provides lithofacies probabilities for drill-core and georadar data. The indicator transform at grid node location is set to 1 for the lithofacies types with the greatest probability values, 0 otherwise. The experimental indicator variograms of open-framework/bimodal gravel couplets, gray gravel, brown gravel, silty gravel, and sand are shown in Fig. 10. The directional variograms, given for specified azimuth and dip, characterize the geometric anisotropy of the sedimentary structure types. They indicate orientations and ranges corresponding to maximum and minimum horizontal and vertical distances of spatial correlation. Variogram information for the nine sedimentary structure types in the study area is given in Table 1. The lithofacies proportions are based on the data density representing a specific structure type. The values written in italics are estimated because the corresponding structure types never have the greatest probabilities and, therefore, the indicator transform is always set to 0 by default for these structure types. The orientation of the sedimentary structure types represents the dominance of the main flow direction of the river Rhine. The relatively large ranges of spatial correlation may be significantly influenced by the resolution of the georadar system and by the density of the sampled data taken from the georadar sections.

Fig. 11 shows a realization of the sequential indicator simulation, visualized within the OpenGL window (Fig. 11, above on the left hand side), and a sectional detail of the XY-plane (Fig. 11, above on the right hand side). The visualization is managed by selecting the left mouse button for 3D rendering, the right mouse button for zooming, the checkboxes for plane selection within the OpenGL window, the sliders for continuous slicing through the simulated volume, and the selection boxes for plane views perpendicular to coordinate axes.

Some of the parameter values used for this realization can be found in Fig. 6 and Table 1. The regular model grid is defined by 110 x 80 x 14 cells with cell sizes of 5 m x 5 m x 1.5 m. The simulated model reproduces the lithofacies proportions with an accuracy of ± 10%. Since the conditional probabilities were estimated by indicator kriging with given indicator variograms, the simulated values taken altogether will reproduce those variograms. The lithofacies types are replaced by hydraulic parameters, where the values are generated randomly based on the defined statistical description. Finally, files are generated and exported for use in groundwater flow and transport simulation models.
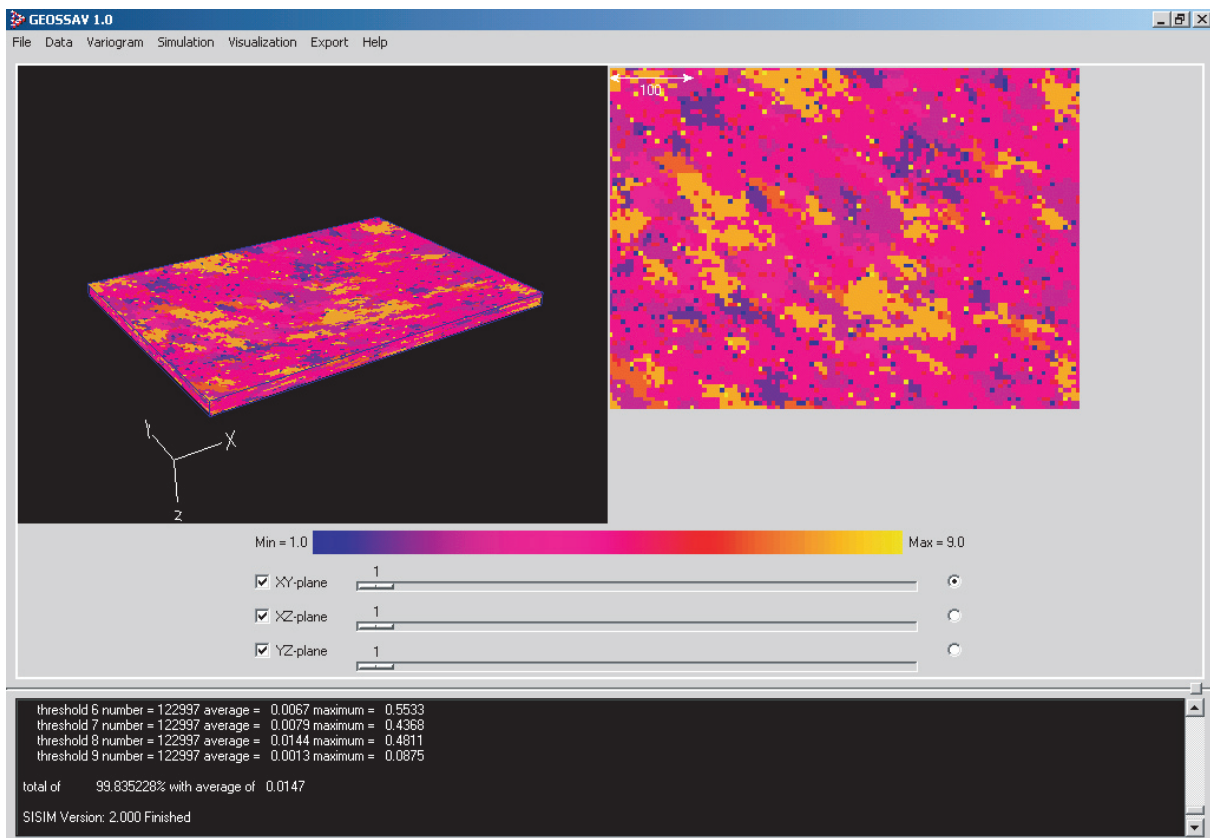
Fig. 11. *Realization of the sequential indicator simulation, visualized within the OpenGL window, and a sectional detail of the XY-plane. The visualization is managed by the control panel, and by the left and right mouse buttons.*

6.3. Discussion

When using the indicator kriging approach for generating parameter distributions, prior data should have regular spatial density. A local accumulation of data points within a particular sedimentary structure type leads to a biased amplified proportion of this type. In such cases, one should first decluster the data (e.g., with the module 'declus' (Deutsch and Journel, 1998)) or choose a uniformly grid pattern for sampling. The grid should be as regular as possible.

If there are many lithofacies types of very small proportions, the reproduction of such small lithofacies proportions is difficult in simulated models. Therefore, the criterions to reject a simulated model have to consider this problem.

In the example shown in Fig. 11, the current main direction of groundwater flow, the directions of hydraulic gradients and the direction of the river Wiese are oriented approximately parallel to the x axis. The geological stuctures, however, show an anisotropy of about 35° to the x axis. Such information is important e.g., for modeling river-groundwater interaction and determination of well capture zones.

The geometric anisotropy of the sedimentary structures was characterized based on data of the entire aquifer. However, changes in orientation and ranges of sedimentary structures may occur due to the interactions of the two rivers over time. Those modifications could be included in the model by partitioning the aquifer vertically into two hydrostratigraphic units. This is actually done in Regli et al. (2003).

7. Conclusions

GEOSSAV is described as a tool for the integration of hard and soft geological and geophysical data in the stochastic simulation and visualization of hydrogeological properties of the subsurface. The implemented software packages (bicalib, gamv, vargplt, and sisim from GSLIB plus OpenGL) support subsurface characterization from data processing through simulation and visualization to final control and data export to external finite-difference groundwater simulation systems (e.g., ASM, MODFLOW based systems).

In particular GEOSSAV allows to model categorical variables such as lithofacies types and continuous variables such as distributions of hydraulic properties. The distinguished lithofacies can be explained based on depositional processes (e.g., fluvial sediment sorting processes). For many practical hydrogeological problems such as determination of well capture zones or risk estimation of groundwater pollutants due to contaminated sites, not only statistical distributions of lithofacies are required but also site-specific structural information. The presented methods allow integration of site-specific structural information into a framework of stochastic description of geological structures.

Although the given example includes a characterization of the simulated geological structures by hydraulic parameters, GEOSSAV can definitely be used for other applications such as groundwater and/or soil contamination, site remediation, air pollution, and ecology. In fact, whenever stochastic solutions are preferred to solve site-specific heterogeneity problems, GEOSSAV can be used as a user-friendly and adequate software solution.

GEOSSAV has been successfully tested on Microsoft Windows NT 4.0/2000/XP and on SuSE Linux 7.3, and has already been applied successfully to hydrogeological problems. Due to the Tcl/Tk integration platform and development environment as well as the modular set-up, GEOSSAV can be easily upgraded and adapted to specific problems, which may be solved using geostatistical methods. The current version of GEOSSAV is available at http://www.unibas.ch/earth/pract.

8. Hardware and software requirements

GEOSSAV may be operated on Windows and on most kinds of Unix based operating systems. The following hardware components are required:

- PC with at least a Pentium II processor running Windows NT 4.0 or higher, or SuSE Linux 7.3 or higher;

- 24-bit color graphics card or better;

- 64 MB or more Ram; and

- 5 MB or more hard disk space.

Tcl/Tk is the software environment that embeds the implemented applications for hydrogeological analysis and allows an integrated use of them. The following open-source software is required to run GEOSSAV:

- Tcl/Tk, release 8.4. Tcl is an extensible scripting language and library. Tcl was chosen due to its easy development environment, its cross-platform deployment, and its ability to embed codes written in other programming languages. Tk is a graphical user interface and is shipped

as an extension with all distributions of Tcl. To enable the writing of graphical applications at the script level, the stand-alone interpreter wish (windowing shell) is provided.

- [incr Tcl], release 3.2. The [incr Tcl] extension is an object-oriented extension for Tcl. Objects are organized into classes with identical characteristics that can inherit functionality from one another. This helps to organize the code into modules that are easier to understand and maintain, and, therefore, larger Tcl/Tk applications can be built.

- [incr Tk], release 3.2. The [incr Tk] extension is an object-oriented framework for building mega-widgets using the [incr Tcl] object system. Mega-widgets are high-level widgets such as a file browser or a tabbed notebook.

- [incr Widgets], release 3.0.0. The [incr Widgets] extension is a set of mega-widgets that are included with the [incr Tcl] object system and the [incr Tk] mega-widget framework. This extension comes bundled with the [incr Tcl] distributions.

- TkTable, release 2.7. The TkTable extension is a full-featured 2D table widget extension for Tk. It supports images, embedded windows, and much more.

- OpenGL, release 1.1. OpenGL is an open, standardized API for 3D rendering, possibly with hardware acceleration. It was chosen because of its cross-platform functionality. The OpenGL code has been integrated into GEOSSAV with a Tcl/Tk extension written in C.

The distributed GEOSSAV executable (which is platform dependent with different versions for the Win32 and Linux platform but sharing the same code base for all platforms) automatically calls all the necessary Tcl/Tk scripts.

9. Distribution information

GEOSSAV is distributed electronically at no cost. The current version is available at http://www.unibas.ch/earth/pract. The package includes everything needed to run GEOSSAV including the current version of GEOSSAV and all the necessary open-source Tcl/Tk interactive-environment software. Although the authors cannot provide any professional support service, they welcome comments and will attempt to respond to questions regarding the software and its application. The authors neither guarantee the integrity nor the proper performance of the software.

10. Further developments

GEOSSAV is useful for many applications in earth sciences and other subsurface investigations because its main target is the simulation and visualization of heterogeneous subsurface properties using hard and soft data. Consequently, we plan to upgrade GEOSSAV with: (1) additional methods for data analysis (e.g., change of coordinate systems, declustering of data); (2) interactive curve fitting for selecting variogram models based on experimental variograms generated from field data; (3) subsurface characterization (e.g., Monte Carlo analysis) and; (4) the option to export additional data files for finite-difference groundwater flow and transport systems. In addition, we anticipate the implementation of a design tool in GEOSSAV that will allow fully object-oriented visualization of model data and simulated structures, which can be added in any order to the display.

Acknowledgments

References

Ayyub, B.M., Gupta, M.M., 1997. Uncertainty Analysis in Engineering and Sciences – Fuzzy Logic, Statistics, and Neural Network Approach. Kluwer Academic Publishers, Boston, 400pp.

Beres, M., Huggenberger, P., Green, A.G., Horstmeyer, H., 1999. Using two- and three-dimensional georadar methods to characterize glaciofluvial architecture. Sedimentary Geology 129, 1-24.

Bundesamt für Wasser und Geologie, 2001. Hydrologisches Jahrbuch der Schweiz 2000. Eidgenössisches Departement für Umwelt, Verkehr, Energie und Kommunikation, Bern, 435pp.

Chiang W.-H., Kinzelbach, W., Rausch, R., 1998. Aquifer Simulation Model for Windows – Groundwater flow and transport modeling, an integrated program. Gebrueder Borntraeger, Berlin, 137pp.

Chiang, W.-H., Kinzelbach, W., 2001. 3D-Groundwater Modeling with PMWIN – A Simulation System for Modeling Groundwater Flow and Pollution. Springer, Berlin, 346pp.

Deutsch, C.V., Journel, A.G., 1998. GSLIB: Geostatistical Software Library and User's Guide, 2nd edn. Oxford University Press, Oxford, 369pp.

Environmental Modeling Systems Inc., 2002. GMS: Groundwater Modeling System. http://www.ems-i.com.

Fosner, R., 1997. OpenGL Programming for Windows 95 and Windows NT, 2nd pr. Addison-Wesley Developers Press, Reading, Massachusetts, 259pp.

Furger, G., 1990. Von der Geologie zum Stofftransportmodell. Dissertation Nr. 9356, Eidgenössische Technische Hochschule, Zürich, 164pp.

Harbaugh, A.W., McDonald, M., 1996. User's documentation for MODFLOW-96, an update to the U.S. Geological Survey modular finite-difference ground-water flow model. U.S. Geological Survey Open-File Report 96-485, Reston, Virginia, 56pp.

Harrison, M., 1997. Tcl/Tk Tools. O'Reilly & Associates, Inc. Cambridge, 653pp.

Huggenberger, P., 1993. Radar facies: recognition of facies patterns and heterogeneities within Pleistocene Rhine gravels, NE Switzerland. In: Best, C.L., Bristow, C.S. (Eds.), Braided Rivers. Geological Society, Special Publication 75, London, 163-176.

Hess, K.M., Wolf, S.H., Celia, M.A., 1992. Large-scale natural gradient test in sand and gravel, Cape Cod, Massachusetts, 3. Hydraulic conductivity and calculated macrodispersivities. Water Resources Research 28 (8), 2011-2027.

Isaaks & Co., 2001. SAGE2001. A Spatial and Geostatistical Environment for Variography. http://www.isaaks.com.

Jol, H.M., Smith, D.G., 1991. Ground-penetrating radar of northern lacustrine deltas. Canadian Journal of Earth Sciences 28 (12), 1939-1947.

Ousterhout, J.K., 1994. Tcl and the Tk Toolkit, 9th pr. Addison-Wesley professional computing series, Reading, Massachusetts, 458pp.

Pannatier, Y., 1996. Variowin – Software for Spatial Data Analysis in 2D. Springer, New York, 91pp.

Poeter, E.P., McKenna, S.A., 1995. Reducing uncertainty associated with ground-water flow and transport predictions. Ground Water 33 (6), 899-904.

Press, W.H., Flannery, B.P., Teukolsky, S.A., Vellerling, W.T., 1988. Numerical recipes in C: the art of scientific computing. Cambridge University Press, Cambridge, 735pp.

Rauber, M., Stauffer, F., Huggenberger, P., Dracos, T., 1998. A numerical three-dimensional conditioned/unconditioned stochastic facies type model applied to a remediation well system. Water Resources Research 34 (9), 2225-2233.

Regli, Ch., Huggenberger, P., Rauber, M., 2002. Interpretation of drill-core and georadar data of coarse gravel deposits. Journal of Hydrology 255, 234-252.

Regli, Ch., Rauber, M., Huggenberger, P., 2003. Analysis of aquifer heterogeneity within a well capture zone, comparison of model data with field experiments: A case study from the river Wiese, Switzerland. Aquatic Sciences 65, 111-128.

Schafmeister, M.-Th., 1999. Geostatistik für die hydrogeologische Praxis. Springer, Berlin, 172pp.

Schroeder, W.J., Avila, L.S., Martin, K.M., Hoffman, W.A., Law, C.C., 2001. The Visualization Toolkit User's Guide. Kitware, Inc., 380pp.

Sensors & Software Inc., 1993. PulseEKKO Software user's guide. Sensors & Software Inc., Mississauga, Ontario, 120pp.

Sudicky, E.A., 1986. A natural-gradient experiment on solute transport in a sand aquifer: Spatial variability of hydraulic conductivity and its role in the dispersion process. Water Resources Research 22 (13), 2069-2082.

Weissmann, G.S., Carle, S.F., Fogg, G.E., 1999. Three-dimensional hydrofacies modeling based on soil surveys and transition probability geostatistics. Water Resources Research 35 (6), 1761-1770.

Wingle, W.L., Poeter, E.P., McKenna, S.A., 1997. UNCERT: A Geostatistical Uncertainty Analysis Package Applied to Groundwater Flow and Contaminant Transport Modeling. Colorado School of Mines, Golden, Colorado, 464pp.

Wright, R.S., Sweet, M., 2000. OpenGL Superbible, 2nd edn. Waite Group Press, Indianapolis, 696pp.

Zechner, E., Hauber, L., Noack, Th., Trösch, J., Wülser, R., 1995. Validation of a groundwater model by simulating the transport of natural tracers and organic pollutants. In: Leibundgut, Ch. (Ed), Tracer Technologies for Hydrological Systems. International Association of Hydrological Sciences Publication 229, 57-64.

Analysis of aquifer heterogeneity within a well capture zone, comparison of model data with field experiments: A case study from the river Wiese, Switzerland

Christian Regli [a], Martin Rauber [b] Peter Huggenberger [a]

[a] *Department of Earth Sciences, Applied and Environmental Geology, University of Basel, Bernoullistr. 16, 4056 Basel, Switzerland*

[b] *Rauber Consulting, Technoparkstr. 1, 8005 Zürich, Switzerland*

Analysis of aquifer heterogeneity within a well capture zone, comparison of model data with field experiments: A case study from the river Wiese, Switzerland

Christian Regli [a], Martin Rauber [b], Peter Huggenberger [a]

[a] *Department of Earth Sciences, Applied and Environmental Geology, University of Basel, Bernoullistr. 16, 4056 Basel, Switzerland*

[b] *Rauber Consulting, Technoparkstr. 1, 8005 Zürich, Switzerland*

Abstract

This paper describes two groundwater models simulating a well capture zone in a heterogeneous aquifer located near an infiltrating river. A deterministic, large-scaled groundwater model (1.8 km x 1.2 km) is used to simulate the average behavior of groundwater flow and advective transport. It is also used to assign the boundary conditions for a small-scaled groundwater model (550 m x 400 m) which relies on stochastically generated aquifer properties based on site-specific drill-core and georadar data. The small-scaled groundwater model is used to include the large subsurface heterogeneity at the location of interest. The stochastic approach in the small-scaled groundwater model does not lead to a clearly defined well capture zone, but to a plane representation of the probability of a certain surface location belonging to the well capture zone. The models were applied to a study site, which is located in an area of artificial groundwater recharge and production, in Lange Erlen near Basel, Northwestern Switzerland. The groundwater at this site contributes to the city's drinking water supply, and the site serves as recreational area to the population of Basel. The river is channelized, but there are initiatives to restore the riverbank to more natural conditions. However, they conflict with the requirements of groundwater protection, especially during flood events. Therefore, a river section of 600 m in the vicinity of a unused and disconnected drinking water well was restored to study changes in the groundwater flow regime depending on hydrologic variations, water supply operation data, progress of river restoration, and subsurface heterogeneity. The results of the groundwater models are compared with data from two tracer experiments using Uranine and the natural Radon isotope Rn-222, and with physical, chemical, and microbiological data sampled in monitoring wells between the river and the drinking water well. The groundwater models document significant variations regarding the dimension of the well capture zone depending on changing boundary conditions and the variability of the hydraulic aquifer properties. The knowledge of the subsurface heterogeneity is important to evaluate transport times and distances of microorganisms from the infiltrating river or the riverbank to the drinking water well. The data from the monitoring wells show that the chemical and microbiological processes predominantly occur in the hyporheic interstitial zone and the riverbank within a range of a few meters up to a few 10s of meters from the river. The methods presented here can be used to define and evaluate groundwater protection zones in heterogeneous aquifers associated with infiltration from rivers under changing boundary conditions, and under the uncertainty of subsurface heterogeneity. Furthermore, they allow to study the site-specific operational alternatives associated with river restorations.

1. Introduction

The fluvial deposits of river valleys are commonly important groundwater aquifers for municipal water supplies. In Switzerland, approximately 42% of the total drinking water demand, which is about 1.1 billion m^3/y, is covered by pumped groundwater. These groundwater aquifers are recharged by precipitation and river infiltration, but the relative contributions have not been examined in detail. Many of the river valleys are relatively narrow; so wells for water supply systems are commonly located near rivers.

In densely populated areas where public open space may be used as recreational areas as well as groundwater protection areas with activity restrictions, numerical methods for comparative assessment of different operational alternatives become a valuable tool. Groundwater models play an important role in decision-making processes (Reichert and Pahl, 1999), especially in the context of better characterization of parameter distributions and prediction of dynamic behavior of a given system. Groundwater models are helpful tools to define well capture zones based on hydrogeological and water supply operation data (e.g., Kinzelbach et al., 1992; Lerner, 1992). They allow to study the sensitivity of the observed system with respect to changing parameters and conditions. However, groundwater models which do not consider site-specific geological information might not be acceptable for site-specific risk estimation of changing groundwater quality.

Vassolo et al. (1998), van Leeuwen et al. (1998), and others applied stochastic methods to cope with significant subsurface heterogeneity. The major advantage of the stochastic approach is its ability to account for uncertainty in the distribution of hydraulic aquifer parameters. In addition, stochastic methods can be used to check technical and operational measures on aquifers, to evaluate their effectiveness, or to evaluate measures for remediation of pollution (e.g., Rauber et al., 1998).

Model accuracy is strongly dependant on both the quantity and the quality of available data (Kinzelbach and Rausch, 1995). Data used in groundwater models may be divided into two basic types: ,hard data' and ,soft data' (Poeter and McKenna, 1995). Hard data (e.g., outcrop data, in some cases drill-core data) can be directly obtained and examined. There is uncertainty in hard data, but it is considered small enough to be ignored. Soft data (e.g., georadar data) are less precise thus greater uncertainties is associated with the soft data values. The problem of adequately modeling subsurface parameter distributions becomes more difficult with increasing heterogeneity and thereby increasing uncertainty with respect to the spatial variability of available data. The technique used to model subsurface structures in a site-specific problem should be chosen based on properties under consideration (e.g., lithofacies, hydraulic conductivity, porosity), available knowledge of the subsurface, and causes of uncertainty (Ayyub and Gupta, 1997; Weissmann et al., 1999). Considering these aspects, calculation, uncertainty estimation, and assessment of operational alternatives can be separated, the discussion in decision-making processes can be de-emotionalized, and discrepancies can be identified (Reichert and Pahl, 1999). A groundwater model based on geological data has accomplished its task, if the solution is robust, geologically and hydrologically resaonable, and if the actual parameter values differ only within a limited range from those of the model (Kinzelbach and Rausch, 1995).

Agricultural use of the floodplain, river corrections, and intensive hydroelectric power generation have deprived most Swiss perialpine rivers of their natural character. Excavation

and the construction of dams and steps have resulted in deeper and narrower river channels with no connection to the adjacent floodplain. Therefore, these rivers often function primarily as conduits for precipitation runoff and overflow sewage, rather than as a natural aquatic biosphere. Different recent initiatives concentrate on restoring at least part of the original biodiversity of former floodplains. According to new legislation in Switzerland, the groundwater shall be protected by prevention of water pollution and implementation of well capture zones, and the ecological value of the rivers shall be increased (Gewässerschutzgesetz, 1991). In many densely populated areas these ideas lead to conflicting opinions about the best use of public open space.
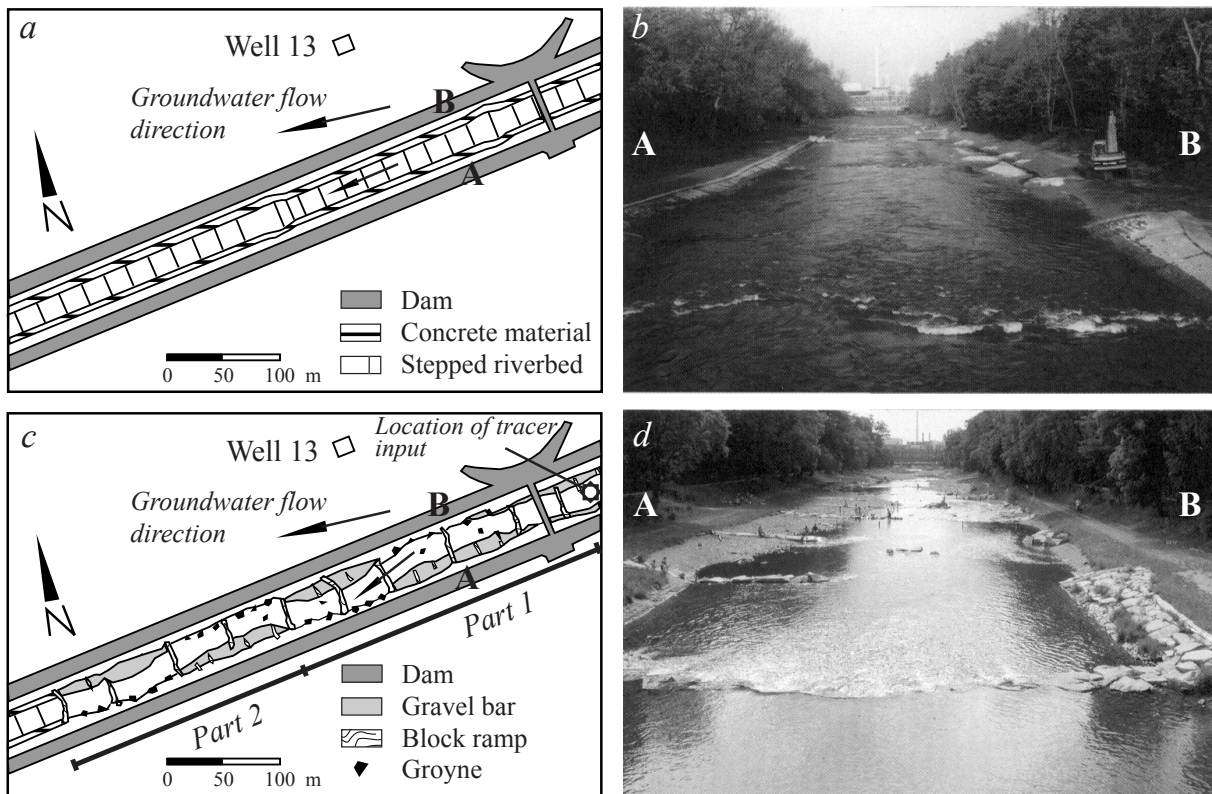
The protection zones legally established are coupled with the licensed extraction volume of groundwater. Most of the existing protection zones legally delineated, however, are not based on the analysis of the dynamic character of the river-groundwater interaction nor on the influence of subsurface heterogenity. The well capture zone is defined as the area from which about 90% of

Fig. 1. *Simplified geological overview of Basel area in Northwestern Switzerland and location of study site – at the lower end of the city's water supply area Lange Erlen – within the ancient confluence of main river Rhine and its tributary Wiese.*

the maximum extracted groundwater originates, assuming a low groundwater table (Gewässerschutzverordnung, 1998). This definition is valid only for time-independent systems. For most groundwater systems, however, the dynamics should be considered, especially if a specific well capture zone is not the only one in the groundwater-bearing formation. In that case, different individual well capture zones mutually compete and influence each other. If the groundwater is polluted by chemicals or particles which are not sufficiently reduced or adsorbed (e.g., hormone effective and endocrine substances, gasoline additives, microorganisms), or if there is a danger of pollution by such substances, the delineation of the well capture zones are of public interest (Gewässerschutzverordnung, 1998).

The main focus of this paper is to define and evaluate groundwater protection zones in heterogeneous aquifers associated with infiltration from rivers under changing boundary conditions, and under the uncertainty of subsurface heterogeneity. For such cases, methods presented here represent helpful tools for risk estimation of changing groundwater quality and quality management of water supplies, and for site-specific evaluation of operational alternatives for river restoration.

This paper starts with a description of the study site. Then deterministic and stochastic modeling of a well capture zone is presented depending on hydrologic variations, water supply operation data, progress of river restoration, and subsurface heterogeneity, including the generation of distributions of hydrogeological properties. This paper concludes with the comparison of results from groundwater models with two tracer experiments using Uranine and the natural Radon isotope Rn-222, and also with physical, chemical, and microbiological data, sampled in monitoring wells between the river and the drinking water well.
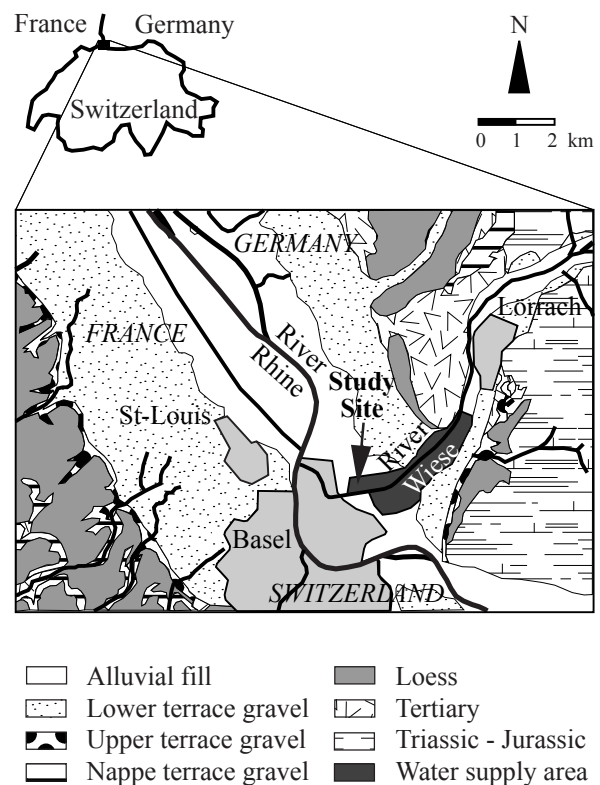
Fig. 2. *Part of river Wiese before and after restoration operation: (a) plan view and (b) photo of straightend and artificially stepped river; (c) plan view and (d) photo of restored river with improved lengthwise and crosswise connectivity through the replacement of steps with block ramps and concrete material with gravelled riparian zones. On the photos the flood protection dams are located within the woods.*

2. Site description

The Lange Erlen serves as recreational area for the population of the city of Basel, as groundwater resource providing a significant portion of the city's drinking water (45'000 m^3/d). This water supply system extends over more than 4 km along the river Wiese as shown in Fig. 1. The study site, at the lower end of the water supply area, is located in the ancient confluence of the main river Rhine (with flow to the Northwest) and its tributary Wiese (with flow to the Southwest).

The aquifer is artificially recharged with treated surface water (fast filtration) from the river Rhine. The water from the river Wiese or its artificial channels is not used to recharge the aquifer, because during the last 40 years, its water was of poorer microbiological quality than Rhine water. Meanwhile, the chemical and microbiological water quality of the river Wiese has improved.

The unconfined aquifer consists of Quaternary unconsolidated coarse alluvial deposits. Tertiary marls underlie these gravels and are considered impermeable for the purposes of the model. The aquifer thickness varies between 13 and 18 meters. The lower 80% of the aquifer consists of Rhine gravel (primarily limestone) and the upper 20% of the aquifer consists of Wiese gravel (primarily silicates and limestone; Zechner et al., 1995). This may be explained by reworking of the Wiese gravel by the river Rhine under landscape-shaping conditions whereby the top sequence of Wiese gravel will be preserved until the next shift of the active channel area of the river Rhine.

The average discharge of the river Rhine over the last 110 years is 1'052 m^3/s and is, therefore, around 90 times larger than the average discharge of the tributary Wiese with 11.4
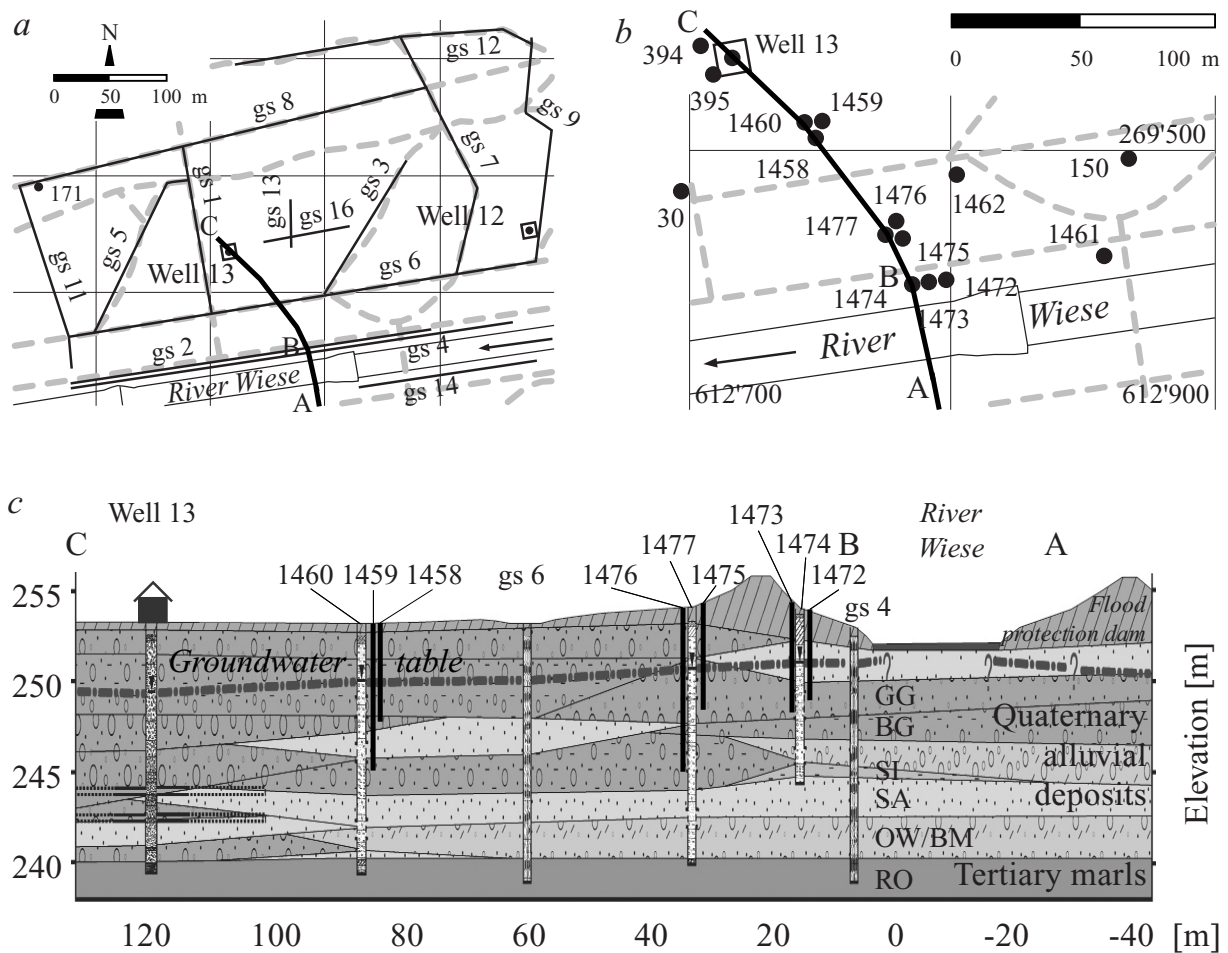
Fig. 3. Plan view of study site and vertical geological section: (a) traces of georadar sections (gs) and drinking water wells; (b) monitoring wells, partially grouped in clusters, sampling the upper, middle, and lower part of the aquifer; (c) vertical geological section (vertically enlarged by a factor of 3) along monitoring wells showing the subsurface heterogeneity within the capture zone of drinking water well 13.

m^3/s over the last 68 years (Bundesamt für Wasser und Geologie, 2001). The river Wiese has been channelized during the last century. Two dams at distances of 55-60 m protect the adjacent plain from flooding. The cross-section is double trapeziform, the actual river width is 20 m. Elevation change in the riverbed is achieved with incremental step hights of about 0.1 m, and the average slope is about 4.5‰.

The riverbed breaks up during floods. It was observed that an increase of the infiltration of river water into groundwater pollutes drinking water wells located near the rivers, especially during flood events. Therefore, river restoration conflicts with the safety requirements of the groundwater protection zones.

The riverbed within the study site has been restored because of its function as a recreational area. The restored section consists of two parts with a total length of approximately 600 m and includes 10 block ramps, 28 groynes, and 4 gravel bars. The weight of the built-in rock blocks was 3'180 tons; however, the volume of these blocks is smaller than that of the concrete material removed. Gravel was only redistributed, no additional gravel material was supplied. Fig. 2 shows the river Wiese before and after restoration operation. The restoration in part 2 is far enough downstream that it has no influence on any well capture zone.

For groundwater monitoring, 11 new boreholes were drilled along hypothetical groundwater flow paths between the river Wiese and drinking water well 13, which is located at a distance of about 120 m from the river and no more used for the water supply. Nine of the new boreholes

are grouped in clusters of three boreholes each as shown in Fig. 3. The boreholes have been drilled to specified aquifer depths. Monitoring wells 1458, 1472, 1473, and 1475 sample the aquifer about 1-2 m below the average groundwater table; monitoring wells 1459, 1461, 1462, and 1476 sample the middle part of the aquifer; and monitoring wells 1460, 1474, and 1477 sample the aquifer a few meters above the relatively impermeable Tertiary marls. Five drill cores covering the whole aquifer thickness have been described sedimentologically. These cores were used to calibrate the 14 vertical georadar reflection sections which were recorded in the vicinity of drinking water well 13 to characterize the subsurface heterogeneity.

The question whether and how river restoration might negatively affect groundwater quality were the objects of an accompanying investigation program. The field experiments as well as the regular and flood-event specific measurements are shown in Table 1.

Table 1. Investigation program accompanying the river restoration within the capture zone of drinking water well 13.

Investigation program	Before river restoration		After river restoration	
	regularly sampling (weekly)	event-specific sampling (daily)	regularly sampling (weekly)	event-specific sampling (daily)
Artificial tracer experiment: *Uranine*		X		X
Natural tracer experiment: *Radon-222*				X
Physical and chemical measurements: *DOC, O_2, pH, Ca, HCO_3, Temperature, Electrical conductivity, NH_4, NO_2, NO_3, PO_4, SO_4, Cl, Turbidity*	X	X	X	X
Microbiological measurements: *Heterotrophic plate counts, Escherichia coli, Enterococcus*	X	X	X	X

3. Aquifer and groundwater modeling

Groundwater flow and coupled advective transport were simulated with two different models using Processing Modflow (PMWIN) from Chiang and Kinzelbach (2001). Fig. 4 shows the situation. Section 3.1. describes the deterministic, large-scaled groundwater model which was used to simulate average groundwater flow and advective transport and allows to define boundary conditions for telescoped model areas. Section 3.2. describes the small-scaled groundwater model which relies on stochastically generated aquifer properties based on site-specific drill-core and georadar data.

3.1. Calibration and results of the large-scaled groundwater model

The large-scaled, two-layer finite-difference groundwater model has a total of 39'032 cells and covers an area of 1'800 m x 1'200 m. The cell size varies from 5 m x 5 m, within the zone of river restoration, to 20 m x 20 m. The model is divided in two layers having a thickness of approximately 4-8 m and homogeneous hydraulic parameters. Model boundary conditions are of the first type (fixed head boundary) along the Eastern and Western side, and of the third type (leakage boundary) along the river Wiese. The Northern and Southern sides are specified as no flow boundaries. The topography of the aquifer bottom (Tertiary marls) is interpolated from the top levels of the bedrock. The available data are based on the drill-core descriptions and georadar recordings.
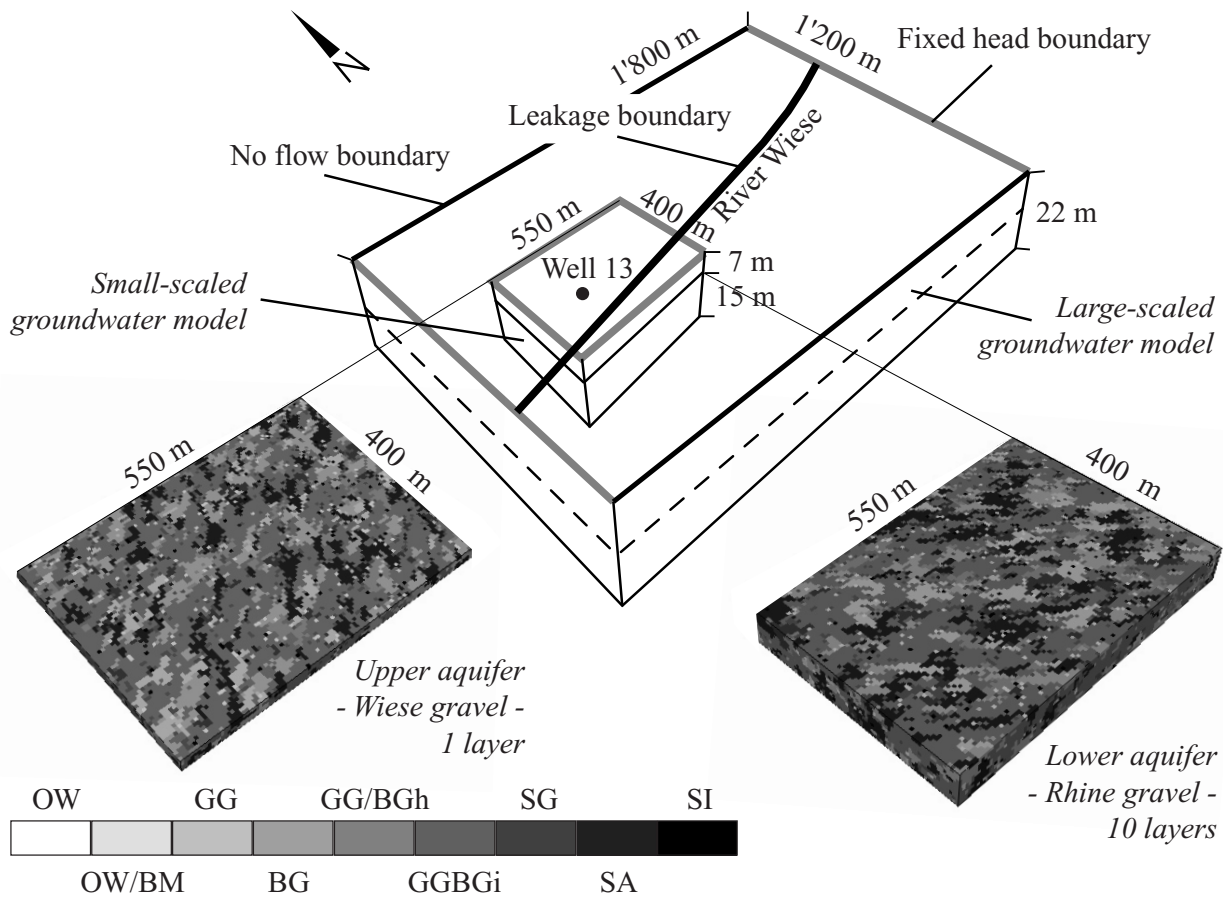
Fig. 4. *Situation of the large-scaled, homogeneous groundwater model and the small-scaled groundwater model, which relies on stochastically generated aquifer properties. OW: open-framework gravel, OW/BM: open-framework/bimodal gravel couplets, GG: gray gravel, BG: brown gravel, GG/BG-horizontal: alternating gray and brown gravel, horizontally layered, GG/BG-inclined: alternating gray and brown gravel, inclined, SG: silty gravel, SA: sand, SI: silt.*

The data-sensitive parameters of the steady-state, large-scaled groundwater model – the hydraulic conductivity of the two model layers and the leakage factor (Chiang and Kinzelbach, 2001) of the riverbed – are calibrated with data from December 9, 1998. The data are based on 69 groundwater head measurements, 4 river stage, and corresponding pumping and recharge rates. Solutions of the groundwater flow equation match the field head data with a mean squared deviation of 0.14 m^2. The calibrated hydraulic conductivity is 5.75 E-3 m/s for both the upper and lower layer. The leakage factor of the river Wiese is 1 E-6 /s.

Fig. 5 shows simulations of the capture zone of drinking water well 13 that was approximately determined by particle tracking for conditions before and after river restoration as well as for low river discharge, moderate and high floods. Fig. 5a represents the calibrated groundwater model. In Fig. 5b-f predictions under changed boundary conditions are given. The well capture zone is strongly influenced by changing river discharge and the structure of the riverbed. River restoration is simulated by increasing the leakage factor by a factor of 10 and 100, respectively, within the restored river channel, assuming moderate and strong increase of the hydraulic conductivity of the riverbed. The leakage factor of the artificially built gravel bars was not increased. The modeled infiltration of river water within the well capture zone varies between < 0.02 m^3/m^2/d (Fig. 5a) and > 3.06 m^3/m^2/d (Fig. 5f). Particularly at high flood events, the model results show a short travel time between the riverbed and the drinking water well 13.

Based on the large-scaled, homogeneous model results, the average groundwater residence time between the river Wiese and drinking water well 13 varies between 20 d (Fig. 5a) and 5
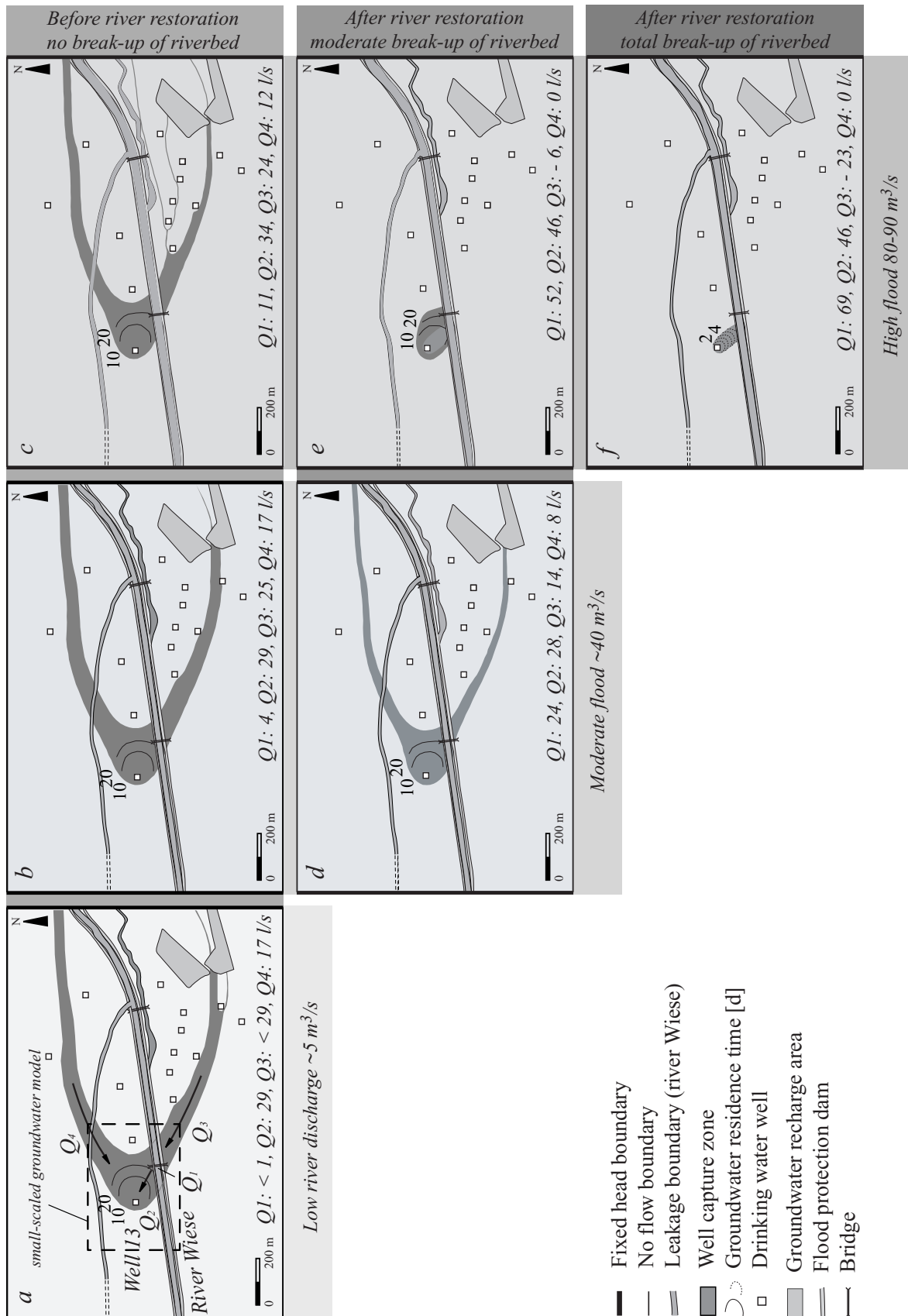
Fig. 5. *Changes of the capture zone of drinking water well 13 in the large-scaled groundwater model depending on river discharge, river restoration, and water supply operation data: (a,b,c) before river restoration; (d-f) after river restoration (increasing the leakage factor by a factor of 10 (d,e) and 100 (f)); (a) low river discharge (~5 m³/s); (b,d) moderate flood (~40 m³/s); (c,e,f) high flood (80-90 m³/s). The groundwater extraction at drinking water well 13 is constant at 0.046 m³/s. Water budgets within the well capture zone [l/s]: Q1: river leakage, Q2: horizontal groundwater flow (right side of river Wiese), Q3: horizontal groundwater flow (left side of river Wiese), Q4: horizontal groundwater flow (Northeastern of drinking water well 13).*

d (Fig. 5f). In general, it is expected that in restored rivers, break-up of the riverbed does not occur at the same time nor to the same extent as before river restoration. Therefore, particularly during flood events, the permeability of the riverbed will vary considerably because of both the higher discharge dynamics in restored rivers compared to channelized rivers and the temporal variability of zones with higher infiltration.

3.2. Generation of aquifer properties and results of the small-scaled groundwater model

At Basel about 3'000 drill-core descriptions from Basel are stored in a data base (Noack, 1993; Noack, 1997). This is a comprehensive source of information for site characterizations. For the generation of aquifer properties at the small scale, a combined sedimentological and geostatistical approach was chosen. The sedimentological approach is based on observations in unweathered outcrops and fluvio-dynamic interpretations of processes in a braided river system (Siegenthaler and Huggenberger, 1993; Jussel et al., 1994) and allows a lithofacies-based interpretation of drill-core and georadar data to provide conditioning data for the stochastic aquifer simulation (Regli et al., 2002). The geostatistical approach matches the sedimentary structures based on the conditioning data and the spatial correlation of the data values (e.g., Deutsch and Journel, 1998). The aquifer properties are then integrated into the small-scaled groundwater model for steady-state flow and coupled advective transport simulation. Observed groundwater heads are used to restrict the choice of aquifer realizations to those yielding acceptable simulated groundwater heads at the observation points.

3.2.1. Sedimentological and geophysical analysis of the Rhine/Wiese aquifer

As noted above the lithology of the Rhine and Wiese sediments is easily distinguished because the sediments are from different source areas which have distinct geological units. Within these two stratigraphic units a number of sedimentary structures are recognized that were generated by sedimentary processes in the braided fluvial system. Lithofacies associated with the sedimentary structures at this location include (Regli et al., 2002): open-framework gravel (OW), open-framework/bimodal gravel couplets (OW/BM), gray gravel (GG), brown gravel (BG), alternating gray and brown gravel layers (GG/BG), horizontally layered or inclined, silty gravel (SG), sand lenses (SA), and silt lenses (SI). The principal relationship of the lithofacies types and the sedimentary processes which form these structure types are described in Siegenthaler and Huggenberger (1993).

The boreholes and georadar investigations (Fig. 3) were made to delineate the main sedimentary structures as described above. The total length of the georadar sections is 3'040 m. The three-step method presented in Regli et al. (2002) was used to interpret the sedimentological and geophysical data. In the first step, the site-specific lithofacies scheme to classify sedimentary structure types is established based on outcrop data. In the second step, the probability that a drill-core layer description represents a certain lithofacies type is estimated. In the last step, drill-core layers and corresponding radarfacies types are related.

This lithofacies-based interpretation of drill-core and georadar data respects differences in data uncertainty and provides lithofacies probabilities for points along boreholes and for grid nodes with arbitrary mesh sizes along georadar sections. The sampled data from the georadar sections at this location are given for grid nodes separated by 5 m x 1 m.

3.2.2. Stochastic generation of aquifer properties

GEOSSAV (<u>Ge</u>ostatistical <u>E</u>nvironment f<u>O</u>r <u>S</u>ubsurface <u>S</u>imulation <u>A</u>nd <u>V</u>isualization) is a tool for the integration of hard and soft data into the 3D stochastic simulation and visualization of distributions of geological structures and hydrogeological properties in the subsurface (Regli et al., submitted). GEOSSAV was used to generate the sedimentary structures and the hydraulic aquifer properties in the vicinity of drinking water well 13, which are integrated into the small-scaled (550 m x 400 m x 22 m), eleven-layer finite-difference groundwater flow and advective transport model. GEOSSAV, as an interface to selected geostatistical programs from the Geostatistical Software LIBrary, GSLIB (Deutsch and Journel, 1998), can be used for data analysis, variogram computation of regularly or irregularly spaced data, and sequential indicator simulation of subsurface heterogeneities. The simulations can be visualized by 3D rendering and slicing perpendicular to the main coordinate axis. The data can be exported into regular grid-based groundwater simulation systems (e.g., GMS (Environmental Modeling Systems Inc., 2002); PMWIN (Chiang and Kinzelbach, 2001)).

The variogram computation is based on the drill-core and georadar data described in section 3.2.1. The variography was run separately for the lower part (Rhine gravel) and the upper part (Wiese gravel) of the aquifer. The indicator transform (Deutsch and Journel, 1998) at grid node locations is set to 1 for the structure types with the greatest probability values, or is set to 0 otherwise. Experimental indicator variograms are calculated for various directions (azimuth, dip, plunge). The resulting variogram information for the nine sedimentary structure types identified in the study site is given in Table 2. Azimuth, dip, plunge, and the ranges corresponding to maximum and minimum horizontal and vertical distances of spatial correlation characterize the geometric anisotropy of the sedimentary structure types (Deutsch and Journel, 1998). The initial probability density functions (Deutsch and Journel, 1998) are based on the data density representing a specific structure type. The values written in italics are estimated because the corresponding structure types never have the greatest probabilities and, thus, the indicator transform always would be set to 0 by default for these structure types.

Table 2. *Variogram information of Rhine and Wiese gravel used for the sequential indicator simulation to define the geometric anisotropy of the sedimentary structure types: OW: open-framework gravel, OW/BM: open-framework/bimodal gravel couplets, GG: gray gravel, BG: brown gravel, GG/BG-horizontal: alternating gray and brown gravel, horizontally layered, GG/BG-inclined: alternating gray and brown gravel, inclined, SG: silty gravel, SA: sand, SI: silt. The values written in italics are estimations; the isotropic nugget constants of the sedimentary structure types are 0; the variogram models are exponential; the dips and plunges of the sedimentary structures are 0.*

|	Sedimentary structure type / Variogram parameter	OW	OW/BM	GG	BG	GG/BG horizontal	GG/BG inclined	SG	SA	SI
Wiese gravel	Probability density function	*0.02*	0.05	0.16	0.05	*0.50*	*0.05*	0.02	0.14	*0.01*
	Sill	*0.13*	0.12	0.18	0.115	*0.13*	*0.13*	0.045	0.18	*0.13*
	Azimuth [°]	*240*	240	240	240	*240*	*240*	270	200	*240*
	Max. horiz. range [m]	*3*	24	60	34	*50*	*7*	14	50	*3*
	Min. horiz. range [m]	*1.5*	18	24	24	*18*	*3*	18	16	*1.5*
	Vertical range [m]	*0.5*	4	6	5	*6*	*1*	4	3	*0.5*
Rhine gravel	Probability density function	*0.02*	0.06	0.12	0.05	*0.50*	*0.05*	0.03	0.16	*0.01*
	Sill	*0.1*	0.095	0.155	0.055	*0.1*	*0.1*	0.04	0.17	*0.1*
	Azimuth [°]	*310*	320	315	300	*310*	*310*	300	300	*310*
	Max. horiz. range [m]	*5*	54	60	40	*70*	*8*	30	60	*5*
	Min. horiz. range [m]	*2*	22	19	22	*30*	*4*	17	22	*2*
	Vertical range [m]	*1*	10	5	11	*10*	*2*	10	8	*1*

The main outcome of the variogram analysis is the orientation of the sedimentary structure types representing the main flow direction of the river Rhine in the lower part of the aquifer and the tributary Wiese in the upper part of the aquifer. The relatively large ranges of spatial correlation of a few meters up to a few 10s of meters for the different sedimentary structure types (Table 2) may be significantly influenced by the resolution of the georadar system and the density of the sampled data taken from the georadar sections. The sedimentary structures of the Rhine gravel are modeled as geostatistical structures that are horizontally around 20% and vertically around 45% larger than the structures of the Wiese gravel.

The aquifer is simulated by sequential indicator simulation (Deutsch and Journel, 1998). The sequential indicator simulation principle allows conditioning by including all data available within the neighbourhood of a model cell, including the original data and all previously simulated values. The steps in the sequential indicator simulation are as follows: In the first step, a grid network and coordinate system is established. In the second step, the existing data is assigned to the nearest grid node. If there is multiple data available, only the closest data is assigned to the nearest grid node. In the third step, a random path through all grid nodes is determined. For a node in the random path: (1) the nearby data and previously simulated grid nodes are searched, and (2) the conditional distribution is estimated by indicator kriging (Deutsch and Journel, 1998). From this distribution (3) a simulated lithofacies is randomly drawn and set as hard data. Then the next node in the random path is selected and the steps (1)-(3) are repeated. This way, the simulation grid is built up sequentially. In the last step, the results are checked. The data and the global proportions (random function hypothesis: limited deviations of the input and output probability density functions of the sedimentary structure types) have to be honored, and the orientations and sizes of the sedimentary structures have to be in accordance with the observed sedimentary structures.

In Fig. 4 one realization of the sequential indicator simulation is shown with separate realizations for the lower and the upper part of the aquifer. The regular model grid of the lower part is defined by 110 x 80 x 10 cells and of the upper part by 110 x 80 x 1 cells. The cell sizes of the lower part are 5 m x 5 m x 1.5 m and of the upper part 5 m x 5 m x 7 m. However, the saturated thickness of the topmost layer is about 1-2 m.

A total of ten combinations of sedimentary structure-type distributions were simulated, each called an aquifer realization. The resulting probability density functions of the sedimentary structure types deviate less than ± 10% from the initial probability density functions. For determining statistical moments and their confidence limits by a Monte Carlo type modeling more than 100 or 1000 realizations are needed. However, to qualitatively examine the effects of subsurface heterogeneity in this boundary condition dominated model (changes in river discharge and permeability of riverbed), a smaller number of aquifer realizations already produces the main trends of groundwater flow and transport behavior.

The changes in orientation and ranges of the sedimentary structures, caused by the above-mentioned interactions of the two rivers over time, are recognized and included in the model by partitioning the aquifer vertically into two hydrostratigraphic units. The generated sedimentary structures are characterized by randomly selecting hydraulic conductivity and porosity values given by means and variances in Jussel et al. (1994) and Rauber et al. (1998). Then, files with the distributions of the hydraulic parameters are generated and exported into PMWIN (Chiang and Kinzelbach, 2001) to perform steady-state groundwater flow and transport simulations.
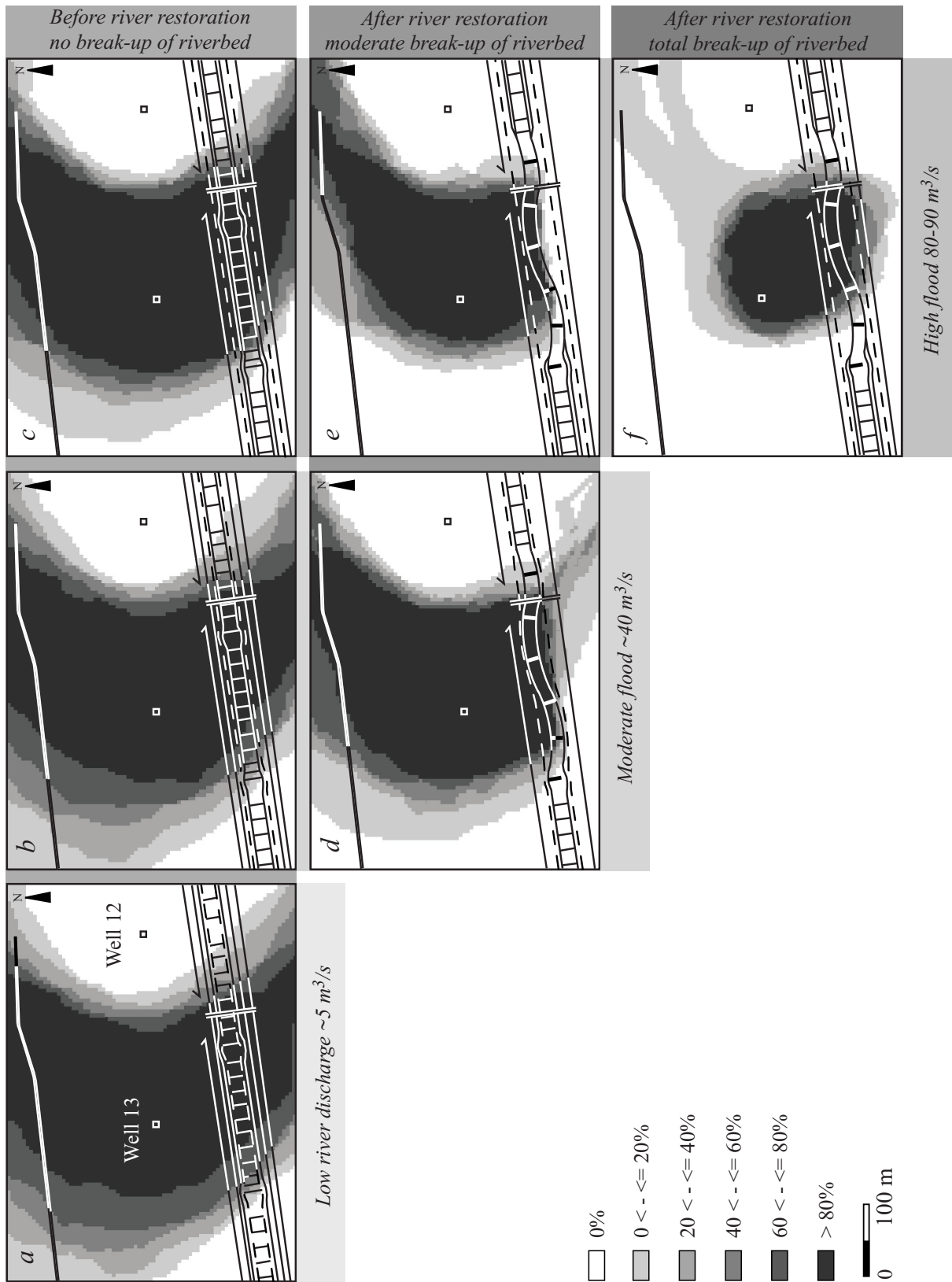
Fig. 6. *Changes of the capture zone distribution of drinking water well 13 in the small-scaled groundwater model depending on river discharge, river restoration, water supply operation data, and subsurface heterogeneity: (a,b,c) before river restoration; (d-f) after river restoration (increasing the leakage factor by a factor of 10 (d,e) and 100 (f)); (a) low river discharge (~5 m³/s); (b,d) moderate flood (~40 m³/s); (c,e,f) high flood (80-90 m³/s). Each capture zone distribution is based on 10 aquifer realizations and describes the probability of a point on the ground surface belonging to the capture zone. The groundwater extraction at drinking water well 13 is constant at 0.046 m³/s.*

3.2.3. Results of the small-scaled groundwater model

For each aquifer realization, a flow model computation was performed and the capture zone for drinking water well 13 was approximately defined by particle tracking. By superposition of all capture zones produced, a probability distribution is obtained that describes the probability of a point on the ground surface belonging to the capture zone. This probability is given by the fraction of capture zones among all realizations containing the point.

Fig. 6 shows probability distributions of the capture zone of drinking water well 13 for conditions before and after river restoration as well as for low river discharge, moderate and high floods. Fig. 6a represents the calibrated groundwater model. The average of the mean squared deviations of observed versus calculated heads over the 10 flow simulations is 0.10 m^2. In Fig. 6b-f, predictions under changed boundary conditions are given, with each probability distribution representing the result of 10 flow and advective transport simulations.

The probability distribution of the well capture zone is strongly influenced not only by changing river discharge and riverbed structure, but also by subsurface heterogeneity. Preferential flow paths can be detected to some extent. In particular, zones along the riverbank with increased infiltration rates of river water can be recognized. River restoration is simulated by increasing the leakage factor by a factor of 10 and 100, respectively, within the restored river channel, assuming moderate and strong increase of the hydraulic conductivity of the riverbed. The leakage factor of the artificially built gravel bars was not increased.

The small-scaled groundwater model produces probable well capture zones depending on the uncertainty of the available data representing sedimentary structure types and the variability of hydraulic conductivity and porosity values for each. The groundwater residence times vary between 1 d and 20 d.

4. Comparison of model results with field data

4.1. Tracer experiments

A first tracer experiment with Uranine was run before river restoration (March 9 – July 3, 1998) during a moderate flood event to determine the stretch of riverbed which should be restored such that no upstream well capture zone would be influenced. The results are also used to determine the sampling frequency for event-specific physical, chemical, and microbiological measurements. The tracer was released into the groundwater between the river Wiese and the right main flood protection dam. The tracer experiment is described in Huggenberger and Regli (1998).

A second tracer experiment with Uranine was run after river restoration (December 13-30, 1999) during a moderate flood event to determine the river-groundwater interaction and groundwater residence times between the river Wiese and drinking water well 13. The tracer was released into the river slightly upstream of the restored river section. Uranine has a retardation factor in sandy gravel of 1.2 and its detection limit is 0.002 ppb (Schudel et al., 2002). To enhance the lateral mixing of the tracer in the river, 10 kg Uranine dissolved in 40 liters of water was evenly distributed over the entire cross-section of the river. The river discharge averaged 39.6 m^3/s during the Uranine release. The groundwater extraction rate at drinking water well 13 was constant at 0.046 m^3/s.

The breakthrough curves at monitoring wells 1461, 1472, 1474, 1475, 1476, 1477, 30, 1459, and 1460 (grouped according to distance from the river) are shown in Fig. 7a-c. They document
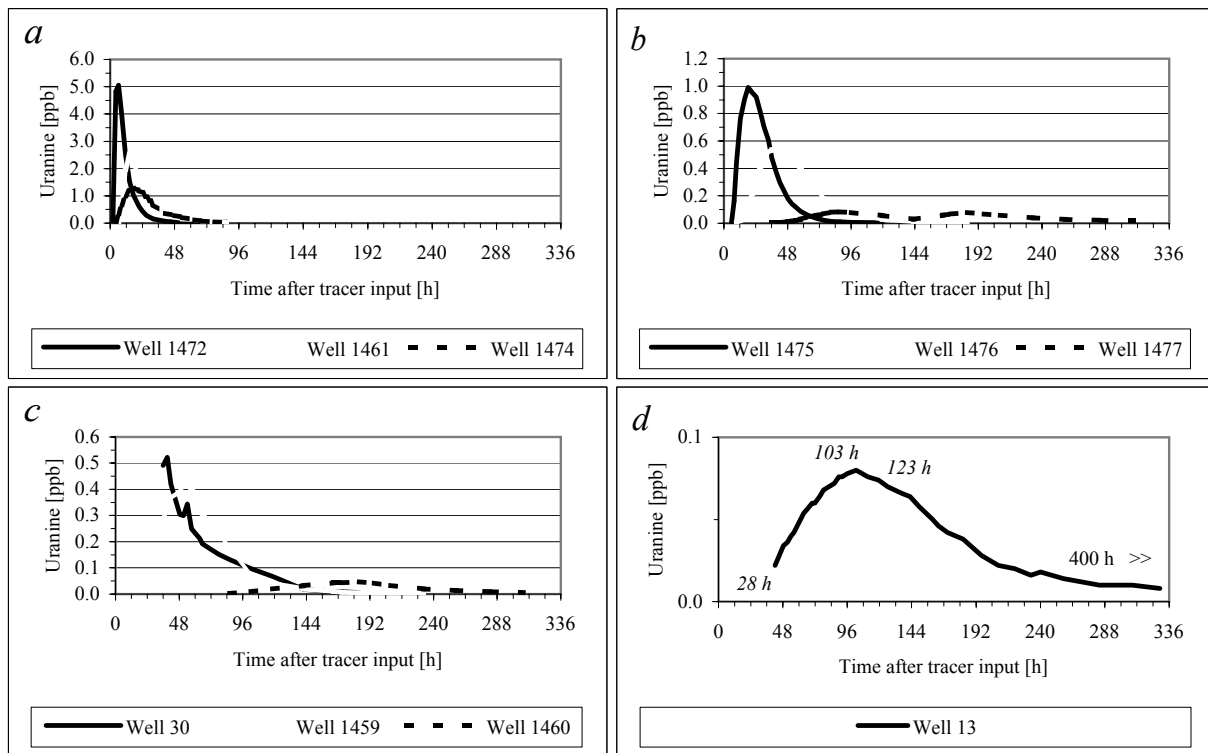
Fig. 7. *Breakthrough curves of Uranine in (a) monitoring wells 1472, 1461, 1474, located 12 meters from the river, (b) monitoring wells 1475, 1476, 1477, located 30 meters from the river, (c) monitoring wells 30, 1459, 160, located 84 meters from the river, – samples were taken in the upper (1472, 1475, 30), middle (1461, 1476, 1459), and lower (1474, 1477, 1460) part of the aquifer, and (d) drinking water well 13, located 124 meters from the river, – samples were taken in the lower part of the aquifer. The moderate flood was 39.6 m³/s. Note variable concentration scales in (a)-(d). See Fig. 3 for well location information.*

a relatively slow vertical mixing of groundwater within the aquifer. The breakthrough of the tracer is delayed and has a decreased peak concentration with increasing depth. The breakthrough curve of monitoring well 1477 is influenced by the second flood event from December 18-21, 1999 which followed the first flood event on December 13, 1999. The breakthrough of wells 1475 and 1476 in the upper part of the aquifer occurred before the second flood event.

The breakthrough curve at drinking water well 13 (Fig. 7d) shows minimum (approximate), dominant, average, and maximum (approximate) groundwater residence times of 28 h (1.2 d), 103 h (4.3 d), 123 h (5.1 d), and 400 h (16.7 d), respectively. These residence times indicate the existence of fast flow paths as predicted by simulations of the small-scaled groundwater model. The maximum tracer concentration in drinking water well 13 was 0.04 ppb and the dilution rate was 1 : 3'500. The recovery of 1.2 g of the tracer in drinking water well 13 documents infiltration of river water within the well capture zone which amounts to approximately 5 l/s/ (area), where the area represents this part of river section which is part of the well capture zone. It corresponds to approximately 10% of the extracted groundwater in drinking water well 13.

In comparison to the results from the large-scaled groundwater model (Fig. 5), the average groundwater residence time of 5.1 d, determined with the Uranine tracer experiment, supports the interpretation of a total break-up of the riverbed as occuring under natural conditions during moderate to high floods or immediately after river restoration. However, the infiltration rate of river water of 5 l/s/(area) indicates no to moderate break-up of the riverbed.
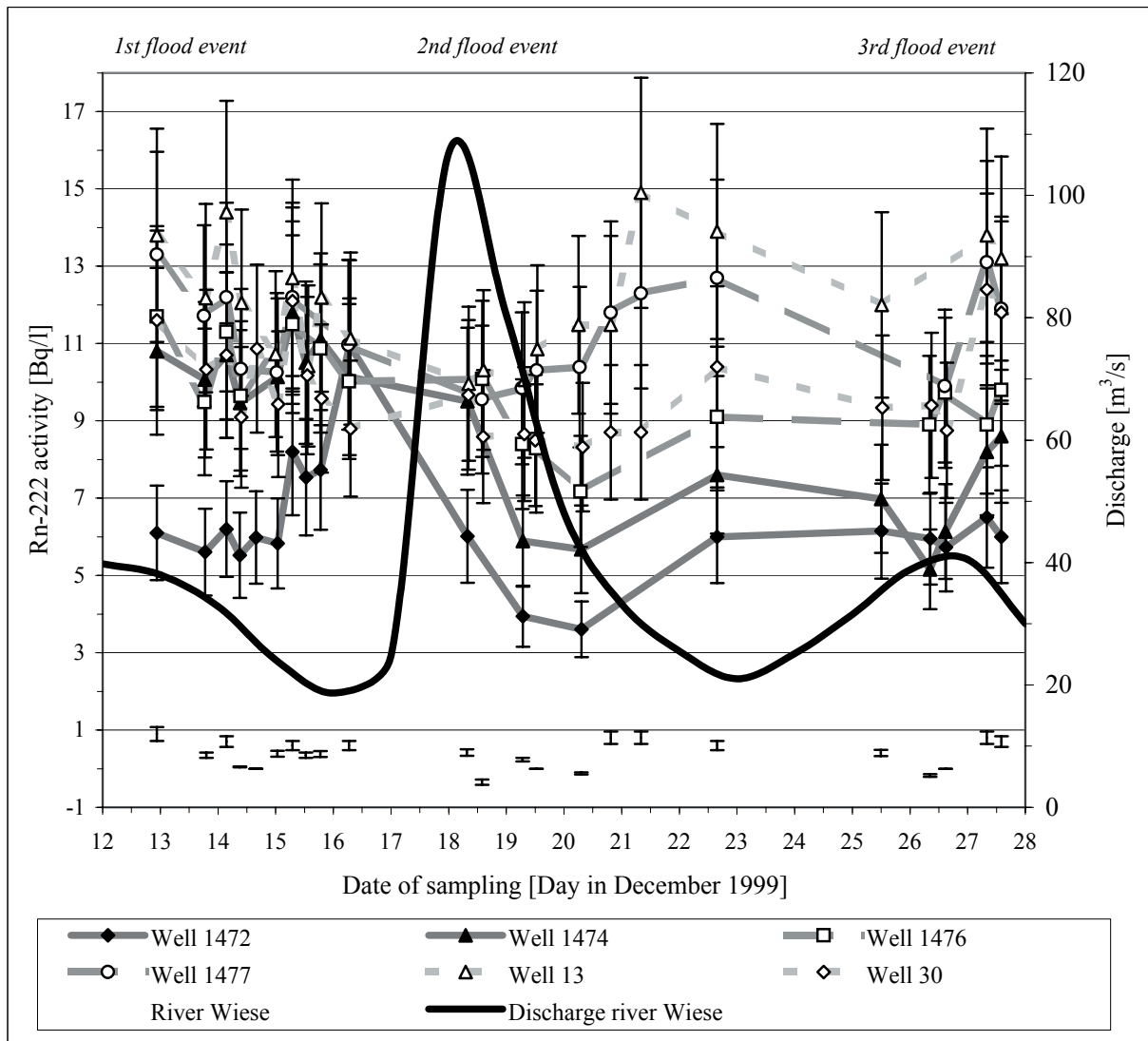
Fig. 8. *Activities of Rn-222 from December 13-28, 1999, in the river Wiese, monitoring wells 1472 and 1474, located 12 meters from the river, monitoring wells 1476 and 1477, located 30 meters from the river, monitoring well 30, located 70 meters from the river, and drinking water well 13 located 124 meters from the river.*

The river-groundwater transition zone is characterized by mixing of river water and ground-water and by changing groundwater residence times (Brunke and Gonser, 1997). Using the natural tracer Radon, the Radon water age can be determined. The theory and the limitations of this method are described by Hoehn and von Gunten (1989). Several authors have demonstrated the use of the dissolved Radon isotope Rn-222 for the determination of the average groundwater residence time (e.g., Hoehn, 2001; Dehnert et al., 1999; Hoehn and von Gunten, 1989). The cited authors assumed plug-flow conditions without mixing of river water and groundwater. The overall error attributed to uncertainties in sampling, measurement method, and counting statistics is estimated to be in the order of ± 20% (Hoehn and von Gunten, 1989).

During the second Uranine tracer experiment, the groundwater as well as the river water was sampled for Rn-222. The Rn-222 activities are shown in Fig. 8. The measurements in the river Wiese show low values during the experiment. The monitoring well 1472 near the river Wiese, which samples the upper part of the aquifer, shows a rapid increase in Rn-222 activity after the first smaller flood event on December 13, 1999, followed by a rapid decrease in Rn-222 activity at the beginning of the second larger flood event from December 18-21, 1999, and a renewed increase in Rn-222 activity at the end of the second flood event. The increase in Rn-222 activity after the first flood event is probably caused by the inclusion of zones with increased Rn-222

production such as iron hydroxide and manganese oxide precipitations on gravel surfaces. The decrease in Rn-222 activity may be caused by the dilution due to high infiltration of river water. Such biogeochemical changes in groundwater-infiltration systems are described for column experiments by von Gunten and Zobrist (1993) and for field experiments by von Gunten et al. (1991). The Rn-222 activity of well 1474 shows a similar shape, except for the initial increase of Rn-222 activity after the first flood event.

The Rn-222 activity of the monitoring wells 1476, 1477, and 30, and of drinking water well 13 varies between 7 and 15 Bq/l. The relative shape of the Rn-222 activity curves of these wells shows a decrease in Rn-222 activity after the first flood event and an increase in Rn-222 activity after the second flood event. However, the changes in Rn-222 activity are not significant, the values of the single wells vary within an error of ± 20%. Therefore, these values do not allow further interpreations.

Assuming a steady-state Rn-222 activity of 19 Bq/l, measured in monitoring well 171 (Fig. 3a), the Radon water age for the extracted groundwater in drinking water well 13 is 4.2-7.5 d (101-180 h). Note that the average residence time for Uranine of 5.1 d falls within this range. Compared to the results from the groundwater models, the dominant time-to-peak and the average groundwater residence times could be accurately determined with Rn-222 measurements.

4.2. Physical and chemical data

The river-groundwater transition zone is characterized by microbiologically mediated redox processes such as aerobic respiration, denitrification, manganoxide reduction, etc. These riverbank-filtration processes are extensively described in von Gunten et al. (1991) and Sigg and Stumm (1996).

Water samples were taken in the river Wiese, in monitoring wells 1474, 1477, 1460, and in drinking water well 13 before, during, and after the river restoration of part 1 (18 different measurement times from November 1998 – Dezember 1999). The water was analyzed on temperature, pH, turbidity, oxygen saturation, dissolved organic carbon, electrical conductivity, chloride, hydrogencarbonate, ammonium, nitrite, nitrate, phosphate, sulfate, and calcium. Table 3 shows some data before, during, and after river restoration.

The measured concentrations in the river Wiese are subject to large fluctuations and, due to the time delay of the signals, they cannot be directly correlated with the concurrently measured concentrations in the monitoring wells 1474, 1477, 1460, and in drinking water well 13. The data in Table 3 show that no significant changes of substance concentrations are noticeable before and after river restoration.

During the aerobic degradation of organic carbon, bacteria are using oxygen as a means for oxidization. The groundwater between the river Wiese and drinking water well 13 is mostly in an oxidizing condition. The carbon dioxide produced dissolves in the groundwater and reacts with the rock-forming minerals, e.g., carbonates and silicates. The weathering processes are responsible for the concentration of the main components calcium, magnesium, bicarbonate, sulfate, and silicic acid in the groundwater. Sodium, potassium, and chloride are probably controlled through these geochemical processes as well. The concentration of nitrate in the groundwater is primarily dependant on the mineralisation of organic nitrogen and secondarily on the nitrification of ammonium. The nitrate does not pose a public-health problem for the groundwater at this location. The phosphate concentration in the groundwater, however, is relatively high and may be attributed to agricultural use of fertilizers within the catchment area.

Table 3. *Data of physical and chemical parameters sampled in the river Wiese, the monitoring wells 1474, 1477, 1460, and drinking water well 13, before, during and after river restoration; n.p.: below detection limit.*

River restoration	Sampling date	Sampling location	Water temperature [°C]	pH [-]	Turbidity [FNU]	Oxygen saturation [% O2]	Dissolved organic carbon [mg C/l]	Electrical conductivity [µS/cm]	Chloride [mg Cl/l]	Hydrogencarbonate [mg HCO3/l]	Nitrate [mg NO3/l]	Nitrite [mg NO2/l]	Phosphate [mg PO4/l]	Sulfate [mg SO4/l]	Ammonium [mg NH4/l]	Calcium [mg Ca/l]
Before	Nov 09, 98	River Wiese	7.9	8.08	4.36	104	1.46	82	2.9	36	4.6	0.005	0.076	6.4	0.020	9.7
		Well 1474	9.9	8.74	3.34	81	0.96	100	2.5	50	4.2	0.030	0.159	6.1	0.020	14.0
		Well 1477	13.5	8.28	3.56	39	0.62	176	5.5	91	5.7	0.014	0.206	12.0	0.010	24.9
		Well 1460	13.6	8.23	0.57	29	0.62	191	6.2	107	6.0	0.010	0.231	13.4	0.020	26.8
		Well 13	13.4	8.05	0.07	67	0.68	183	3.9	98	5.5	n.p.	0.178	9.3	<0.009	27.6
	Dez 01, 98	River Wiese	4.2	7.90	1.44	101	1.08	135	9.0	53	6.0	0.016	0.091	10.3	0.030	26.8
		Well 1474	6.5	8.58	3.95	89	0.70	136	6.7	59	5.8	0.010	0.159	10.1	<0.009	19.3
		Well 1477	10.1	8.41	1.37	58	0.57	160	4.3	83	5.2	<0,01	0.235	9.6	n.p.	22.6
		Well 1460	13.5	8.29	0.62	43	0.51	175	5.1	91	5.6	<0,01	0.250	11.3	n.p.	25.9
		Well 13	12.8	8.10	0.05	76	0.52	170	4.2	91	5.6	n.p.	0.205	9.7	n.p.	26.8
	Jan 19, 99	River Wiese	4.9	7.87	2.11	101	1.36	116	6.6	49	5.3	0.024	0.062	9.0	0.052	14.2
		Well 1474	5.6	8.61	2.37	83	0.76	134	9.0	58	5.8	n.p.	0.163	9.1	<0.009	18.5
		Well 1477	5.6	8.53	1.05	83	0.59	140	6.5	68	5.6	n.p.	0.225	8.9	n.p.	20.3
		Well 1460	11.6	8.40	0.29	80	0.49	150	5.9	77	5.6	n.p.	0.238	9.3	n.p.	22.1
		Well 13	10.2	8.18	0.13	87	0.52	163	6.8	83	5.9	n.p.	0.178	9.3	n.p.	25.0
During	Feb 16, 99	River Wiese	1.8	7.94	1.20	101	1.17	122	7.6	51	5.8	0.035	0.098	10.2	0.089	14.9
		Well 1474	3.6	8.57	3.32	95	0.82	138	8.2	62	6.2	n.p.	0.133	10.2	<0.009	19.5
		Well 1477	6.5	8.60	6.47	89	0.82	136	8.2	63	5.8	n.p.	0.202	8.8	<0.009	20.3
		Well 1460	7.9	8.49	0.13	91	0.63	143	7.8	68	5.9	n.p.	0.196	8.9	<0.009	20.5
		Well 13	9.8	8.26	0.12	84	0.57	180	7.4	94	6.3	n.p.	0.181	10.7	<0.009	29.0
	Mrz 16, 99	River Wiese	6.2	7.78	1.80	102	1.02	75	4.8	29	3.9	0.006	0.034	5.3	0.031	7.9
		Well 1474	5.9	8.77	1.09	97	0.84	99	5.3	44	4.3	n.p.	0.165	5.9	<0.009	12.9
		Well 1477	5.9	8.62	0.20	106	0.67	136	9.2	58	5.8	n.p.	0.229	8.3	n.p.	18.5
		Well 1460	6.5	8.56	0.21	110	0.71	136	8.4	59	5.9	n.p.	0.241	8.1	n.p.	18.9
		Well 13	6.8	8.16	0.10	114	0.75	163	7.1	79	6.7	n.p.	0.166	9.2	n.p.	26.2
	Apr 20, 99	River Wiese	5.5	8.30	8.17	103	1.83	108	5.9	45	4.4	0.013	0.072	7.4	0.020	14.4
		Well 1474	7.5	8.71	0.69	85	0.94	118	5.4	51	4.5	n.p.	0.167	7.4	<0.009	16.8
		Well 1477	6.7	8.69	0.20	80	0.51	116	5.3	54	4.6	n.p.	0.282	6.8	<0.009	16.3
		Well 1460	6.6	8.66	0.22	82	0.52	116	5.2	54	4.6	n.p.	0.294	6.7	<0.009	16.7
		Well 13	7.7	8.23	0.13	86	0.49	170	6.0	82	6.1	n.p.	0.198	9.0	<0.009	26.5
After	Jun 22, 99	River Wiese	14.1	8.12	0.13	67	0.76	160	5.9	79	5.4	n.p.	0.163	11.4	n.p.	21.6
		Well 1477	12.3	8.52	0.13	64	0.67	149	5.7	72	5.5	n.p.	0.247	11.0	n.p.	18.3
		Well 1460	10.7	8.49	0.08	61	0.63	144	5.4	70	5.3	n.p.	0.254	10.2	0.010	18.9
		Well 13	12.6	8.12	0.10	69	0.65	167	5.7	86	5.4	n.p.	0.192	11.1	n.p.	25.9
	Sep 21, 99	River Wiese	14.0	8.09	1.29	96	1.95	237	14.7	86	8.9	0.043	0.086	28.6	0.040	26.2
		Well 1474	17.5	7.98	0.17	35	0.66	238	10.9	104	7.5	n.p.	0.083	23.8	0.240	32.4
		Well 1477	16.3	8.24	0.16	33	0.52	217	9.7	96	7.4	n.p.	0.194	19.8	0.010	31.9
		Well 1460	15.9	8.21	0.11	35	0.52	221	9.8	97	7.3	n.p.	0.193	20.1	n.p.	32.5
		Well 13	16.0	7.89	0.07	54	0.52	252	9.8	118	7.1	n.p.	0.128	20.5	n.p.	39.2
	Dez 07, 99	River Wiese	3.9	8.00	3.65	94	1.34	102	5.5	41	5.2	<0.01	0.074	7.6	0.015	13.0
		Well 1474	4.6	8.42	0.69	79	1.17	152	8.3	66	6.4	n.p.	0.167	9.1	<0.009	20.0
		Well 1477	9.1	8.31	0.94	78	0.83	197	8.3	91	6.9	n.p.	0.207	14.8	<0.009	28.7
		Well 1460	10.2	8.24	0.09	77	0.57	198	8.1	90	6.9	n.p.	0.231	14.7	<0.009	32.2
		Well 13	11.9	8.19	0.10	81	0.51	315	7.6	103	6.8	n.p.	0.171	14.2	<0.009	31.6

Additional biweekly temperature measurements show a clear horizontal layering of the groundwater, which remains virtually unchanged up to drinking water well 13 during the winter and the summer months. Through the groundwater extraction a vertical mixing eventually takes place. The rather large temperature differences between winter and summer amount to 16 °C near the river Wiese and to 7 °C near the drinking water well 13. They support the modeling and tracer experiment results that a significant amount of groundwater recharge by the river Wiese occurs. The horizontal temperature distribution indicates the existence of preferential flow paths.

The physical and chemical data show that the chemical processes associated with infiltration of river water into the groundwater system predominantly occur in the hyporheic interstitial and in the riverbank within a range of a few meters up to a few 10s of meters from the river.

4.3. Microbiological data

The microbiological data from the groundwater of drinking water well 13 in Fig. 9a-c document peak concentrations of microorganisms during flood events. The highest concentration in the river water is 3'000'000 cfu/ml (cfu: colony-forming unit) for heterotrophic plate counts, 10'600 cfu/100 ml for Escherichia coli, and 2'600 cfu/100 ml for Enterococcus. The concentration of microorganisms in drinking water well 13 increased during restoration activities (February 3 – June 8, 1999) and moderate flood events (river discharge > 40 m^3/s) due to dredging and increase in permeability of the riverbed (179 cfu/ml for heterotrophic plate counts, 41 cfu/100 ml for Escherichia coli, 7 cfu/100 ml for Enterococcus). This represents a deterioration of the groundwater quality. After completion of the river restoration, the concentration of microorganisms increased during flood events due to increase in permeability of the riverbed (232 cfu/ml for heterotrophic plate counts, 11 cfu/100 ml for Escherichia coli, 7 cfu/100 ml for Enterococcus). However, for low and average river discharges, the concentration of microorganisms is comparable to that before the river restoration. The delay of the flow peak in the river compared to the measured peak concentration of microorganisms in the drinking water well 13 amounts to 1-2 d (24-48 h) only.

Fig. 9d-f shows average, minimum, and maximum concentrations of microorganisms along a hypothetical flow path between the river Wiese and drinking water well 13. The microorganisms predominantly occur in the hyporheic interstitial and within a few to a few 10s of meters of the riverbank. A few microorganisms are able to reach drinking water well 13 by following the fast flow paths with larger and more pervious pores. The filtering effect along the fast flow paths is insufficient to hold back these microorganisms.

The fast flow paths in the study site occur primarily in open-framework gravel (OW, OW/BM). The occurrence frequency and size of open-framework gravel deposits strongly determine the variance and the correlation length of the hydraulic conductivity. Transport experiments by Rehmann et al. (1999) show that the breakthrough of microorganisms is dependant on the variance of hydraulic conductivity within the aquifer. Thus, in heterogeneous systems the breakthrough of microorganisms occurs faster than that of conservative tracers. In the case of the Rhine and Wiese gravels, the hydraulic conductivity varies over four orders of magnitude (Jussel et al., 1994; Regli et al., 2002) and the correlation length of the highly permeable structure type OW/BM is 36 m for Rhine gravel and 16 m for Wiese gravel (Table 2).

The observations at the study site confirmed the assumption that the reduction in concentration of microorganisms in the groundwater is dependant on the river discharge and the concentration of microorganisms in the river water, the filtering effect of the riverbed and the
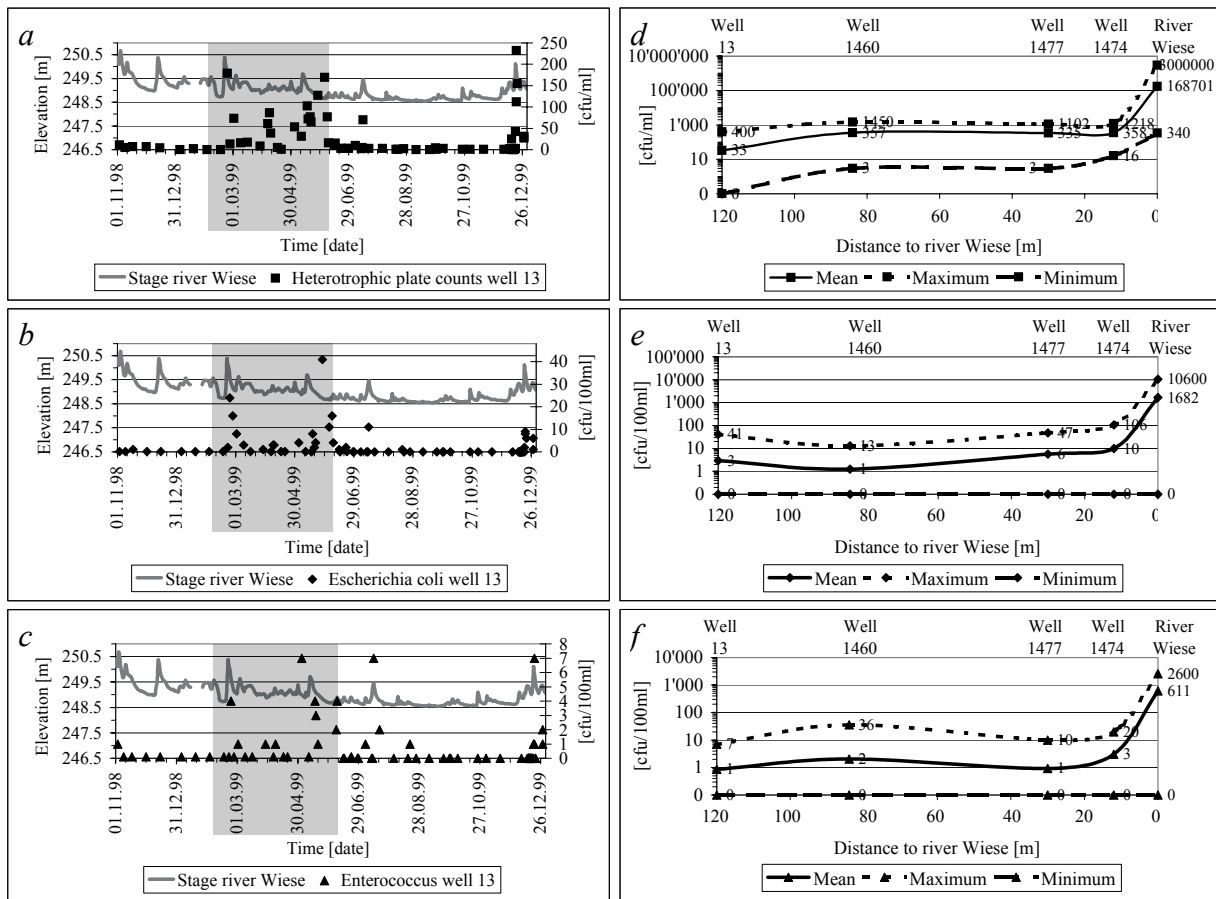
Fig. 9. *Concentrations of microorganisms measured in drinking water well 13 (left column) and along a hypothetical flow path – river Wiese, monitoring wells 1474, 1477, 1460, and drinking water well 13 – (right column) from November 1998 – December 1999: (a,d) Heterotrophic plate counts; (b,e) Escherichia coli; (c,f) Enterococcus. The groundwater extraction at drinking water well 13 amounts to 0.0 m³/s in November 1998, 0.06 m³/s from November 1998 – October 1999, and thereafter 0.046 m³/s; cfu: colony-forming units; gray rectangel: time of restoration activities. Number of measurements (right column): 36 in river Wiese, 17 in monitoring well 1474, 19 in monitoring well 1477, 20 in monitoring well 1460, and 75 in drinking water well 13.*

riverbank, the operation of drinking water well 13, the subsurface heterogeneitiy regarding permeability (filtering effect of the aquifer), and the biogeochemical conditions of the groundwater (Huggenberger, 2003).

5. Discussion and conclusions

The investigations demonstrate that well capture zones in the vicinity of infiltrating rivers might drastically change in size and orientation with respect to changing river infiltration, e.g., during high flow conditions. In order to accurately assess well capture zones, it is important to understand the boundary conditions and the influence of subsurface heterogeneity. In particular, the knowledge of highly permeable zones may help to define groundwater protection zones but also to define river sections where the structure of the riverbed and the riverbank can be restored to more natural conditions.

The use of stochastic methods is an effective and objective way to generate distributions of aquifer properties based on site-specific geological data of different quality. The integration of such distributions into groundwater flow and transport models is needed to determine

well capture zones taking into account data uncertainty. To manage the integration of hard and soft data into the stochastic simulation and visualization of the subsurface, the software tool GEOSSAV (Regli et al., submitted) was used, which has been successfully tested and demonstrated with field experiments.

The results of the stochastic aquifer generation for the Lange Erlen study site include orientations of the sedimentary structure types representing the main flow directions of the river Rhine in the lower part of the aquifer and the tributary Wiese in the upper part of the aquifer. The spatial correlations of the sedimentary structure types of the Rhine gravel are horizontally around 20% and vertically around 45% larger than those of the Wiese gravel. In each aquifer realization the initial probability density functions of the sedimentary structure types deviate less than ± 10% from those which result in the probabilistic models.

The large-scaled, homogeneous groundwater model produced different possible well capture zones depending on changing boundary conditions (e.g., river discharge, riverbed structure). The runs with the small-scaled groundwater model show that the geometry of the well capture zone is strongly influenced not only by changing river discharge and riverbed structure, but also by subsurface heterogeneity. The stochastic approach in the small-scaled groundwater model does not lead to a clearly defined well capture zone, but to a plane representation of the probability of a certain surface location belonging to the capture zone, reflecting the uncertainty of the available data representing sedimentary structure types and the variability of their hydraulic conductivity and porosity values. This model takes into account the identified sedimentary structures and the statistical properties of the aquifer. As the number of aquifer realizations is relatively small, the results have more qualitative character. However, they clearly illustrate the relative contribution of boundary fluxes and subsurface heterogeneity to changes in the well capture zone.

With the large-scaled, homogeneous groundwater model, the average groundwater residence time were determined and vary between 5 and 20 d depending on the boundary conditions. In comparison to the model results, the average groundwater residence time of 5.1 d (determined with the Uranine tracer experiment) is consistent with a flux boundary of an unclogged riverbed as occuring under natural conditions during moderate to high river discharge or immediately after river restoration. However, the corresponding river water infiltration at a rate of 5 l/s/(area) is more consistent with the model results when assuming no to moderate break-up of the riverbed.

The physical and chemical data show that the chemical processes associated with infiltration of river water into the groundwater system predominantly occur in the hyporheic interstitial and in the riverbank within a range of a few meters up to a few 10s of meters from the river. During the observation period of one year significant changes in groundwater chemistry could not be detected.

The breakthrough of microorganisms during moderate and high flow conditions is dependant on the concentration of microorganisms in the river, the variance of the hydraulic conductivity within the aquifer, and the correlation length of the highly permeable structure types. The fast breakthrough occurrence of microorganisms and Uranine within 1-2 d in drinking water well 13 is in accordance with the sedimentological and geostatistical analysis of the aquifer.

The microbiological groundwater quality in the drinking water wells near the river Wiese is below drinking water standards during moderate and high flood events. Due to the frequency of flood events of about 10-12 times per year, it may not be possible to maintain operational security for groundwater extraction near the infiltrating river.

The concept of well capture zones as a planning instrument to prevent groundwater pollution in the vicinity of wells is not effective enough for drinking water wells with a significant amount

of river water infiltration. Results from this study indicate that as long as the water quality in the river is not adequately controlled to avoid significant impacts on the operation of drinking water wells near the river, the concept of well capture zones proposed in Switzerland should be more rigorous. However, if these aspects are taken into account (e.g., operation of water supply according to river discharge and river water quality), it should be possible to perform river restorations within capture zones of wells which will still allow extracted groundwater to meet drinking water standards. As a consequence for conflicting situations in groundwater protection and river restoration, the understanding of the dynamics of the well capture zones at different flow conditions and the influence of subsurface heterogeneity between the river and the wells are basic requirements for a sustainable management of groundwater resources including the needs of river ecology.

Acknowledgments

References

Ayyub, B.M., Gupta, M.M., 1997. Uncertainty Analysis in Engineering and Sciences: Fuzzy Logic, Statistics, and Neural Network Approach. Kluwer Academic, Dordrecht.

Brunke, M., Gonser, T., 1997. The ecological significance of exchange processes between rivers and groundwater. Freshwater Biology, 37 (1), 1-33.

Bundesamt für Wasser und Geologie (BWG), 2001. Hydrogeologisches Jahrbuch der Schweiz 2000.

Chiang, W.-H., Kinzelbach, W., 2001. 3D-Groundwater Modeling with PMWIN. Springer, Heidelberg.

Dehnert, J., Nester, W., Freyer, K., Treutler, H.-C., 1999. Messung der Infiltrationsgeschwindigkeit von Oberflächengewässer mit Hilfe des natürlichen Isotops Radon-222. Grundwasser, 1, 18-30.

Deutsch, C.V., Journel, A.G., 1998. GSLIB: Geostatistical Software Library and User's Guide, Second Edition, Applied Geostatistics Series. Oxford University Press, Oxford.

Environmental Modeling Systems Inc. (EMS-I), 2002. GMS: Groundwater Modeling System, EMS-I, South Jordan, Utah.

Gewässerschutzgesetz (GSchG, vom 24. Januar 1991, Stand 21. Dezember 1999).

Gewässerschutzverordnung (GSchV, vom 28. Oktober 1998, Stand 18. Dezember 2001).

Hoehn, E., 2001. Exchange processes between rivers and groundwaters - The hydrological and geochemical approach. Griebler, C. et al. (Eds.). Groundwater ecology: a tool

for management of water resources. European Commission Environment and climate programme. 55-68.

Hoehn, E., von Gunten, H.R., 1989. Radon in groundwater – a tool to assess infiltration from surface waters to aquifers. Water Resources Research, 25 (8), 1795-1803.

Huggenberger, P., 2003. Transport von Mikroorganismen. Auckenthaler, A., Huggenberger, P. (Eds). Pathogene Mikroorganismen im Grund- und Trinkwasser, Transport – Nachweismethoden – Wassermanagement. Birkhäuser, Basel, 55-77.

Huggenberger, P., Regli, Ch., 1998. Pilotprojekt Revitalisierung Wiese: Voruntersuchungen Grundwasser, Markierversuch Lange Erlen, Brunnen 8013. Tiefbauamt Basel-Stadt.

Huggenberger, P., 1993. Radar facies: recognition of facies patterns and heterogeneities within Pleistocene Rhine gravels, NE Switzerland. Best, C.L., Bristow, C.S. (Eds.). Braided Rivers. Geological Society Special Publication 75, 163-176.

Jol, H.M., Smith, D.G., 1991. Ground-penetrating radar of northern lacustrine deltas. Canadian Journal of Earth Sciences 28 (12), 1939-1947.

Jussel, P., Stauffer, F., Dracos, T., 1994. Transport modeling in heterogeneous aquifers: 1. statistical description and numerical generation of gravel deposits. Water Resources Research, 30 (6), 1803-1817.

Kinzelbach, W., Rausch, R., 1995. Grundwassermodellierung, Eine Einführung mit Übungen. Gebrüder Bornträger, Berlin.

Kinzelbach, W., Marburger, M., Chiang, W.-H., 1992. Bestimmung von Brunneneinzugsgebieten in zwei und drei räumlichen Dimensionen. Geologisches Jahrbuch, Reihe C, Heft 61, Bundesanstalt für Geowissenschaften und Rohstoffe und Geologische Landesämter in der Bundesrepublick Deutschland, Hannover.

Lerner, D.N., 1992. Well catchments and time-of-travel zones in aquifers with recharge. Water Resources Research, 28 (10), 2621-2628.

Noack, T., 1993. Geologische Datenbank der Region Basel. Eclogae Geologicae Helveticae, 86, 283-301.

Noack, T., 1997. Geologische Datenbank der Region Basel - Konzept und Anwendungen. Mitteilungen der Schweizerischen Gesellschaft für Boden- und Felsmechanik, 133, 13-18.

Poeter, E.P., McKenna, S.A., 1995. Reducing uncertainty associated with ground-water flow and transport predictions. Ground Water 33 (6), 899-904.

Rauber, M., Stauffer, F., Huggenberger, P., Dracos, T., 1998. A numerical three-dimensional conditioned/unconditioned stochastic facies type model applied to a remediation well system. Water Resources Research 34 (9), 2225-2233.

Regli, Ch., Rosenthaler, L., Huggenberger, P. GEOSSAV: a simulation tool for subsurface applications. Submitted to Computers & Geoscience, December 2002.

Regli, Ch., Huggenberger, P., Rauber, M., 2002. Interpretation of drill core and georadar data of coarse gravel deposits. Journal of Hydrology 255, 234-252.

Rehmann, L.L.C., Welty, C., Harvey, R.W., 1999. Stochastic analysis of virus transport in aquifers. Water Resources Research, 35 (7), 1987-2006.

Reichert, P., Pahl, C., 1999. Wie können Modelle zu Umweltentscheiden beitragen? EAWAG news 47d, 3-5.

Rohrmeier, M., 2000. Geologische Modelle im Anströmbereich von Wasserfassungen. Diplomarbeit, Universität Basel.

Schudel, B., Biaggi, D., Dervey, T., Kozel, R., Müller, I., Ross, J.H., Schindler, U., 2002. Einsatz künstlicher Tracer in der Hydrogeologie – Praxishilfe. Bundesamt für Wasser und Geologie, Bern.

Sensors & Software Inc., 1993. PulseEKKO Software user's guide. Sensors & Software Inc., Mississauga, Ontario.

Siegenthaler, C., Huggenberger, P., 1993. Pleistocene Rhine gravel: deposits of a braided river system with dominant pool preservation. Best, C.L., Bristow, C.S. (Eds.). Braided Rivers. Geological Society Special Publication 75, 147-162.

Sigg, L., Stumm, W., 1996. Aquatische Chemie: Eine Einführung in die Chemie wässeriger Lösungen und natürlicher Gewässer. vdf Hochschulverlag an der ETH Zürich.

van Leeuwen, M., te Stroet, Ch.B.M., Butler, A.P., Tompkins, J.A., 1998. Stochastic determination of well capture zones, Water Resources Research, 34 (9), 2215-2223.

Vassolo, S., Kinzelbach, W., Schäfer, W., 1998. Determination of a well head protection zone by stochastic inverse modeling. Journal of Hydrology 206 (3-4), 268-280.

von Gunten, U., Zobrist, J., 1993. Biogeochemical changes in groundwater-infiltration systems: column studies. Geochimica et Cosmochimica Acta 57, 3895-3906.

von Gunten, H.R., Karametaxas, G., Krähenbühl, U., Kuslys, M., Giovanoli, R., Hoehn, E., Keil, R., 1991. Seasonal biogeochemical cycles in riverborne groundwater. Geochimica et Cosmochimica Acta 55, 3597-3609.

Weissmann, G.S., Carle, S.F., Fogg, G.E., 1999. Three-dimensional hydrofacies modeling based on soil surveys and transition probability geostatistics. Water Resources Research, 35 (6), 1761-1770.

Zechner, E., Hauber, L., Noack, Th., Trösch, J., Wülser, R., 1995. Validation of a groundwater model by simulating the transport of natural tracers and organic pollutants. Leibundgut, Ch. (Ed.). Tracer Technologies for Hydrological Systems. IAHS Publ., 229, 57-64.

Summary

Coarse fluvial deposits in river valleys of the alpine foreland are important aquifers for municipal water supplies. The complexity of the sedimentary and erosional processes in these formerly braided river environments lead to highly heterogeneous distributions of geological structures and hydrogeological properties such as hydraulic conductivity and porosity, which control groundwater flow as well as solute and particle transport.

Many of the present problems in hydrogeology such as old waste disposal sites, polluted grounds, and the risk of the infiltration of contaminated riverwater concern the protection of groundwater. Solutions of qualitative and quantitative, site-specific groundwater problems require the knowledge of the site-specific heterogeneity of the subsurface. Therefore, the following approaches are combined: (1) descriptive methods which translate sedimentological facies models into hydrofacies models with characteristic aquifer properties, (2) structure-imitating methods which match sedimentary structures based on geostatistical techniques, and (3) process-imitating methods which solve governing flow and transport equations based on calibration techniques (Koltermann and Gorelick, 1996).

Data used in subsurface and groundwater modeling may be divided into two basic types: 'hard data' and 'soft data' (Poeter and McKenna, 1995). Hard data can be directly obtained and examined. Examples of hard data include outcrop data and, in some cases, drill-core data because these explicitly define sedimentary structure types and structure properties. There is measurement or interpretation uncertainty in hard data, but it is considered small enough to be ignored. Soft data are less precise and generally indirect, thus greater uncertainties are associated with the soft data values. Ground-penetrating radar data is an example of soft data.

Three contributions to the above-mentioned methods are presented:

(1) Sedimentlogical and geophysical data – outcrop, drill-core, and georadar data – are combined in a lithofacies-based interpretation and processed to be used for stochastic simulations of sedimentary structures. This interpretation respects differences in data uncertainty and provides lithofacies probabilities for points along boreholes and grid nodes with arbitrary mesh sizes along georadar sections. The estimation of probabilities that drill-core layer descriptions and radarfacies patterns represent specified lithofacies types is based on the significance of the information included in drill-core layer descriptions and the interpretation of the structural information of radarfacies patterns. The specification of the lithofacies types is based on outcrop data. The application of this interpretation shows the importance of a detailed sedimentological analysis of outcrops and drill cores, and its significance on the distinction of lithofacies types.

The method allows a differentiation between the highly permeable open-framework gravel and the open-framework/bimodal gravel couplets, which are only rarely described in the classic literature on the stratigraphy of braided river systems. As these lithofacies types show a high hydraulic conductivity, they act as preferential pathways and, therefore, strongly influence groundwater transport. In addition, older outcrop and drill-core data can be reinterpreted and integrated in the proposed lithofacies scheme.

(2) GEOSSAV (Geostatistical Environment fOr Subsurface Simulation And Visualization) has been developed for the integration of hard and soft data into the stochastic simulation and visualization of distributions of geological structures and hydrogeological properties in the subsurface. GEOSSAV, an interface to selected geostatistical modules (bicalib, gamv, vargplt, and sisim) from the Geostatistical Software LIBrary, GSLIB (Deutsch and Journel,

1998), can be used for data analysis, variogram computation of regularly or irregularly spaced data, and sequential indicator simulation of subsurface heterogeneities. Sequential indicator simulation, based on various kriging techniques (simple, ordinary, and Bayesian), is suitable for the simulation of either continuous variables such as hydraulic conductivity of an aquifer or chemical concentrations at a contaminated site, or categorical variables which indicate the presence or absence of a particular lithofacies.

The data integration platform and development environment of GEOSSAV is Tcl (Tool command language) with its graphical user interface, Tk (Toolkit (Ousterhout, 1994)), and a number of Tcl/Tk extensions (Harrison, 1997). The standard OpenGL API (application programming interface) is used for rendering of 3D data distributions and for slicing perpendicular to the main coordinate axis. Export options for finite-difference groundwater models (e.g. GMS (Environmental Modeling Systems Inc., 2002); PMWIN (Chiang and Kinzelbach, 2001)) allow either files that characterize single model layers (which are saved in ASCII matrix format) or files that characterize the complete 3D flow model set-up for MODFLOW-based groundwater simulation systems (which are saved in bcf package format (Harbaugh and McDonald, 1996)). GEOSSAV has been successfully tested on Microsoft Windows NT 4.0/2000/XP, and on SuSE Linux 7.3. The current version is available at http://www.unibas.ch/earth/pract.

(3) The developed lithofacies-based interpretation of geological and geophysical data and the software GEOSSAV was applied on a field example in the groundwater recharge and production area Lange Erlen, a formerly braided river environment near Basel, Northwestern Switzerland. Two different groundwater models are used to simulate a capture zone of a well located near the infiltrating river Wiese, depending on the hydrological variations (river discharge, hydraulic conductivity of the riverbed), the water supply operation, the progress of river restoration, and the heterogeneity of the subsurface. A deterministic, large-scaled groundwater model (1.8 km x 1.2 km) is used to simulate the average behavior of groundwater flow and advective transport. It is also used to assign the hydraulic boundary conditions for a small-scaled groundwater model (550 m x 400 m), which relies on stochastically generated aquifer properties based on site-specific drill-core and georadar data. The small-scaled groundwater model is used to cope with large subsurface heterogeneity at the location of interest. The stochastic approach in the small-scaled groundwater model does not lead to a clearly defined well capture zone, but to a well capture zone distribution reflecting the uncertainty of the knowledge of the aquifer parameters.

The orientation of the modeled lithofacies types represents the dominance of the flow direction of the river Rhine, in the lower, and the tributary Wiese, in the upper part of the aquifer. The single lithofacies types are spatially correlated in the order of a few meters to a few 10s of meters. The spatial correlations of the sedimentary structures of the Rhine gravel are horizontally around 20% and vertically around 45% larger than those of the Wiese gravel. In each aquifer realization the initial probability density functions of the lithofacies types deviate less than ± 10% from those which result in the probabilistic models.

The results of the groundwater models are compared with two tracer experiments (Uranine and the natural Radon isotope Rn-222) and with physical, chemical, and microbiological data, sampled in monitoring wells between the river and the drinking water well. The groundwater models document strong variations regarding the dimension of the well capture zone depending on changing hydraulic boundary conditions and the variability of the hydraulic aquifer properties. In particular at the small scale (10s to a few hundred of meters), the knowledge of the subsurface heterogeneity is important to evaluate transport-time and -distance of microorganisms between the infiltrating river and the drinking water well. With the large-scaled, homogeneous groundwater model, the average groundwater residence time can be

simulated which varies between 5 and 20 d depending on the hydraulic boundary conditions. In comparison to the model results, the average groundwater residence time of 123 h, determined with the Uranine tracer experiment during an average flood event, indicates a strong increase of the hydraulic conductivity of the riverbed. With the small-scaled groundwater model, the whole range of the groundwater residence times, which varies between 1 and 20 d, can be simulated due to the integration of the subsurface heterogeneity. With the natural tracer Rn-222, the dominant and the average groundwater residence times could be determined.

The data of the monitoring wells show that the chemical and microbiological processes predominantly occur in the hyporheic interstital and the riverbank within a range of a few me-ters to a few 10s of meters from the river.

The breakthrough of microorganisms is dependant on the variance of the hydraulic conductivity within the aquifer. In the case of the Rhine and Wiese gravel, the hydraulic conductivity varies over 3-4 orders of magnitude and the correlation length of the highly permeable open-framework/bimodal gravel couplets is 36 m for Rhine and 16 m for Wiese gravel. The fast occurrence of microorganisms and the tracer Uranine within 1-2 d in the drinking water well is, therefore, in accordance with the sedimentological and geostatistical analysis of the aquifer.

The developed methods and tools allow the integration of geological and geophysical data of different quality into the stochastic description of aquifers. They can be used, e.g., to define and evaluate groundwater protection zones in heterogeneous aquifers associated with infiltration from rivers under changing boundary conditions and under the uncertainty of subsurface heterogeneity. They are useful for the assessment of the groundwater quality of municipal water supplies and for the site-specific evaluation of possibilities for river restorations.

References

Chiang, W.-H., Kinzelbach, W., 2001. 3D-Groundwater Modeling with PMWIN. Springer, Heidelberg.

Deutsch, C.V., Journel, A.G., 1998. GSLIB: Geostatistical Software Library and User's Guide, Second Edition, Applied Geostatistics Series. Oxford University Press, Oxford.

Environmental Modeling Systems Inc. (EMS-I), 2002. GMS: Groundwater Modeling System, EMS-I, South Jordan, Utah.

Harbaugh, A.W., McDonald, M., 1996. User's documentation for MODFLOW-96, an update to the U.S. Geological Survey modular finite-difference ground-water flow model. U.S. Geological Survey Open-File Report 96-485.

Harrison, M., 1997. Tcl/Tk Tools. O'Reilly & Associates, Inc. Cambridge.

Koltermann, C.E., Gorelick, S.M., 1996. Heterogeneity in sediment deposits: A review of structure-imitating, process-imitating, and descriptive approaches. Water Resources Research 32, 2617-2658.

Ousterhout, J.K., 1994. Tcl and the Tk Toolkit. Professional Computing Series. Addison-Wesley, Reading, Massachusetts.

Poeter, E.P., McKenna, S.A., 1995. Reducing uncertainty associated with ground-water flow and transport predictions. Ground Water 33 (6), 899-904.

Scientific achievements

1st author papers

Regli, C., Rosenthaler, L., Huggenberger, P.: GEOSSAV: a simulation tool for subsurface applications. Submitted to Computers & Geosciences, December 2002.

Regli, C., Rauber, M., Huggenberger, P. (2003): Analysis of aquifer heterogeneity within a well capture zone, comparison of model data with field experiments: A case study from the river Wiese, Switzerland. Aquatic Sciences 65, 111-128.

Regli, C., Huggenberger, P., Rauber, M. (2002): Interpretation of drill-core and georadar data of coarse gravel deposits. Journal of Hydrology 255, 234-252.

Co-authored paper

Huggenberger, P., Regli, C.: Sedimentological model of coarse braided river deposits with regard to integrate data of different quality in the stochastic framework of hydraulic aquifer properties. Submitted to Braided Rivers, August 2003.

Course script

Huggenberger, P., Regli, C. (2001): Hydraulische Heterogenität von Lockergesteinsaquiferen und ihre Behandlung: Beobachtungen, stochastische Ansätze, räumliche Korrelationen, Up-Scaling. NDK Blockkurs 18, Zürich. Unterlagen, Reg. L, 1-13.

Abstracts

Huggenberger, P., Regli, C. (2001). Integration of information of different quality in the stochastic description of aquifers. GPR in Sediments, Geological Society of London, Abstracts p. 25.

Regli, C., Huggenberger, P., Rauber, M. (2001): Interpretation of drill-core and georadar data of coarse gravel deposits. 9th Meeting of Swiss Sedimentologists, Fribourg. Abstracts p. 35.

Regli, C., Huggenberger, P., Rauber, M. (2000): Interpretation von Bohr- und Georadardaten grober Kiesablagerungen basierend auf Aufschluss- und Laboruntersuchungen. HydroGeoEvent, Heidelberg. Schriftenreihe der Deutschen Geologischen Gesellschaft (SDGG), Heft 12, S. 198.

Huggenberger, P., Regli, C. (2000): Influence of the heterogeneity on the filtration properties of the aquifer. HydroGeoEvent, Heidelberg. SDGG, Heft 12, S. 105.

Regli, C., Huggenberger, P., Rauber, M., Einstein, H. (1999): Temporal and spatial behavior of the riparian zone as a key issue for the understanding of biogeophysical processes between river and groundwater. AGU Fall Meeting, San Francisco. CA, EOS, v. 80, no. 46, p. F45.

Regli, C., Huggenberger, P., Rohrmeier, M., Einstein, H., Rauber, M. (1998): Integration of field-data of different quality into flow and transport models: case studies from river Wiese and river Toess, Switzerland. EGS Meeting, Nice. AG, sup. II to v. 16, p. C431.

Curriculum vitae

Christian Regli
Born in Andermatt on April 8, 1967

Education

1997 - 2002	University of Basel, Ph.D. Studies of Earth Sciences, present Ph.D. thesis
1995 - 1997	Swiss Federal Institute of Technology (ETH) Zürich and Swiss Federal Institute for Environmental Science and Technology (EAWAG) Dübendorf, Postgraduate Studies of Water Resources Management and Water Pollution Control, Post-Diploma
1987 - 1992	University of Bern, Studies of Geology, Mineralogy, and Chemistry, Diploma
1980 - 1987	Highschool Altdorf, Matura C (natural sciences)
1974 - 1980	Primary school Andermatt

Professional Experience

1997 - 2002	University of Basel, Applied and Environmental Geology, Research assistance for facies based groundwater flow and transport modeling and river-groundwater interaction
1994 - 1995	Geoplan, Altdorf, Consultancy for water protection and foundation testing
1992 - 1993	Büro für Hydrogeologie, Altdorf, Consultancy for water protection and groundwater heat use

Membership

Swiss Association of Geologists – CHGEOL
Swiss Hydrogeological Society – SGH
European Geosciences Union – EGU

Address

University of Basel
Department of Earth Sciences
Applied and Environmental Geology
Bernoullistr. 16, 4056 Basel, Switzerland
christian.regli@unibas.ch

Appendices

Appendix A   Interpretation of drill-core and georadar data

App. A1   Source codes of georadar data processing programs   CD ROM 1

App. A2   Georadar data   CD ROM 2

App. A3   Drill-core data   CD ROM 2

Appendix B   Source code of GEOSSAV   CD ROM 1

Appendix C   Subsurface and groundwater models

App. C1   Large-scaled groundwater models   CD ROM 2

App. C2   Geostatistics and small-scaled aquifer models   CD ROM 2

App. C3   Small-scaled groundwater models   CD ROM 2

App. C4   Data of field experiments and measurements   CD ROM 2

CD ROM 1: inside

CD ROM 2: archive of Geological Institute